FOR OFFICIAL USE ONLY

JPRS L/8242

25 January 1979

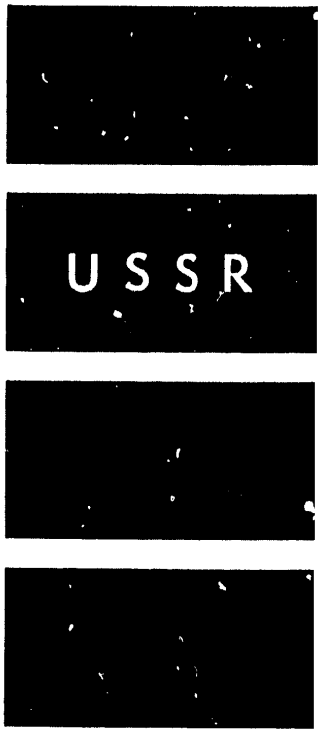

TRANSLATIONS FROM THE LENINGRAD POLYTECHNICAL INSTITUTE'S MONOGRAPH ON QUANTUM ELECTRONICS

U. S. JOINT PUBLICATIONS RESEARCH SERVICE

FOR OFFICIAL USE ONLY

NOTE

JPRS publications contain information primarily from foreign newspapers, periodicals and books, but also from news agency transmissions and broadcasts. Materials from foreign-language sources are translated; those from English-language sources are transcribed or reprinted, with the original phrasing and other characteristics retained.

Headlines, editorial reports, and material enclosed in brackets [] are supplied by JPRS. Processing indicators such as [Text] or [Excerpt] in the first line of each item, or following the last line of a brief, indicate how the original information was processed. Where no processing indicator is given, the information was summarized or extracted.

Unfamiliar names rendered phonetically or transliterated are enclosed in parentheses. Words or names preceded by a question mark and enclosed in parentheses were not clear in the original but have been supplied as appropriate in context. Other unattributed parenthetical notes within the body of an item originate with the source. Times within items are as given by source.

The contents of this publication in no way represent the policies, views or attitudes of the U.S. Government.

APPROVED FOR RELEASE: 2007/02/08: CIA-RDP82-00850R000100010049-6

50272-101

REPORT DOCUMENTATION PAGE	1. REPORT NO. JPRS L/8242	2.	3. Recipient's Accession No.
4. Title and Subtitle: TRANSLATIONS FROM THE LENINGRAD POLYTECHNICAL INSTITUTE'S MONOGRAPH ON QUANTUM ELECTRONICS			5. Report Date: 25 January 1979 6.
7. Author(s): K. P. Seleznev (editor)			8. Performing Organization Rept. No.
9. Performing Organization Name and Address: Joint Publications Research Service 1000 North Glebe Road Arlington, Virginia 22201			10. Project/Task/Work Unit No. 11. Contract(C) or Grant(G) No. (C) (G)
12. Sponsoring Organization Name and Address: As above			13. Type of Report & Period Covered 14.

15. Supplementary Notes: TRUDY LPI (LENINGRADSKIY ORDENA LENINA POLITEKHNICHESKIY INSTITUT IMENI M.I. KALININA): KVANTOVAYA ELEKTRONIKA, Leningrad, 1975

16. Abstract (Limit: 200 words)

This report contains theoretical and experimental papers in the field of quantum generators, optical data processing and holography. The following problems are discussed: physical phenomena in gas (helim--neon and argon) and solid-state (glass and yttrium-aluminum garnet with neodymium admixture) lasers; the methods of selection and synchronization of the type of oscillations in lasers; the methods of automatic frequency control and stabilization; the theory and application of acoustooptical devices in optical data processing systems; the application of holography in experimental equipment; resonance and decelerating systems masers.

17. Document Analysis a. Descriptors

USSR
Laser
Helium
Neon
Argon
Yttrium-aluminum
Neodymium
Polarization
Light Modulation
Light guides

b. Identifiers/Open-Ended Terms

c. COSATI Field/Group 20E 20J

18. Availability Statement	19. Security Class (This Report)	21. No. of Pages
For Official Use Only. Limited Number of Copies Available From JPRS.	UNCLASSIFIED	166
	20. Security Class (This Page) UNCLASSIFIED	22. Price

(See ANSI-Z39.18) See Instructions on Reverse OPTIONAL FORM 272 (4-77) (Formerly NTIS-35) Department of Commerce

JPRS L/8242

25 January 1979

TRANSLATIONS FROM THE LENINGRAD POLYTECHNICAL INSTITUTE'S MONOGRAPH ON QUANTUM ELECTRONICS

Leningrad TRUDY LPI (LENINGRADSKIY ORDENA LENINA POLITEKHNICHESKIY INSTITUT IMENI M.I. KALININA): KVANTOVAYA ELEKTRONIKA in Russian No 344, 1975 signed to press 26 Jun 75 pp 1-111

[Book edited by K.P. Seleznev, Leningrad Polytechnical Institute Press, 800 copies]

CONTENTS

CONTENTS (Continued)

CONTENTS (Continued) Page

PUBLICATION DATA

English title	:	TRANSLATIONS FROM THE LENINGRAD POLITECHNICAL INSTITUTE'S MONOGRAPH ON QUANTUM ELECTRONICS
Russian title	:	TRUDY LPI (LENINGRADSKIY ORDENA LENINA POLITEKHNICHESKIY INSTITUT IMENI M.I. KALININA): KVANTOVAYA ELEKTRONIKA
Author (s)	:	
Editor (s)	:	K. P. Seleznev
Publishing House	:	Leningradskiy Politekhnicheskiy Institut
Place of Publication	:	Leningrad
Date of Publication	:	1975
Signed to press	:	26 June 75
Copies	:	800
COPYRIGHT	:	Leningradskiy Politekhnicheskiy Institut imeni M. I. Kalinina, 1975

ANNOTATION

/Text/ This collection was approved by the Chief Council on Radiophysics of the Ministry of Higher and Middle Specialized Education of the RSFSR.

It was recommended for publication by the Scientific Council of the Radiophysics Department of Leningrad Polytechnical Institute imeni M. I. Kalinin.

The theoretical and experimental papers in the field of quantum generators (lasers and masers), optical data processing and holography are published in this collection. The following problems are discussed: physical phenomena in gas (helium -- neon and argon) and solid-state (glass and yttrium-aluminum garnet with neodymium admixture) lasers; the methods of selection and synchronization of the type of oscillations in lasers; the methods of automatic frequency control and stabilization; the theory and application of acousto-optical devices in optical data processing systems; the application of holography in experimental equipment; resonance and decelerating systems for masers.

The collection is designed for a broad class of physicists and engineers in the field of quantum electronics and adjacent areas and also for post-graduates and students in the advanced courses.

EQUATIONS DESCRIBING THE MULTIMODE OPERATION OF AN ANNULAR LASER

[Article by S. L. Galkin, B. V. L'vov, V. M. Nikolayev]

[Text] Annular lasers are at the present time attracting the attention of a broad class of researchers. The overwhelming majority of published papers on this topic have been devoted to their single-mode operation. The calculation was made within the framework of the semiclassical method proposed by Lamb [1]. Terms have been introduced into the equations which take into account the backscattering similarly to how this was done in references [2, 3] for the single-mode operation. The synchronization of the longitudinal modes was calculated by the method proposed in [4] for a laser with a Fabry-Perot resonator. The equations obtained in our paper are not limited to the case of purely doppler broadening of the line, which extends the range of their application by comparison with the equations for the multimode annular lasers obtained in [5].

In semiclassical laser theory, the electromagnetic field is considered classical, subject to the Maxwell equations, which in the open resonator are reduced to the approximate one-dimensional weighed equation [1, 6]

$$\frac{\partial^2 E}{\partial z^2} - \varepsilon_0\mu_0 \frac{\nu}{Q} \frac{\partial E}{\partial t} - \varepsilon_0\mu_0 \frac{\partial^2 E}{\partial t^2} = -\mu_0 \nu^2 P. \qquad (1)$$

The solution for the electric field E will be found in the form

$$E(z, t) = \sum_n \{E_{1n}(t) \exp[-i\nu_n t - i\varphi_{1n}(t) + iK_n z] + E_{2n}(t) \exp[-i\nu_n t - i\varphi_{2n}(t) - iK_n z]\}, \qquad (2)$$

and for the macroscopic polarization P in the form

$$P(z, t) = \sum_n \{[C_n(t) + iS_n(t)] \exp[-i\nu_n t - i\varphi_{1n}(t) + iK_n z] + [\tilde{C}_n(t) + i\tilde{S}_n(t)] \exp[-i\nu_n t - i\varphi_{2n}(t) - iK_n z]\}, \qquad (3)$$

where $E_{1,2,n}(t)$, $\varphi_{1,2,n}(t)$, $C_n(t)$, $\tilde{C}_n(t)$, $S_n(t)$, $\tilde{S}_n(t)$ are slowly varying functions; $\exp(iK_n z)$ and $\exp(-iK_n z)$ are the eigenfunctions of the resonator; $K_n = 2\pi n/L$; L is the length of the resonator.

Considering the orthogonalness of the eigenfunctions and neglecting the second derivatives of $E_n(t)$ and $\varphi_n(t)$ with respect to time and also the terms with $\nu_n \dot{E}_n/Q_n$; $\dot{\varphi}_n \dot{E}_n$, $\nu_n \dot{\varphi}_n \frac{E_n}{Q_n}$ from equation (1), the system of equations for the amplitudes and phases of the types of oscillations in opposite waves was obtained

$$\dot{E}_{1n} + \frac{1}{2}\frac{\nu}{Q_n} E_{1n} = -\frac{1}{2}\frac{\nu}{\varepsilon_0} S_n; \tag{4}$$

$$(\nu_n + \dot{\varphi}_{1n} - \Omega_{1n}) E_{1n} = -\frac{1}{2}\frac{\nu}{\varepsilon_0} C_n; \tag{5}$$

$$\dot{E}_{2n} + \frac{1}{2}\frac{\nu}{Q_n} E_{2n} = -\frac{1}{2}\frac{\nu}{\varepsilon_0} \tilde{S}_n; \tag{6}$$

$$(\nu_n + \dot{\varphi}_{2n} - \Omega_{2n}) E_{2n} = -\frac{1}{2}\frac{\nu}{\varepsilon_0} \tilde{C}_n. \tag{7}$$

Here $\Omega_{1,2,n} = \Omega_0 + 2\pi n \frac{C}{L} \pm K_n \frac{2A\dot{\theta}}{L}$ are the eigenfrequencies of the moving resonator ($|\Omega_{1n} - \Omega_{2n}| \ll \Omega_{1,2,n}$); $\dot{\theta}$ is the angular velocity of the resonator; A is the area bounded by the resonator.

The active medium in the semiclassical model of a gas laser is considered as a quantum system with two excited levels a and b where the interaction with the electromagnetic field is considered by the methods of perturbation theory.

The polarization of the medium in the first order of perturbation theory [1, 6]

$$P^{(1)}(z, t) = -i\frac{p_{ab}^2}{\hbar} N(z, t) \int_{-\infty}^{\infty} dv\, W(v) \int_{-\infty}^{t} dt' E[z - v(t - t')] \times \exp[(\gamma_{ab} + i\omega)(t' - t)] + \text{к.с.}, \tag{8}$$

where p_{ab} is the matrix element of the electric dipole moment taken between the states a and b; γ_a, γ_b and $\gamma_{ab} = (1/2)(\gamma_a + \gamma_b)$ describe the transition from the excited levels a and b to the basic (unexcited) level; N(z, t) is the stationary density of the inverse population of levels a and b in the absence of the field. The medium is considered to consist of moving molecules with velocity distribution W(v). Only the z-component of the velocity is taken into account.

Let us substitute the value of E from expression (2) in the equality (8) considering only $\exp[i(\omega-\nu_n)t']$ and neglecting the quickly varying terms of the type $\exp[i(\omega+\nu_n)t']$.

Now let us assume that the velocity distribution is Maxwell, that is,

$$W(v)=\frac{1}{u\sqrt{\pi}}\exp\left[-\frac{v^2}{u^2}\right].$$

Let us integrate (8) with respect to v, and then let us proceed to the spatial Fourier polarization component

$$\left.\begin{aligned}P_n^{(1)}(t)&=\frac{2}{L}\int_0^L dz\,P^{(1)}(z,t)\exp[-iK_nz];\\ \tilde{P}_n^{(1)}(t)&=\frac{2}{L}\int_0^L dz\,P^{(1)}(z,t)\exp[iK_nz].\end{aligned}\right\}\qquad(9)$$

On integration over z we neglect the rapidly varying terms of the type $\exp[\mp i(K_n+K_\mu)]$, for they do not make a noticeable contribution to the polarization under the condition that N(z, t) varies little at the distance on the order of the wave length of the optical emission.

After carrying out the indicated transformations and integrating (8) with respect to t', we obtain

$$P_n^{(1)}(t)=-\frac{p_{ab}^2}{\hbar Ku}\left\{\sum_{\mu=1}^{M}E_{1\mu}(t)\exp[-i(\nu_\mu t+\varphi_{1\mu}(t)]\,N_{n-\mu}(t)Z(\nu_\mu-\omega)\right\}.\qquad(10)$$

Here

$$N_{n-\mu}(t)=\frac{1}{L}\int_0^L dz\,N(z,t)\exp\left[i(\mu-n)\frac{2\pi z}{L}\right]$$

(everywhere hereafter the point z=0 will be located at the center of the active body and considered constant within the limits of the active body N(z, t); $Z(y)=2i\int_{-\infty}^{iy}dt\exp[-(t^2+y^2)]$ is the plasma dispersion function.

Replacing 1μ by 2μ and also $N_{n-\mu}$ by $N_{\mu-n}$, from (10) we obtain the expression for $\tilde{P}_n^{(1)}(t)$.

Calculating the coefficients $C_n^{(1)}$, $S_n^{(1)}$, $\tilde{C}_n^{(1)}$, $\tilde{S}_n^{(1)}$ found in (3) from (10) and the analogous expression for $\tilde{P}_n^{(1)}$, and substituting them in the system of equations for the field (4)-(7), we obtain the equations for the annular laser in the first approximation

$$\dot{E}_{1n} + \frac{1}{2}\frac{\nu}{Q_n}E_{1n} = \frac{1}{2}\frac{\nu}{\varepsilon_0}\frac{p_{ab}^2}{\hbar K u}\bar{N}Z_i(\nu_n - \omega)E_{1n}; \tag{11}$$

$$\dot{E}_{2n} + \frac{1}{2}\frac{\nu}{Q_n}E_{2n} = \frac{1}{2}\frac{\nu}{\varepsilon_0}\frac{p_{ab}^2}{\hbar K u}\bar{N}Z_i(\nu_n - \omega)E_{2n}; \tag{12}$$

$$(\nu_n + \dot{\varphi}_{1n} - \Omega_{1n})E_{1n} = \frac{1}{2}\frac{\nu}{\varepsilon_0}\frac{p_{ab}^2}{\hbar K u}\bar{N}Z_r(\nu_n - \omega)E_{1n}; \tag{13}$$

$$(\nu_n + \dot{\varphi}_{2n} - \Omega_{2n})E_{2n} = \frac{1}{2}\frac{\nu}{\varepsilon_0}\frac{p_{ab}^2}{\hbar K u}\bar{N}Z_r(\nu_n - \omega)E_{2n}. \tag{14}$$

Here $\bar{N} \equiv N_0(t)$.

As is obvious from expressions (11)-(14) in the first procedure of perturbation theory the equations for amplitudes and phases of the oscillations in each of the two opposite waves do not depend on each other. The interaction between the waves in this approximation is absent (with the exception of the case of reflection of waves from nonuniformity in the resonator investigated below).

When finding $P_n^{(3)}(t)$, we shall consider only the slowly varying terms with respect to z and drop the terms of the type

$$\exp[\pm i(K_\mu \mp K_\rho + K_\sigma) - iK_n]z \text{ and } \exp[-i(K_\mu + K_\rho - K_\sigma + K_n)]z.$$

As before, the velocity distribution will be considered Maxwell, and after integrating over v we obtain

$$P_n^{(3)}(t) = \frac{ip_{ab}^4}{4\hbar^3}\sum_\mu\sum_\rho\sum_\sigma |[E_{1\mu}E_{1\rho}E_{1\sigma}N_{\mu-\rho+\sigma-n} \times$$
$$\times \exp[-i(\nu_\mu t + \varphi_{1\mu}) + i(\nu_\rho t \mp \varphi_{1\rho}) - i(\nu_\sigma t + \varphi_{1\sigma})] \times$$
$$\times \int_0^\infty d\tau' \int_0^\infty d\tau'' \int_0^\infty d\tau''' \exp\left[-\frac{1}{4}K^2u^2(\tau' + \tau''')^2\right] +$$
$$+ N_{\mu+\rho-\sigma-n}E_{1\mu}E_{2\rho}E_{2\sigma}\exp[-i(\nu_\mu t \mp \varphi_{1\mu}) \mp$$

$$+ i(\nu_\rho t + \varphi_{2\rho}) - i(\nu_\sigma t + \varphi_{2\sigma})\Big] \int_0^\infty d\tau' \int_0^\infty d\tau'' \int_0^\infty d\tau''' \times$$
$$\times \exp\left[-\frac{1}{4} K^2 u^2 (\tau' - \tau''')^2\right] + E_{2\mu} E_{2\rho} E_{1\sigma} N_{-\mu+\rho+\sigma-n} \exp\left[-i(\nu_\mu t + \varphi_{2\mu}) + \right.$$
$$+ i(\nu_\rho t + \varphi_{2\rho}) - i(\nu_\sigma t + \varphi_{1\sigma})\Big] \int_0^\infty d\tau' \int_0^\infty d\tau'' \int_0^\infty d\tau''' \times$$
$$\times \exp\left[-\frac{1}{4} K^2 u^2 (\tau' + 2\tau'' + \tau''')^2\right]\Big] \exp\left[-(\gamma_{ab} - i\nu_\mu + i\nu_\rho - i\nu_\sigma + i\omega)\tau' - \right.$$
$$- (\gamma_a + i\nu_\rho - i\nu_\sigma)\tau'' - (\gamma_{ab} + i\omega - i\nu_\sigma)\tau'''\Big] + \Big[E_{1\mu} E_{2\rho} E_{2\sigma} N_{\mu-\rho+\sigma-n} \times$$
$$\times \exp\left[-i(\nu_\mu t + \varphi_{1\mu}) - i(\nu_\rho t + \varphi_{2\rho}) + i(\nu_\sigma t + \varphi_{2\sigma})\right] \int_0^\infty d\tau' \int_0^\infty d\tau'' \int_0^\infty d\tau''' \times$$
$$\times \exp\left[-\frac{1}{4} K^2 u^2 (\tau' + \tau''')^2\right] + E_{1\mu} E_{1\rho} E_{1\sigma} N_{\mu+\rho-\sigma-n} \times$$
$$\times \exp\left[-i(\nu_\mu t + \varphi_{1\mu}) - i(\nu_\rho t + \varphi_{1\rho}) + i(\nu_\sigma t + \varphi_{1\sigma})\right] \int_0^\infty d\tau' \int_0^\infty d\tau'' \int_0^\infty d\tau''' \times$$
$$\times \exp\left[-\frac{1}{4} K^2 u^2 (\tau' - \tau''')^2\right] + E_{2\mu} E_{1\rho} E_{2\sigma} N_{-\mu+\rho+\sigma-n} \times$$
$$\times \exp\left[-i(\nu_\mu t + \varphi_{2\mu}) - i(\nu_\rho t + \varphi_{1\rho}) + i(\nu_\sigma t + \varphi_{2\sigma})\right] \int_0^\infty d\tau' \int_0^\infty d\tau'' \int_0^\infty d\tau''' \times$$
$$\times \exp\left[-\frac{1}{4} K^2 u^2 (\tau' + 2\tau'' + \tau''')^2\right]\Big] \times \exp\left[-(\gamma_{ab} - i\nu_\mu - i\nu_\rho + i\nu_\sigma + \right.$$
$$+ i\omega)\tau' - (\gamma_a - i\nu_\rho + i\nu_\sigma)\tau'' - (\gamma_{ab} - i\omega + i\nu_\sigma)\tau'''\Big] +$$

+ the same thing but changing places with a and b. (15)

We obtain the expression for $\tilde{P}_n^{(3)}(t)$ from (15) by interchanging the indexes 1 and 2 and also by changing the signs in all of the indexes for N (for example, $N_{-n+\mu-\rho+\sigma}$ is replaced by $N_{n-\mu+\rho-\sigma}$, and so on).

Integrating (15) with respect to τ', τ'' and τ''', we have the final form of the equations for the amplitudes and phases of the oscillations in the third procedure of perturbation theory

$$\dot{E}_{1n} = \alpha_n E_{1n} - \sum_{\mu\rho\sigma} \delta_{\mu+\rho-\sigma-n} E_{1\mu} E_{1\rho} E_{1\sigma} \left|\theta'_{\mu\rho\sigma n}\right| \sin\left[(\nu_n - \nu_\mu - \nu_\rho + \nu_\sigma)t + \right.$$
$$+ \varphi_{1n} - \varphi_{1\mu} - \varphi_{1\rho} + \varphi_{1\sigma} + \arg\theta'_{\mu\rho\sigma n}\Big] - \sum_{\mu\rho\sigma} \delta_{\mu+\rho-\sigma-n} E_{1\mu} E_{2\rho} E_{2\sigma} \left|\theta_{\mu\rho\sigma n}\right| \times$$
$$\times \sin\left[(\nu_n - \nu_\mu - \nu_\rho + \nu_\sigma)t + \varphi_{1n} - \varphi_{1\mu} - \varphi_{2\rho} + \varphi_{2\sigma} + \arg\theta_{\mu\rho\sigma n}\right]; \quad (16)$$

$$(\dot{\varphi}_{1n} + \nu_n - \Omega_{1n}) E_{1n} = \alpha_n E_{1n} - \sum_{\mu\rho\sigma} \delta_{\mu-\rho-\sigma-n} E_{1\mu} E_{1\rho} E_{1\sigma} \left|\theta'_{\mu\rho\sigma n}\right| \times$$
$$\times \cos\left[(\nu_n - \nu_\mu - \nu_\rho + \nu_\sigma)t + \varphi_{1n} - \varphi_{1\mu} - \varphi_{1\rho} + \varphi_{1\sigma} + \arg\theta'_{\mu\rho\sigma n}\right] -$$
$$- \sum_{\mu\rho\sigma} \delta_{\mu+\rho-\sigma-n} E_{1\mu} E_{2\rho} E_{2\sigma} \left|\theta_{\mu\rho\sigma n}\right| \times$$
$$\times \cos\left[(\nu_n - \nu_\mu - \nu_\rho + \nu_\sigma)t + \varphi_{1n} - \varphi_{1\mu} - \varphi_{2\rho} + \varphi_{2\sigma} + \arg\theta_{\mu\rho\sigma n}\right]. \quad (17)$$

Here

$$\alpha_n = \frac{1}{2} \frac{\nu}{\varepsilon_0} \frac{P_{ab}^2}{bKu} \overline{N} Z_i(\nu_n - \omega) - \frac{1}{2} \frac{\nu}{Q_n};$$

$$\alpha_n = \frac{1}{2} \frac{\nu}{\varepsilon_0} \frac{P_{ab}^2}{bKu} \overline{N} Z_r(\nu_n - \omega);$$

$$\delta_{\mu+\rho-\sigma-n} = \begin{cases} 1 & \text{for } \mu+\rho-\sigma-n = 0; \\ 0 & \text{for } \mu+\rho-\sigma-n \neq 0; \end{cases}$$

$$\theta'_{\mu\rho\rho n} = |\theta'_{\mu\rho\rho n}| \exp(i \arg \theta'_{\mu\rho\rho n}) = \frac{ip_{ab}^4}{4h^3} \frac{8'}{(Ku)^2} \frac{\nu}{\omega_0} \times$$
$$\times \left\{ \frac{N_{\mu+\rho-\rho-n}}{4i(\eta_{ca} - i\xi_\Delta)(-i\xi_\mu - i\xi_\Delta + i\xi_\rho + 2\eta)} [Z(\eta; \xi_\mu + \xi_\Delta) + Z(\eta; -\xi_\rho)] + \right.$$
$$\left. + \frac{N_{\mu+\rho-\rho-n}}{4i(\eta_{ca} - i\xi_\Delta)(i\xi_\mu + i\xi_\Delta - i\xi_\rho)} [Z(\eta; \xi_\mu + \xi_\Delta) - Z(\eta; \xi_\rho)] \right\} +$$

+ the same, but changing places with a and b; (18)

$$\theta_{\mu\rho\rho n} = |\theta_{\mu\rho\rho n}| \exp(i \arg \theta_{\mu\rho\rho n}) = \frac{i}{\omega_1} \frac{p_{ab}^4}{h^3} \frac{8}{(Ku)^2} \frac{\nu}{\omega_0} \times$$
$$\times \left\{ \frac{N_{\mu-\rho+\rho-n}}{4i(\eta_{ca} - i\xi_\Delta)(2\eta - i\xi_\mu - i\xi_\Delta - i\xi_\rho)} [Z(\eta; \xi_\mu + \xi_\Delta) + Z(\eta; \xi_\rho)] + \right.$$
$$\left. + \frac{N_{\mu-\rho+\rho-n}}{4i(\eta_{ca} - i\xi_\Delta)(i\xi_\mu - i\xi_\Delta + i\xi_\rho)} [Z(\eta; \xi_\mu + \xi_\Delta) - Z(\eta; -\xi_\rho)] \right\} +$$
$$+ \frac{4N_{\mu-\rho+\rho-n}}{-\sqrt{2}(2\eta - \eta_{ca} - i\xi_\mu - i\xi_\rho)(2\eta - \eta_{ca} - 2i\xi_\rho + i\xi_\rho - i\xi_\mu)} Z\left(\frac{\eta_{ca}}{2}; -\frac{\xi_\rho - \xi_\mu}{2}\right) +$$
$$+ \frac{2N_{\mu-\rho+\rho-n}}{\sqrt{2}(-i\xi_\rho + i\xi_\rho)(2\eta - \eta_{ca} - i\xi_\mu - i\xi_\rho)} Z(\eta; \xi_\rho - \xi_\rho + \xi_\mu) -$$
$$- \frac{2N_{\mu-\rho+\rho-n}}{2(-i\xi_\rho + i\xi_\rho)(2\eta - \eta_{ca} - i\xi_\mu + i\xi_\rho - 2i\xi_\rho)} Z(\eta; \xi_\mu) +$$
$$+ \frac{4N_{\mu-\rho+\rho-n}}{-\sqrt{2}(2\eta - \eta_{ca} + i\xi_\rho + i\xi_\mu)(2\eta - \eta_{ca} - 2i\xi_\rho - i\xi_\mu + i\xi_\rho)} Z\left(\frac{\eta_{ca}}{2}; -\frac{\xi_\mu - \xi_\rho}{2}\right) +$$
$$+ \frac{2N_{\mu-\rho+\rho-n}}{\sqrt{2}(-i\xi_\mu - i\xi_\rho)(2\eta - \eta_{ca} + i\xi_\rho + i\xi_\mu)} Z(\eta; \xi_\rho - \xi_\mu + \xi_\rho) -$$
$$- \frac{2N_{\mu-\rho+\rho-n}}{\sqrt{2}(-i\xi_\mu - i\xi_\rho)(2\eta - \eta_{ca} + i\xi_\rho - i\xi_\mu - 2i\xi_\rho)} Z(\eta; -\xi_\rho) +$$

+ the same but changing places with a and b.[1] (19)

[1] The analogous expressions were obtained by Sargent and O'Bryan [7].

Here

$$\xi_\sigma = \frac{\nu_\sigma - \omega}{Ku}; \quad \xi_\mu = \frac{\nu_\mu - \omega}{Ku}; \quad \xi_\rho = \frac{\nu_\rho - \omega}{Ku}; \quad \xi_\Delta = \frac{\nu_\rho - \nu_\sigma}{Ku};$$

$$\eta = \frac{\gamma_{ab}}{Ku}; \quad \eta_a = \frac{\gamma_a}{Ku}; \quad \eta_b = \frac{\gamma_b}{Ku}.$$

The equations for $\dot{E}_{2n}$ and $\dot{\phi}_{2n}$ were obtained from (16) and (17) by interchanging the indexes 1 and 2.

Let us note that in the approximation of the purely doppler broadening of the line, that is, for $\eta \ll 1$, in the expression (15) the integrals containing

$$\exp\left[-\frac{1}{4}K^2u^2(\tau' - \tau''')^2\right],$$

can be replaced by the integrals of the δ-function with the argument $(\tau'-\tau''')$, and it is possible to neglect the remaining integrals.

Then the expressions for θ and θ' assume the form

$$\theta'_{\mu\rho\sigma n} = \frac{ip_{ab}^4}{4\hbar^3}\frac{\nu}{\varepsilon_0}\frac{8}{(Ku)^3}\frac{\sqrt{\pi}}{4}\left\{\frac{N_{\mu+\rho-\sigma-n}}{(2\eta_i - i\xi_\mu - i\xi_\rho + 2i\xi_\sigma)(\eta_a + i\xi_\sigma - i\xi_\rho)} + \right.$$
$$\left. + \frac{N_{\mu+\rho-\sigma-n}}{(2\eta_i - i\xi_\mu - i\xi_\rho + 2i\xi_\sigma)(\eta_b + i\xi_\sigma - i\xi_\rho)}\right\};$$
$$\theta_{\mu\rho\sigma n} = \frac{ip_{ab}^4}{4\hbar^3}\frac{8}{(Ku)^3}\frac{\nu}{\varepsilon_0}\frac{\sqrt{\pi}}{4}\left\{\frac{N_{\mu-\rho+\sigma-n}}{(2\eta_i - i\xi_\mu + i\xi_\sigma - 2i\xi_\rho)(\eta_a - i\xi_\rho + i\xi_\sigma)} + \right.$$
$$\left. + \frac{N_{\mu-\rho+\sigma-n}}{(2\eta_i - i\xi_\mu + i\xi_\sigma - 2i\xi_\rho)(\eta_b - i\xi_\rho + i\xi_\sigma)}\right\}.$$

Let us consider the generation mode in which the oscillation frequencies are equidistant. Setting $\nu_n = \Omega_0 + n\nu_m$; $\dot{\Omega}_{1,2,n} = \Omega_0 + n\Delta \pm \Omega$ and considering that for equidistance modes $\dot{\varphi}_{1n} = \dot{\varphi}_{1n+1} = \ldots = \dot{\varphi}_1$, $\dot{\varphi}_{2n} = \dot{\varphi}_{2n+1} = \ldots = \dot{\varphi}_2$, we have

$$\dot{E}_{1n} = \alpha_n E_{1n} - \sum_{\mu\rho\sigma} \delta_{\mu+\rho-\sigma-n} E_{1\mu}E_{1\rho}E_{1\sigma}|\theta'_{\mu\rho\sigma n}| \times$$
$$\times \sin(\varphi_{1n} - \varphi_{1\mu} - \varphi_{1\rho} + \varphi_{1\sigma} + \arg\theta'_{\mu\rho\sigma n}) -$$
$$- \sum_{\mu\rho\sigma} \delta_{\mu+\rho-\sigma-n} E_{1\mu}E_{2\rho}E_{2\sigma}|\theta_{\mu\rho\sigma n}| \sin(\varphi_{1n} - \varphi_{1\mu} - \varphi_{2\rho} + \varphi_{2\sigma} + \arg\theta_{\mu\rho\sigma n});$$
$$[\dot{\varphi}_1 + n(\nu_m - \Delta) + \tilde{\Omega}]E_{1n} = \alpha_n E_{1n} - \sum_{\mu\rho\sigma} E_{1\mu}E_{1\rho}E_{1\sigma}|\theta'_{\mu\rho\sigma n}|\delta_{\mu+\rho-\sigma-n} \times$$
$$\times \cos(\varphi_{1n} - \varphi_{1\mu} - \varphi_{1\rho} + \varphi_{1\sigma} + \arg\theta'_{\mu\rho\sigma n}) - \sum_{\mu\rho\sigma} \delta_{\mu+\rho-\sigma-n} E_{1\mu}E_{2\rho}E_{2\sigma}|\theta_{\mu\rho\sigma n}| \times$$
$$\times \cos(\varphi_{1n} - \varphi_{1\mu} - \varphi_{2\rho} + \varphi_{2\sigma} + \arg\theta_{\mu\rho\sigma n}).$$

The equations for $\dot{\varphi}_2$ and $\dot{E}_{2n}$ are obtained, just as before, by interchanging the indexes 1 and 2.

The investigated mode is called synchronization of the types of oscillations, and its range of existence depends on the type of coefficients α, σ, θ and θ'.

As a rule, in order to obtain stable synchronization, modulation of the losses or the dielectric constant inside the resonator with a frequency ν_m close to the distance between adjacent natural frequencies of the resonator is used [4, 8-10].

In the case of loss modulation, the term of [4] is added to the polarization:

$$\cdot i\varepsilon_0\Delta\chi''(z)[1+\cos(\nu_m t)]E(z,t).$$

The additional term in P_n has the form

$$-i\frac{\varepsilon_0\delta_0 c}{\nu L}E_{1n}\exp[-i(\nu_n t+\varphi_{1n})]-$$
$$i\frac{\varepsilon_0 c}{\nu L}[E_{1n+1}\delta_+\exp[-i(\nu_n t+\varphi_{1n+1})]+E_{1n-1}\delta_-\exp[-i(\nu_n t+\varphi_{1n-1})]],$$

where

$$\delta_0=\frac{2\nu}{c}\int_0^L\Delta\chi''(z)\,dz;$$
$$\delta_\pm=\frac{\nu}{c}\int_0^L\Delta\chi''(z)\exp\left(\mp\frac{i2\pi z}{L}\right)dz.$$

For small dimensions of the modulator by comparison with the length of the resonator

$$\delta_\pm=\delta\exp\left(\mp\frac{i2\pi z_p}{L}\right),$$

where

$$\delta=\frac{\nu}{c}\int_0^L\Delta\chi''(z)\,dz=\frac{\delta_1}{2};$$

z_p is the center of the modulator.

In the case of modulation of the dielectric constant, the term of [4] is added to the polarization:

$$\varepsilon_0 \Delta\chi'(z)\cos(\nu_m t)E(z, t)$$

and the additional term in P_n is equal to

$$\frac{\varepsilon_0 c}{L}\left[E_{1n-1}\delta'_{+}\exp\left[-i(\nu_n t+\varphi_{1n+1})\right]+E_{1n-1}\delta'_{-}\exp\left[-i(\nu_n t+\varphi_{1n-1})\right]\right],$$

where

$$\delta'_{\pm}=\frac{\nu}{c}\int_0^L \Delta\chi'(z)\exp\left(\mp i\frac{2\pi z}{L}\right)dz,$$

and for small dimensions of the modulator

$$\delta'_{\pm}=\delta'\exp\left(\mp\frac{i2\pi z_p}{L}\right),\ \text{where}\ \delta'=\frac{\nu}{c}\int_0^L \Delta\chi'(z)\,dz.$$

Thus, for loss modulation, the following terms are added to equation (16)

$$-\frac{c}{L}\left[\delta_0 E_{1n}+\delta E_{1n+1}\cos\left(\varphi_{1n+1}-\varphi_{1n}+\frac{2\pi z_p}{L}\right)+\right.$$
$$\left.+\delta E_{1n-1}\cos\left(\varphi_{1n-1}-\varphi_{1n}-\frac{2\pi z_p}{L}\right)\right], \qquad (20)$$

and the following terms, to equation (17)

$$-\frac{c}{L}\left[\delta E_{1n-1}\sin\left(\varphi_{1n+1}-\varphi_{1n}+\frac{2\pi z_p}{L}\right)+\right.$$
$$\left.+\delta E_{1n-1}\sin\left(\varphi_{1n-1}-\varphi_{1n}-\frac{2\pi z_p}{L}\right)\right]. \qquad (21)$$

For dielectric constant modulation, the additional terms in equation (16) have the form

$$\frac{c}{L}\left[\delta' E_{1n+1}\sin\left(\varphi_{1n-1}-\varphi_{1n}+\frac{2\pi z_p}{L}\right)+\right.$$
$$\left.+\delta' E_{1n-1}\sin\left(\varphi_{1n-1}-\varphi_{1n}-\frac{2\pi z_p}{L}\right)\right], \qquad (22)$$

and in equation (17) they are equal to

$$\frac{c}{L}\left[\delta' E_{1n-1}\cos\left(\varphi_{1n-1}-\varphi_{1n}+\frac{2\pi z_p}{L}\right)+\right.$$
$$\left.+\delta' E_{1n-1}\cos\left(\varphi_{1n-1}-\varphi_{1n}-\frac{2\pi z_p}{L}\right)\right]. \qquad (23)$$

In the equations for $\dot{E}_{2n}$ and $\dot{\phi}_2$, in the additional terms in both cases the index 1 is replaced by 2, and the sign in front of $2\pi z_p/L$ is changed everywhere.

If there is a dispersing agent in the annular resonator at the point z_{disp} (for example, the complex dielectric constant of the medium at this point varies discontinuously by some amount), then reflected waves appear, and the field in the resonator assumes the form

$$E = \sum_n [E_{1n} \exp(iK_n z - i\nu_n t - i\varphi_{1n}) + E_{2n} \exp(-iK_n z - i\nu_n t - i\varphi_{2n}) + \\ + |m_1| E_{2n} \exp(i\chi_1 + iK_n z - i\nu_n t - i\varphi_{2n} - i\psi_n) + \\ + |m_2| E_{1n} \exp(i\chi_2 - iK_n z - i\nu_n t - i\varphi_{1n} + i\psi_n)].$$

Here $m_1 = |m_1| \exp(i\chi_1)$; $m_2 = |m_2| \exp(i\chi_2)$ are the backscattering coefficients, $\psi_n = z_{disp} K_n = \psi_0 + n\psi$; $\psi = 2\pi z_{disp}/L$.

In practice, in view of the smallness of the values of m, it is possible to limit ourselves to the contribution of the reflected wave to the polarization in the first procedure of perturbation theory. The following term appears in equation (16)

$$M_1 E_{2n} \sin(\varphi_{2n} - \varphi_{1n} + n\dot{\psi} + \dot{\psi}_0 - \chi_1); \quad (24)$$

In the equation analogous to it for $\dot{E}_{2n}$

$$M_2 E_{1n} \sin(\varphi_{2n} - \varphi_{1n} + n\dot{\psi} + \dot{\psi}_0 + \chi_2). \quad (25)$$

In the equation (17)

$$M_1 E_{2n} \cos(\varphi_{2n} - \varphi_{1n} + n\dot{\psi} + \dot{\psi}_0 - \chi_1), \quad (26)$$

and in the euqation for $\dot{\phi}_2$

$$M_2 E_{1n} \cos(\varphi_{2n} - \varphi_{1n} + n\dot{\psi} + \dot{\psi}_0 + \chi_2). \quad (27)$$

Here

$$M_{1,2} = \frac{1}{2} \frac{\nu}{\omega} \frac{p_{ab}^2}{\hbar K u} \bar{N} |m_{1,2}|.$$

The equations obtained considering the terms (18-27) offer the possibility of investigating a number of specific phenomena in an annular multimode laser connected with the interaction of the generated mode and backscattering, in particular, the self-synchronization conditions and synchronization of longitudinal modes and also capture of the counter wave frequencies.

BIBLIOGRAPHY

1. Lamb, W. E. PHYS REV., No 134, A1429, 1964.

2. Klimontovich, Yu. L.; Landa, P. S.; Lariontsev, Ye. G. ZHETF [Journal of Experimental and Theoretical Physics], No 52, 1967, p 1616.

3. Landa, P. S.; Lariontsev, Ye. G. RADIOTEKHNIKA I ELEKTRONIKA [Radioengineering and Electronics], No 15, 1970, p 1214.

4. Harris, S. E.; McDuff, O. P. IEEE J. OF QUANT. ELECTR., 1965, p 245.

5. Miyashita Toyokatay. JAP. J. APPL. PHYS., No 10, 1971, p 1051.

6. Aronowitz, F. PHYS. REV., No 139, 1965, p A635.

7. Sargent, O'Bryan. PHYS. REV., No 6, 1973, p A8.

8. Buholz, N.; Chodorow, M. IEEE J. OF QUANTUM ELECTRONICS, QE-3, 1967, p 454.

9. Wax, S. I.; Chodorow, M. IEEE J. OF QUANTUM ELECTRONICS, QE-8, 1972, P 343.

10. Kruglik, G. S.; Kutsak, A.A. ZHPS, No 14, 1971, p 59.

EFFECT OF AN AXIAL MAGNETIC FIELD ON THE INTERACTION OF THE COUNTER WAVES OF AN ANNULAR HE-NE LASER WITH SYNCHRONIZATION OF THE LONGITUDINAL MODES

[Article by S. L. Galkin, B. V. L'vov, V. M. Nikolayev, V. Yu. Petrun'kin]

[Text] One of the important factors determining the practical application of annular lasers is the stability of the beat frequency of the counter waves. The interaction of the counter waves in the active medium leads to the fact that the magnitude of the beat frequency between them differs from the frequency caused by rotation of the system or the phase-shifter. Under the conditions of synchronization of longitudinal modes, the competition between the counter waves leads to the fact that the beat frequency depends essentially on the modulating frequency difference with respect to the intermodal, the modulation depths, the displacement of the modulator from the point of encounter of the pulses [1-3]. The enumerated factors have a sharp effect on the stability of the frequency of the counter waves, for they can change in the operating process. Consequently, the attenuation of the competition of the counter waves in the active medium increases the stability of the beat frequency.

The experimental study of the annular He-Ne laser with synchronization of the longitudinal modes performed by us [3] demonstrated that the axial magnetic field applied to the active Ne-Ne medium with a natural mixture of neon isotopes significantly decreases the effect of the position of the modulator and the variation of the parameters of the modulating signal on the magnitude of the beat frequency on the counter waves. It was proposed that this stabilizing effect of the magnetic field is connected with a decrease in the competition of the counter waves in the active medium, that is, that the Zeeman splitting of the amplification circuit attenuates the interaction of the counter waves to some degree analogously to how this occurs in the active medium with equal content of neon isotopes.

This paper contains the results of the theoretical investigation which confirmed the above-discussed proposition. In addition, the analysis has demonstrated that in some range of intensities of the magnetic field the interaction between the counter waves can even be greater than in the absence of the field, and it depends sharply on its magnitude. The performed experiment confirmed these results.

The equations describing the operation of the multimodal annular gas laser were obtained by us in reference [4]. The coefficients $\theta_{\mu\rho\sigma n}$ in these equations are the coefficients of the relation between the modes of the counter waves in the absence of a magnetic field. For determination of the type of these coefficients on placement of the active medium in the axial magnetic field, we used the results of reference [5]. We shall consider that as a result of the presence of Brewster windows in the laser resonator there is only one linear polarization of the electromagnetic field. Then the expression for the coefficients of the relation between the modes of the counter waves of the annular laser, the active medium of which is placed in the axial magnetic field assumes the form:

$$\theta_{\mu\rho\sigma n} = \frac{iv\sqrt{\pi}N_{\mu-\rho+\sigma-n}}{\varepsilon_0\gamma\sqrt{2}\hbar^3k^{11}}\left\{\frac{\sum_{a'-b'=1}P^4_{a'b'}}{(2\gamma_{ab}-iv_\mu+iv_\sigma-2iv_\rho+2i\omega_0+2i\Delta\omega)(\gamma_a+iv_\sigma-iv_\rho)}+\right.$$

$$+\frac{\sum_{a'-b'=1}P^4_{a'b'}}{(2\gamma_{ab}-iv_\mu+iv_\sigma-2iv_\rho-2i\omega_0-2i\Delta\omega)(\gamma_a+iv_\sigma-iv_\rho)}+$$

$$+\frac{\sum_{a'-b'=1}P^4_{a'b'}}{(2\gamma_{ab}-iv_\mu+iv_\sigma-2iv_\rho+2i\omega_0+2i\Delta\omega)(\gamma_b+iv_\sigma-iv_\rho)}+$$

$$+\frac{\sum_{a'-b'=1}P^4_{a'b'}}{(2\gamma_{ab}-iv_\mu+iv_\sigma-2iv_\rho+2i\omega_0-2i\Delta\omega)(\gamma_b+iv_\sigma-iv_\rho)}+$$

$$+\frac{\sum_{a'-b'=1}P^2_{a'b'}P^2_{a',b'-2}}{(2\gamma_{ab}-iv_\mu+iv_\sigma-2iv_\rho+2i\omega_0)(\gamma_a+iv_\sigma-iv_\rho)}+$$

$$+\frac{\sum_{a'-b'=1}P^2_{a'b'}P^2_{a',b'+2}}{(2\gamma_{ab}-iv_\mu+iv_\sigma-2iv_\rho+2i\omega_0+2i\Delta\omega)(\gamma_b+2i\Delta\omega+iv_\sigma-iv_\rho)}+$$

$$+\frac{\sum_{a'-b'+1}P^2_{a'b'}P^2_{a'-2,b'}}{(2\gamma_{ab}-iv_\mu+iv_\sigma-2iv_\rho+2i\omega_0+2i\Delta\omega)(\gamma_a+2i\Delta\omega+iv_\sigma-iv_\rho)}+$$

$$+\frac{\sum_{a'-b'+1}P^2_{a'b'}P^2_{a'-2,b'}}{(2\gamma_{ab}-iv_\mu+iv_\sigma-2iv_\rho+2i\omega_0)(\gamma_b+iv_\sigma-iv_\rho)}+$$

$$+\frac{\sum_{a'-b'-1}P^2_{a'b'}P^2_{a',b'-2}}{(2\gamma_{ab}-iv_\mu+iv_\sigma-2iv_\rho+2i\omega_0)(\gamma_a+iv_\sigma-iv_\rho)}+$$

$$+\frac{\sum_{a'-b'-1}P^2_{a'b'}P^2_{a',b'-2}}{(2\gamma_{ab}-iv_\mu+iv_\sigma-2iv_\rho+2i\omega_0-2i\Delta\omega)(\gamma_b-2i\Delta\omega+iv_\rho-iv_\sigma)}+$$

$$+\frac{\sum_{a'-b'-1}P^2_{a'b'}P^2_{a'-2,b'}}{(2\gamma_{ab}-iv_\mu+iv_\sigma-2iv_\rho+2i\omega_0-2i\Delta\omega)(\gamma_a-2i\Delta\omega+iv_\rho-iv_\sigma)}+$$

$$\left.+\frac{\sum_{a'-b'-1}P^2_{a'b'}P^2_{a'+2,b'}}{(2\gamma_{ab}-iv_\mu+iv_\sigma-2iv_\rho+2i\omega_0)(\gamma_b+iv_\sigma-iv_\rho)}\right\}. \qquad (1)$$

The notation corresponds to that selected by us in reference [4] except that $\Delta\omega=\mu_B gH$; μ_B is the Bohr magneton; g is the Lande factor; H is the intensity of the axial magnetic field; $P_{a'b'}$ are the matrix elements of the dipole moment, and the indexes a', b' correspond to the magnetic sublevels.

It must be noted that the expression for the coefficient θ was obtained in the purely doppler approximation $\gamma_a, \gamma_b, \gamma_{ab} \ll ku$.

The analysis of expression (1) demonstrated that in the multimode regime the coefficients of the relation between the modes of the counter waves essentially depend on the intensity of the axial magnetic field applied to the active medium. It is obvious that the absolute values of θ, and, consequently, the interaction between the modes of the oppositely directed waves have maxima with halfwidth γ_{ab} on satisfaction of one of the conditions

$$\omega_0 - \Delta\omega = \frac{\nu_\mu - \nu_\sigma + 2\nu_\rho}{2}; \qquad (2)$$

$$\omega_0 + \Delta\omega = \frac{\nu_\mu - \nu_\sigma + 2\nu_\rho}{2} \qquad (3)$$

for any combination of indexes μ, σ, ρ of the generated modes.

It is obvious that the equality (2) is satisfied in two cases:

1) The magnitude of the splitting $\Delta\omega = \mu_B g H$ is such that the central frequency of the transitions with righthand circular polarization coincides with the frequency of one of the modes of the generation spectrum;

2) The magnitude of the splitting $\Delta\omega$ is such that the central frequency of the transitions with right circular polarization is in the middle of one of the intermodal intervals.

The equality (3) has analogous meaning except that $\omega_0 + \Delta\omega$ is the central frequency of the transitions with left circular polarization. However, equalities (2) and (3) cannot be satisfied if

$$\omega_0 - \Delta\omega < \nu_{\mu, \sigma, \rho, n} < \omega_0 + \Delta\omega, \qquad (4)$$

that is, in the case where the magnitude of the Zeeman splitting $2\Delta\omega = 2\mu_B g H$ is greater than the spectral width of the generated modes. On satisfaction of condition (4) the modulus $\theta_{\mu\sigma\rho n}$ is a monotonically decreasing function of the magnetic field intensity.

Thus, the results of the calculation indicate that the axial magnetic field decreases the interaction between the counter waves of the multimode annular laser only in the case where the Zeeman splitting of the contour of the application line is greater than the spectral width of the generated mode. Otherwise the interaction between the counter waves will essentially depend on the magnitude of the magnetic field and the spectral tuning of the modes, which leads to additional instability of the beat frequency of the counter waves.

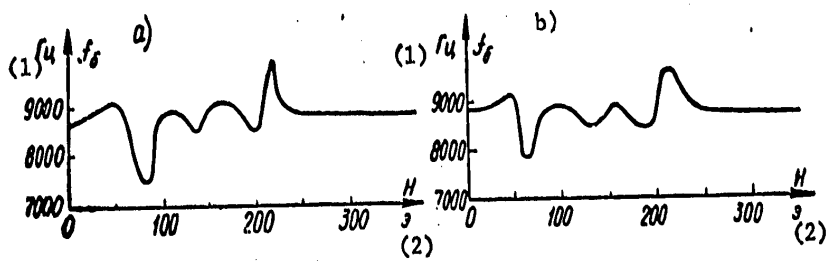

Key:
1. hertz
2. oersteds

As a supplement to reference [3], an experiment was performed permitting estimation of the effect of the axial magnetic field on the interaction of the counter waves of an annular He-Ne laser and to compare the experimental data with the calculation results. The experimental setup was exactly the same as in [3]. The annular He-Ne laser operated on a wave length of 0.63 microns in the longitudinal mode synchronization regime. The generation occurred on 6 longitudinal modes, which corresponded to a spectral width of $\Delta\nu$=800 Mhertz. The modulator was placed at the meeting point of the pulses; the modulation frequency corresponded to the center of the mode synchronization band. Measurements were taken of the beat frequency of the counter waves as a function of the magnitude of the axial magnetic field applied to the active medium. Measures were taken to eliminate the phase anisotropy in the laser resonator by the procedure of reference [6].

Graphs are presented in the figure for the beat frequency f_b of the counter waves as a function of the magnetic field intensity on the tubes. The given frequency difference of the counter waves was created by a Faraday cup, and it was 8,750 hertz. From the graph presented in Fig a it is obvious that the beat frequency of the counter waves essentially depends on the magnitude of the magnetic field to 250 oersteds. The variations of the beat frequency are explicitly of a nonmonotonic resonance nature, and they are well reproduced during repeated measurements. This is illustrated by the graph presented in Fig b. In addition, the nature of the function does not change with variation of the intensity of the field applied to the active medium: the presented graphs correspond to the opposite directions of the magnetic field on the tubes. Beginning with the value of the magnetic field of 250 oersteds, the beat frequency of the counter waves in practice does not depend on the magnitude of the magnetic field.

Thus, the axial magnetic field applied to the gas discharge tubes H>250 oersteds significantly decreases the competition of the counter waves in the annular laser with a natural mixture of neon isotopes and, as a consequence, it increases the stability of the beat frequency of the counter waves, making it less sensitive to the frequency tuning of the generated modes with respect to the amplification line than for H=0.

BIBLIOGRAPHY

1. Buholz, N.; Chodorow, M. IEEE J. OF QUANTUM ELECTRONICS, QE-3, 1967, p 454.

2. Wax, S. I.; Chodorow, M. IEEE J. OF QUANTUM ELECTRONICS, QE-8, 1972, p 343.

3. Galkin, S. L.; Nikolayev, V. M.; Okunev, R. I.; Petrun'kin, V. Yu. ZHTF [Journal of Technical Physics], No 43, 1973, p 1995.

4. Galkin, S. L.; L'vov, B. V.; Nikolayev, V. M. See the present collection, p 3.

5. Sargent, M.; Lamb, W. PHYS. REV., No 164, 1967, p 436.

6. Petrun'kin, V. Yu.; Kozhevnikov, N. M.; Nikolayev, V. M.; Okunev, R. I. ZHTF, No 43, 1973, p 1099.

STUDY OF THE CONDITIONS OF FREQUENCY SELF-SYNCHRONIZATION OF THE MODES OF A LINEAR HE-NE LASER (λ=0.63 MICRONS)

[Article by V. V. Kozlov, O. I. Kotov, B. V. L'vov, V. Yu. Petrun'kin]

[Text] It is possible to separate the operating conditions of the multimode gas laser into three groups with respect to its characteristics and its possibilities for application: 1) the free generation modes; 2) the conditions of complete self-synchronization of modes (CSS); 3) the conditions of partial self-synchronization modes (PSS).

The majority of the experimental and political papers are devoted to the study of the conditions of CSS of laser modes [1, 2]. However, as the experiments have shown, the conditions of PSS of the modes are most frequently encountered. The free generation and CSS conditions are extreme cases of the more common state of the gas laser -- the PSS [3, 4].

In this paper an experimental study was made of the conditions of PSS of longitudinal modes of a linear He-Ne laser (λ=0.63 microns) and the effect of an axial magnetic field on it.

An experimental device was used which was analogous to the one described in reference [5]. Special attention was given to the investigation of the optical spectra and the low-frequency components of the output emission.

It is known that the occurrence of the CSS is characterized by stabilization of the amplitudes of the optical spectral modes [1]. Under the PSS condition, the nature of the optical spectrum changes noticeably: the amplitudes of certain modes fluctuate, the envelope of mode amplitudes loses regularity of variation on making the transition from one mode to another. For the example of Fig 1, two characteristic optical spectra are presented.

The most characteristic attribute of the CSS is the appearance in the output emission of regular low-frequency pulsations. The spectrum of the low-frequency pulsations was investigated using a low-frequency spectral analyzer. Several spectral components with multiple frequencies have been observed (Fig 2).

The low-frequency pulsation frequency depends in complex fashion on the tuning of the mode spectrum with respect to the center of the atomic line. The experiments were performed with a natural mixture of neon isotopes and with equal-isotopic composition. In the second case, the frequency and amplitude of the low-frequency pulsations vary insignificantly on frequency tuning of the mode spectrum.

In addition, the frequency of the low-frequency pulsations depends on the magnitude of the relative excitation (the amount that the amplification exceeds the losses): the increase in relative excitation leads to a decrease in pulsation frequency.

The experiments in which the active medium of the gas laser was placed in an axial magnetic field are the most important for revealing the mechanism of PSS. It was discovered that the frequency of the low-frequency pulsations essentially depends on the magnitude of the magnetic field (see Fig 3). In the presented relation two important characteristics are isolated: 1) with an increase in the magnetic field, a general trend toward a decrease in the frequency of the low-frequency pulsations appears; 2) in the resonance values of the magnetic field $H=H_0$, $2H_0$, $3H_0\ldots$, where the splitting of the σ-components of the amplification line is equal to or a multiple of the intermode interval, the monotonic decrease of the curve is disturbed, and transition to other operating conditions of the laser are possible [5].

Figure 1

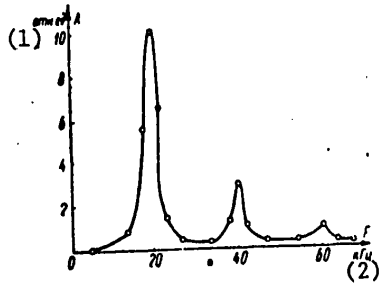

Figure 2

Key:
1. Relative units
2. Kilohertz

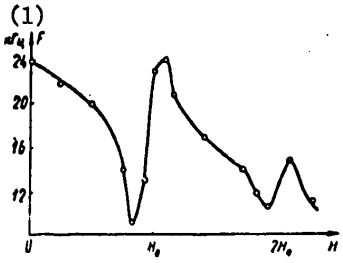

Figure 3

Key:
1. Kilohertz

According to the results of reference [4], the complete self-synchronization mode occurs on satisfaction of the inequality $\sigma^2<A^2+B^2$, where σ describes the frequency pulling and exclusion effects, and A and B are the phase-dependent effects of cross saturation of the modes and the combination tones.

The opposite inequality, on the basis of the great nonlinearity of the dispersion curve ($\sigma\neq0$) or the insufficient magnitude of the amplitudes of the combination tones leads to the appearance of a non-zero difference in magnitudes of the different intermodal intervals, and it causes establishment of the partial self-synchronization. The differences in magnitudes of the intermodal intervals determine the frequency of the low-frequency pulsations. In turn, the magnitudes of the intermodal interval depend on the pulling and exclusion effects of the modes influencing the dispersion curve of the active material.

The tuning of the mode spectrum with respect to the center of the atomic line of neon, the variation in magnitude of the relative excitation cause variation of the mode exclusion effects and, consequently, the curvature of the dispersion curve [3]. Thus, an increase in relative excitation, as a rule, improves the linearity of the dispersion curve, which leads to a decrease in frequency of the low-frequency pulsations.

The experiments with respect to investigating the optical spectrum of the gas laser with windows at the Brewster angle, the active medium of which is placed in an axial magnetic field demonstrated that with an increase in the magnetic field, the apex of the amplification line will become flatter and, consequently, the dispersion curve will become more linear. Under PSS conditions, this, of course, leads to a reduction in the frequency of the low-frequency pulsations with an increase in the magnetic field. In the resonance values of the magnetic field [5] as a result of the nonlinear relation of the σ-components leading to intensification of the relation between axial modes, the mode exclusion effects vary intensely. The latter fact is also one of the causes of the appearance of resonance self-synchronization [5] and also disturbance of the monotonicity of the frequency variation of the low-frequency pulsations (Fig 3).

The phenomena of partial self-synchronization are observed clearly and stably in a large range of variation of the laser parameters in the case of relatively short lasers (the resonator length is less than 70 cm). In the lasers with long optical resonators, the partial self-synchronization "belts" the complete self-synchronization zone [5]. As a rule, the transitions from the free generation mode to the complete self-synchronization or the inverse occur through the conditions of partial self-synchronization of the modes.

BIBLIOGRAPHY

1. Smith, P. W. IEEE J. OF QUANTUM ELECTRONICS, QE-3, 1967, p 627.

2. Zeyger, S. G. OPTIKA I SPEKTROSKOPIYA [Optics and Spectroscopy], No 34, 1973, p 133.

3. Uchida, T.; Ueki, A. IEEE J. OF QUANTUM ELECTRONICS, QE-3, 1967, p 17.

4. Lamb, W. E. PHYS. REV., No 134, 1964, p 1429.

5. Petrun'kin, V. Yu.; Nikolayev, V. M.; Kotov, O. I.; L'vov, B. V. ZHTF [Journal of Technical Physics], No 44, 1974, p 2598.

BEAT FREQUENCY OF THE COUNTER WAVES IN AN ANNULAR LASER AS A FUNCTION OF THE GENERATION FREQUENCY (λ=0.63 MICRONS) CONSIDERING BACKSCATTERING

[Article by V. M. Nikolayev, R. I. Okunev, V. Yu. Petrun'kin]

[Text] The lock-on of the counter wave frequencies in an annular laser occurs basically as a result of back reflections from the optical elements of the resonator and the interaction of the waves on intensification of them by the common groups of atoms of the active medium [1-3]. Accordingly, it is of interest to investigate the effect of the scattering on the frequency of the counter waves and their dependence on the position of the generation frequency on the amplification line for the active media with equal isotopic composition. Usually the scattering is characterized by the value of $|r_i| \exp(j\varepsilon_i)$, where ε_i determines the phase of the corresponding scattered wave i=1, 2, and $|r_i|$ determines the amplitude. The scattering coefficients themselves r_i are calculated as the sum of the scattering coefficients of the individual elements of the resonator considering the phase drifts. We shall consider that the values of $|r_i|$, ε_i are defined; then the effect of backscattering on the beat frequency of the counter waves in the annular laser can be taken into account in the following way.

Considering the relation between the counter waves linear and assuming the unimodal operation of generation of the annular laser, the amplitude and frequency equations for the counter waves with mixed isotopic composition of the active medium can be described in the form of [4], adding the terms describing the backscattering to them

$$\dot{E}_1 + \frac{1}{2}\left(\frac{\omega}{Q}\right)E_1 = -\frac{A\varepsilon^{1/2}}{2}\left(\frac{\omega}{\varepsilon_0}\right)E_1\left\{f\left[\frac{Z_1\xi_1}{Z_1(0)} - I_1\exp(-\xi_1^2) - I_2\exp(-\xi_2^2)L(\xi)\right] + f'\left[\frac{Z_1\xi_1'}{Z_1(0)} - I_1\exp(-\xi_1'^2) - I_2\exp(-\xi_2'^2)L(\xi')\right] - \sqrt{\frac{I_2}{I_1}}|r_1|\sin\left(\frac{\omega}{c}\ldots - \varepsilon_1\right)\right\}; \quad (1)$$

$$E_1 + \frac{1}{2}\left(\frac{\omega}{Q}\right)\dot{E}_1 =$$

$$= \frac{A\pi^{1/2}}{2}\left(\frac{\omega}{\omega_0}\right)E_1\left\{f\left[\frac{Z_1(\xi_1)}{Z_1(0)} - I_2\exp(-\xi_2^2) - I_1\exp(-\xi_1^2)L(\xi)\right] + \right.$$

$$+ f'\left[\frac{Z_1(\xi_2')}{Z_1(0)} - I_2\exp(-\xi_2') - I_1\exp(-\xi_1')L(\xi')\right] +$$

$$\left. + \sqrt{\frac{I_1}{I_2}}|r_2|\sin(\psi + \varepsilon_2)\right\}; \qquad (2)$$

$$\omega_1 + \dot{\Phi}_1 - \Omega_1 = \frac{A}{2}\left(\frac{\omega}{\omega_0}\right)\left\{f\left[Z_r(\xi_1) + I_2 Z_1(\xi_2)\frac{\xi}{\eta}L(\xi)\right] + \right.$$

$$\left. + f'\left[Z_r(\xi_1') + I_2\frac{\xi'}{\eta}Z_1(\xi_2')L(\xi')\right] - \sqrt{\frac{I_2}{I_1}}|r_1|\cos(\psi - \varepsilon_1)\right\}; \qquad (3)$$

$$\omega_2 + \dot{\Phi}_2 - \Omega_2 = \frac{A}{2}\left(\frac{\omega}{\omega_0}\right)\left\{f\left[Z_r(\xi_2) + I_1\frac{\xi}{\eta}Z_1(\xi_1)L(\xi)\right] + \right.$$

$$\left. + f'\left[Z_r(\xi_2') + I_1\frac{\xi'}{\eta}Z_1(\xi_1')L(\xi')\right] - \sqrt{\frac{I_1}{I_2}}|r_2|\cos(\psi + \varepsilon_2)\right\}, \qquad (4)$$

where $\xi_{1,2} = \frac{\omega_{1,2} - \omega_0}{k\omega}$ is the reduced frequency difference of the wave generation with respect to the transition frequency of the Ne^{20} isotopes; $\xi'_{1,2}$ are the analogous values taken only with respect to the transition of the Ne^{22} isotope; f is the proportion of the Ne^{20} isotope in the active medium; $f' = \left(\frac{m'}{m}\right)^{1/2}(1-f)$; m, m' are the masses of the atoms of the Ne^{20} and Ne^{22} isotopes respectively; $I_{1,2} = \frac{|\mu_{a,b}|\mathcal{E}_{1,2}}{2\hbar\gamma_a\gamma_b}$ are the dimensionless intensities of the counter waves. The values of relative variables entering into equation (1)-(4) correspond to [4, 5].

The solution of the nonlinear differential equations (1)-(4) presents defined difficulties. However, in this paper we are interested in the beat frequency of the counter waves $\Delta\omega = d\psi/dt$ (averaging with respect to some measurement time interval) in the stationary mode. Therefore it is sufficient to find the solution of system (1)-(4) only for the stationary case. It must be noted that in the equations there are terms which depend on time. Accordingly, we shall find the solution of the system by the quasistationary ($\dot{E}_1 \approx \dot{E}_2 \approx 0$) method: considering that $E_{1,2}$ fluctuate under these conditions with low amplitudes (on the order of $|r_{1,2}|$) about their stationary values with the beat period of the counter waves significantly exceeding the time of establishment of the stationary amplitudes ($\sim Q/\omega$). In practice this is realized with greater precision, for the difference between them is several orders. In addition, we shall consider the cases of operation of an annular laser most frequently encountered in practice: a) far from the lock-on range of the counter wave frequencies ($\Delta\Omega$ -- the frequency difference of the resonator for the counter waves is sufficiently large); b) the generation frequency does not coincide with the transition frequency for the single-isotopic composition of the active medium.

After the remarks that have been made, let us solve the equation (1)-(2) with respect to I_1, I_2, considering $\dot{E}_1=\dot{E}_2=0$. Substituting the values found in (3-4) and taking their difference, let us define $\omega_1-\omega_2=d\psi/t$ in terms of the ratio of the intensities of the counter waves (in this expression it is also assumed that $\phi_1=\phi_2=0$, which does not limit the generality of the results obtained)

$$\omega_1-\omega_2=\Delta\Omega_0+\frac{A}{2}\left(\frac{\omega}{t_0}\right)\left\{|r_1|\sqrt{\frac{I_2}{I_1}}[2\pi^{1/2}R(\xi,\xi')\sin(\psi-\varepsilon_1)-\right.$$
$$\left.-\cos(\psi-\varepsilon_1)]+|r_2|\sqrt{\frac{I_1}{I_2}}[2\pi^{1/2}R(\xi,\xi')\sin(\psi+\varepsilon_2)+\cos(\psi+\varepsilon_2)]\right\}, \quad (5)$$

where

$$\Delta\Omega_0=\Delta\Omega[1-f\Phi(\xi)-f'\Phi(\xi')]+R(\xi,\xi')\frac{\omega}{2}\left(\frac{1}{Q_1}-\frac{1}{Q_2}\right),$$

$\Delta\Omega=\Omega_1-\Omega_2$ is the frequency difference of the resonator for the counter waves,

$$\Phi(\xi)=\frac{A}{ku}\left(\frac{\omega}{t_0}\right)\exp(-\xi^2)\left[1+2\xi^2-2\xi\int_0^{\xi}\exp(x^2)dx\right],$$

$\phi(\xi')$ is the analogous function except ξ is replaced by ξ', $Q_{1,2}$ is the Q-factor of the resonator for the counter waves, $\xi=\frac{\xi_1+\xi_2}{2}$, ξ' is the analogous value;

$$R(\xi,\xi')=\frac{f\exp(-\xi^2)\frac{\xi}{\eta}L(\xi)+f'\exp(-\xi'^2)\frac{\xi'}{\eta}L(\xi')}{f\exp(-\xi^2)\left(\frac{\xi}{\eta}\right)^2L(\xi)+f'\exp(-\xi'^2)\left(\frac{\xi'}{\eta}\right)^2L(\xi')};$$

$$L(\xi)=\left[1+\left(\frac{\xi}{\eta}\right)^2\right]^{-1};$$

$L(\xi')$ is the analogous value, $\eta=\gamma_{ab}/ku$.

In order to determine ψ in the first approximation with respect to small values of $|r_{1,2}|$, let us substitute the value of ψ in the zero approximation in the righthand side of equation (5) $\psi_0=\Delta\Omega_0 t$ and, integrating it with respect to time under the condition

$$\left(\frac{I_1}{I_2}\right)^{1/2}\approx\left(\frac{I_2}{I_1}\right)^{1/2}\simeq 1,$$

we find

$$\psi_1 = \Delta\Omega_0 t + \frac{A}{2\Delta\Omega_0}\left(\frac{\omega}{t_0}\right)\{-2\pi^{1/2}R(\xi,\xi')\{|r_1|\cos(\psi_0-\varepsilon_1)+ \\ +|r_2|\cos(\psi_0+\varepsilon_2)\}+|r_2|\sin(\psi+\varepsilon_2)-|r_1|\sin(\psi_0-\varepsilon_1)\}+\text{const.} \quad (6)$$

Substituting (6) in the righthand side of equation (5) and the intensity ratios $(I_1/I_2)^{1/2}$, $(I_2/I_1)^{1/2}$ found from equations (1)-(2), in the first approximation with respect to $|r_{1,2}|$ we calculate the "instantaneous" beat frequency of the counter waves in the second approximation

$$\frac{d\psi_1}{dt} = \Delta\Omega_0 + \frac{A}{2\Delta\Omega_0}\left(\frac{\omega}{t_0}\right)\left\{2\pi^{1/2}R(\xi,\xi')\{|r_2|\sin(\psi_1+\varepsilon_2)+|r_1|\sin(\psi_1-\varepsilon_1)\}+ \right. \\ +|r_2|\cos(\psi_1+\varepsilon_2)-|r_1|\cos(\psi_1-\varepsilon_1)\}+ \\ +B\{2\pi^{1/2}R(\xi,\xi')\{|r_1|^2\sin^2(\psi_1-\varepsilon_1)-|r_2|^2\sin^2(\psi_1+\varepsilon_2)\}- \\ \left.-\frac{|r_1|^2}{2}\sin 2(\psi_1-\varepsilon_1)-\frac{|r_2|^2}{2}\sin 2(\psi_1+\varepsilon_2)-|r_1||r_2|\sin(2\psi_1+\varepsilon_2-\varepsilon_1)\}\right\}. \quad (7)$$

Here

$$B = \frac{f\exp(-\xi^2)\{1+L(\xi)\}+f'\exp(-\xi'^2)\{1+L(\xi')\}}{\{f\exp(-\xi^2)\{1-L(\xi)\}+f'\exp(-\xi'^2)\{1-L(\xi')\}\}H(\xi,\xi')},$$

$$H(\xi,\xi') = f\exp(-\xi^2)+f'\exp(-\xi'^2)-\varepsilon_0(\pi^{1/2}AQ)^{-1}.$$

The measured beat frequency of the counter waves $\Delta\omega$ in the second approximation will be equal to the mean value found (7) in the measurement time interval, that is

$$\Delta\omega \simeq \Delta\Omega_0 - \frac{1}{2\Delta\Omega_0}\left[\frac{A}{2}\left(\frac{\omega}{t_0}\right)\right]^2\{|r_1|^2+|r_2|^2-2|r_1||r_2|\cos(\varepsilon_1+\varepsilon_2)- \\ -4\pi R^2(\xi,\xi')\{|r_1|^2+|r_2|^2+2|r_1||r_2|\cos(\varepsilon_1+\varepsilon_2)\}+ \\ +\frac{A\omega\pi^{1/2}}{2t_0}R(\xi,\xi')B(|r_1|^2-|r_2|^2). \quad (8)$$

The approximate equality sign (8) means that the averaging was carried out considering smallness of the values of $|r_{1,2}|$. The terms containing $|r_{1,2}|$ to a power higher than the second are omitted.

For the single-isotopic composition of the active medium ($f=1$, $f'=0$) formula (8) is simplified and assumes the following form:[1]

[1]The analogous formula was obtained in reference [6].

$$\Delta\omega \approx \Delta\Omega_0 - \frac{1}{2\Delta\Omega_0}\left(\frac{A\omega}{2i_0}\right)^2\left\{|r_1|^2+|r_2|^2-2|r_1||r_2|\cos(\varepsilon_1+\varepsilon_2)-\right.$$
$$-4\pi^{1/2}\frac{\nu_1}{\xi}|r_1||r_2|\sin(\varepsilon_1+\varepsilon_2)+4\pi\left(\frac{\nu_1}{\xi}\right)^2\left[|r_1|^2+|r_2|^2+\right.$$
$$\left.\left.+2|r_1||r_2|\cos(\varepsilon_1+\varepsilon_2)\right]\right\}+\frac{A\omega\pi^{1/2}\nu_1}{2i_0\xi}\frac{1+L(\xi)}{[1-L(\xi)]\,\Pi(\xi)}(|r_1|^2-|r_2|^2), \quad (9)$$

where

$$\Delta\Omega_0 = \Delta\Omega\,[1-\Phi(\xi)]+\frac{\omega\nu_1}{2\xi}\left(\frac{1}{Q_1}-\frac{1}{Q_2}\right).$$

From expression(9) it is obvious that the presence of backscattering always decreases the beat frequency of the counter waves, at the same time permitting lock-on of the generation frequencies. The case of complex-conjugate values of r_1 and r_2 for which the effect of the reflections on the beat frequency is significantly attenuated constitutes an exception. The effect of the backscattering can also be diminished if we increase the frequency difference of the resonator $\Delta\Omega$ for the counter waves.

A comparison of formulas (8), (9) indicates that the dependence of the beat frequency of the counter waves on the generation frequency is determined to a great extent by the isotopic composition of the active medium. This is also confirmed by the curves for the frequency of the counter waves in the annular laser as a function of the generation frequency for different values of the moduli of the reflection coefficient calculated on the computer, by formula (8) for the natural f=0.92 (Fig 1) and equal-isotopic f=0.50 (Fig 2) mixture of active medium. The values of the remaining parameters were assumed equal to the following values: $Q_1=Q_2$, $|r_1|=|r_2|=|r|$, $\omega=2\pi\cdot5\cdot10^{14}$ hertz, $ku=2\pi\cdot1.5\cdot10^9$ hertz, $\Delta\Omega=2\pi\cdot10^4$ hertz, $\eta=0.08$.

Graphs are presented in Figures 3 and 4 for the relations taken on the device described in [7]. A comparison of the calculated and experimental curves indicates that they agree well.

On the basis of the discussed results of the investigation it is possible to draw the conclusion that for equal-isotopic composition of the active medium the beat frequency of the counter waves varies less from the generation frequency tuning than for the natural mixture of neon isotopes. Decreasing the reflection coefficient straightens out the curve of this function.

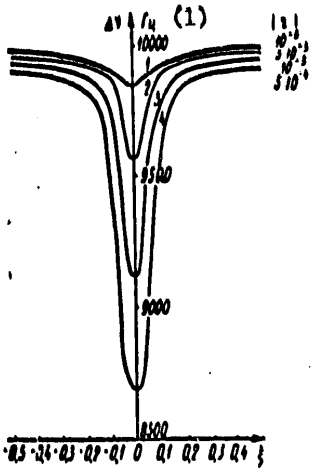

Figure 1

Key:
1. hertz

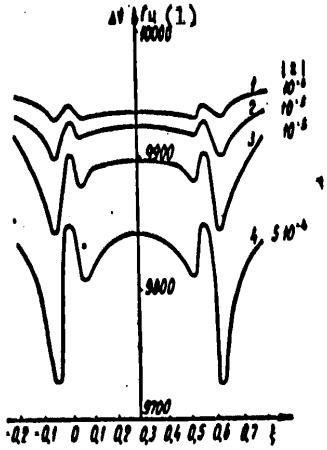

Figure 2

Key:
1. hertz

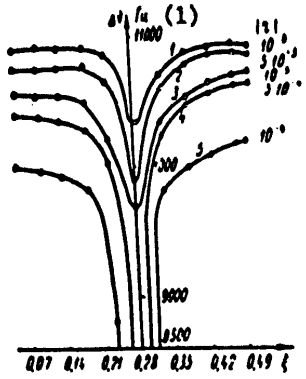

Figure 3

Key:
1. hertz

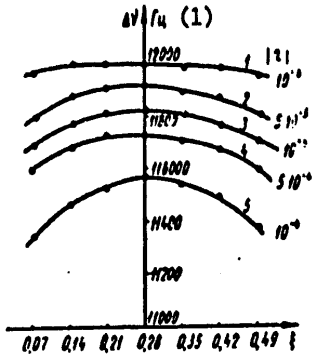

Figure 4

Key:
1. hertz

BIBLIOGRAPHY

1. Klimontovich, Yu. L.; Kuryatov, V. N.; Landa, P. S. ZHETF [Journal of Experimental and Theoretical Physics], No 51, 1966, p 3.

2. Kruglik, G. S. PRIKLADNAYA SPEKTROSKOPIYA [Applied Spectroscopy], No 7, 1967, p 569.

3. Klimontovich, Yu. L.; Landa, P. S.; Lariontsev, Ye. G. ZHETF, No 52, 1967, p 1616.

4. Aronowitz, F. PHYS. REV., No 139, 1965, p 635.

5. Galkin, S. L.; L'vov, B. V.; Nikolayev, V. M. See this collection, p 3.

6. Landa, P. S.; Lariontsev, Ye. G. RADIOTEKHNIKA I ELEKTRONIKA [Radioengineering and Electronics], No 15, 1970, p 1215.

7. Vysotskiy, M. G.; Nikolayev, V. M.; Okunev, R. I.; Petrun'kin, V. Yu. ZHTF [Journal of Technical Physics], No 43, 1973, p 881.

STABILIZATION OF THE RADIATION FREQUENCY OF AN ANNULAR HE-NE LASER

[Article by V. N. Arzumanov, G. F. Zaytsev]

[Text] In the modern radiation frequency stabilization systems of gas lasers broad use has been made of the methods connected with using the power resonances both in the generator itself and in various types of external absorbing cells. The majority of the developed stabilization procedures can also be used in annular lassers, but along with them the narrow radiation power peaks in them can be obtained as a result of the effect of competition of counter waves at the center of the amplification line of the active medium [1]. The basic results of investigating the possibility of stabilization of the radiation frequency of an annular laser using the effect of the interaction of counter waves are presented in this report.

In the first phase of this work a study is made of the conditions of obtaining the power peaks of the output radiation in an annular laser on a wavelength of 0.6328 microns. The two gas discharge tubes 4, 5 of the OKG-16 type laser with a natural mixture of Ne^{20} and Ne^{22} isotopes placed in solenoids, the mirrors 1-3 and the phase plate 6 form an anisotropic 3-mirror resonator with a 75 cm perimeter.

As is known [2], the anomalous dispersion of the active medium in the presence of an axial magnetic field leads to nonmutual Faraday rotation of the polarization plane of two counter running waves. The phase plate placed in the resonator is arranged at an angle which compensates the rotation of the polarization plane of one of the waves and increases it for the other. The presence in the laser resonator of Brewster windows leads to amplitude anisotropy as a result of the loss difference between the two counter waves and suppression of one of them (for the corresponding increase in radiation power of the other) at the center of the amplification line of the active medium where the competition phenomenon is expressed most sharply. Here, narrow peaks (see Fig 2a) appear in the shape of the output radiation curve of each of the waves, the width of which is determined by the resonator parameters and the active medium, and it can be regulated by variation of the magnetic field created by the solenoids. For weak fields (in the described experiment less than 50 oersteds), the widths of the peaks diminished with an increase in the field, and it

reached a value of 10 to 20 megahertz with respect to the halfheight from the maximum level. Further constriction of the power peaks was noted by the distortions caused by the appearance of peaks between the waves, for high intensities of the magnetic field. This phenomenon is connected with the phase anisotropy of the resonator caused by the Faraday effect in the active medium. However, for weak fields as a result of scattering of the light on the optical surfaces and dust particles, the frequencies of the counter waves are mutually synchronized. With an increase in the synchronization field intensity, each of the waves generates on a frequency determined by the optical length of the resonator for this wave.

The threshold value of the field causing loss of synchronization is the detuning function and has a maximum at the center of the amplification line of the active medium.

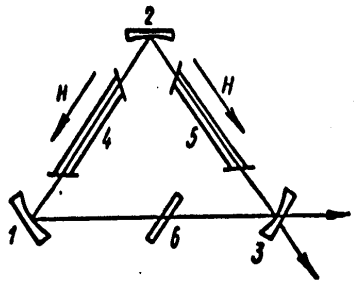

Figure 1

Figure 2

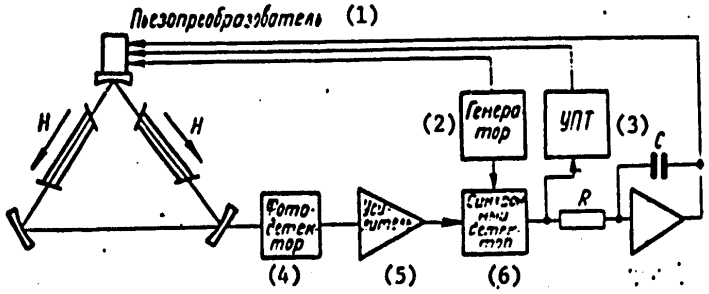

Figure 3

Key:

1. piezoconverter
2. generator
3. DC amplifier
4. Photodetector
5. Amplified
6. Synchronous detector

In itself, the absence of synchronization of the counter waves must not have a significant effect on the shape of the peak, but as a result of the mentioned dispersion of the light, in addition to the basic waves, part of the reflected second wave is incident on the photodetector. The beats between the waves occurring here can significantly distort the shape of the output radiation curve (Fig 2, b). Let us note that even for a field which is close to threshold, undesirable deformation of the shape of the peak is observed. Accordingly, magnitude of the magnetic field intensity for the existence of the frequency stabilization was selected within the limits of 40 to 50 oersteds. Here a peak width of less than 10 megahertz could not be obtained in the performed experiment.

The experimental setup of the frequency stabilization system of the annular laser is presented in Fig 3. In order to lower the losses and the number of scattering surfaces, the phase plate was not installed in the resonator. Its role was played by the Brewster window of the gas-discharge tubes in which twin beam refraction is observed caused by residual stresses in the glass [3]. Even weak rotation of one of the tubes around the longitudinal axis causes high amplitudinal anisotropy in the resonator. The conditions of obtaining power peaks and their shape did not differ significantly in this case from those investigated above.

In order to realize stabilization, the output emission of the laser was frequency modulated and sent to the photoreceiver of the automatic frequency control system. The latter contains two automatic control loops, the first with small time constants is designed for compensation for comparatively fast frequency fluctuations, and the second, for selecting slow drifts. The circuitry of the second loop includes an integrator which is executed on the basis of the K1UT401B integrated circuit. The tuning was realized with respect to the maximum of the radiation output power peak. The long-term frequency stability obtained in the experiments (in 60 minutes) was no worse than 10^{-9} in this case.

BIBLIOGRAPHY

1. Lisitsyn, V. N.; Troshin, B. I. OPTIKA I SPEKTROSKOPIYA [Optics and Spectroscopy], No 22, 1967, p 666.

2. Burrell, G. J.; Hetherington, A.; Moss, M. S. J. PHYS., No B1, 1968, p 692.

3. Malacora, D.; Morales, A.; Rizo, I. APPLIED OPTICS, No 10, 1971, p 1984.

EFFECT OF GAS PRESSURE ON THE INTERACTION OF THE POLARIZATION MODES IN A LASER ON THE 3.39 MICRON LINE

[Article by Ye. Yu. Andreyeva, Ye. N. Zhmin'ko, D. K. Terekhin, S. A. Fridrikhov]

[Text] Increasing the pressure of the gas mixture can significantly affect the polarization and frequency characteristics of the laser in a magnetic field [1-4].

In this paper a report is given on the results of the experiments to study the effect of pressure on the relation between the polarization modes of the laser in a wide range of magnetic fields. The choice of the transition with a wavelength of λ=3.39 microns is explained by the fact that the pressure has a significant effect on the nature of the broadening. According to [5], the uniform line width γ_{ab}=25 megahertz+30·p megahertz/torr at the same time as the doppler width k_u~180 megahertz.

The single-frequency laser was a discharge tube 3 mm in diameter and 210 mm long sealed by windows perpendicular to the axis and placed in a solenoid, and the resonator of the plane-sphere type with spacing between the axial modes of 500 megahertz. The transverse modes were selected by the diaphragm. The length of the resonator was varied using piezoceramics fastened to the flange of a spherical mirror.. The emission with σ^+ or σ^- polarization was isolated using the $\lambda/4$ plate and polarizer. The application of the S1-29 storing oscillograph made it possible with continuous frequency scanning of the resonator simultaneously to obtain oscillograms of the intensities of σ^+ and σ^- polarization modes I_+, I_- and to observe their variation as a function of the resonator detuning and magnitude of the magnetic field. In order to exclude the effect of the isotopic composition of the mixture on the shape of the amplification line, the Ne^{20} isotope was used for the measurements.

As is obvious from the oscillograms presented in Fig 1, in the magnetic field both the functions $I_{+,-}(\nu)$ (Fig 1, a, b, c) are distorted, and the function $I_\Sigma(\nu)$ (Fig 1, d), where $I_\Sigma=I_+ +I_-$. The "chips" or distortions on the curves $I_{-,-}(\nu)$ lead to constriction of the region of simultaneous generation of the σ-modes. Similar phenomenona were observed in [6] for a pressure of 2 torr, and they were explained by the authors as competition or a strong relation between the polarization modes on the transition with λ=3.39 microns.

However, from [7, 8] it is known that even for a weak relation between the modes C, the generation on both modes of the resonator exists if the effective unsaturated amplification coefficient $\alpha'_{\pm}>0$, where $\left(\frac{\pm\theta}{\pm\mp\theta}\right)$.

Here the coefficients β and θ characterize the saturation of each mode by its field and the field of the strange mode respectively [7]. The oscillograms that we obtained analogous to those presented in Fig 1 made it possible directly to determine the magnitude of the coupling coefficient $C=\frac{\theta_{+-}\theta_{-+}}{\beta_{-}\beta_{-}}$ for the central tuning with various intensities of the magnetic field H and different pressures p. Let us consider the procedure for processing the experimental data. According to [7] for weak coupling C<1 the intensities of the polarization modes with central tuning of the resonator $I_+=I_-=I=\frac{\alpha}{\beta}\frac{1}{1+\sqrt{C}}$;

$$C=\left[\frac{\alpha/\beta}{I}-1\right]^2.$$

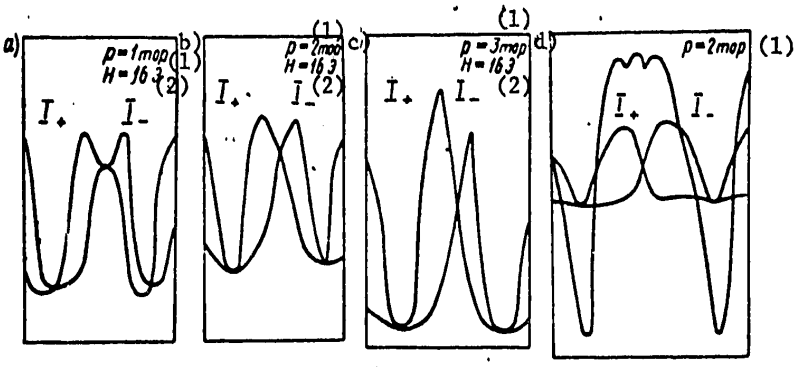

Figure 1

Key:
1. torr
2. oersteds

Here the value of α/β determines the intensity of the single-frequency generation. For the λ=3.39 microns line where the Lamb trough is weakly expressed even for low pressures (see Fig 1), the approximation $\beta\sim1$ is admissible. The intensity I was determined from the oscillograms, and the unsaturated amplification α on a frequency of $\nu=\nu_0$ was calculated for the doppler curve as a function of its shift equal to $g\mu H$ (g=1.1).

The data obtained on the functions C(H) make it possible to draw the conclusion that increasing the pressure leads to an increase in the coupling coefficient, but the coupling on the 3.39 micron line remains weak. For comparison of the experimental values of C with the theoretical values, a calculation was made of C(H) by the formulas presented in [7]

for a pressure of 1 torr with central tuning of the resonator. The calculated and experimental values of C are as follows:

H, oersteds	16	26	32	36	46
C_{exp}	0.065	0.06	0.061	0.056	0.04
C_{calc}	0.08	0.063	0.059	0.055	0.052

From the presented data it is obvious that the calculated values of the magnitudes of the coupling compare well with the experimental values. This serves as confirmation of the fact that the proposed procedure can be used to determine the magnitude of the coupling coefficient in any case in the investigated magnetic field range. A quantitative comparison of theory with experiment was made only for low pressure inasmuch as the theory of [7] was created in the approximation of strong doppler broadening of the amplification line ($\gamma_{ab} \ll ku$), and for the line λ=3.39 microns, the increase in pressure disturbs this condition [3, 5].

The investigation of the relation between the polarization mode of the laser includes not only the problem of the interaction of split modes of the resonator, but also the problem of the interaction of the axial modes generating on the well-separated Zeeman components of the amplification line. When the Zeeman splitting $\Delta\nu_3$ is a multiple of the distance between the modes Δ, according to the theory [7], the relation between modes increases, and in the relation for the total intensity as a function of the magnetic field I_Σ (H) troughs must appear. The ratios of the maximum intensities of the modes I_1/I_2 on variation of the magnetic field are presented in Fig 2. For $\Delta\nu_3 \sim 1/2\Delta$ and $\Delta\nu_3 \sim \Delta$, when H is on the order of 170 and 340 oersteds, respectively, the value of I_1/I_2 decreases significantly. The depth of the troughs increases with an increase in pressure, which indicates an increase in the coupling between the modes in these regions. A decrease in I_1/I_2 is also accompanied by troughs in the functions I_Σ (H). The small difference in intensities I_1 and I_2 observed for all pressures in the entire range of magnetic field is obviously connected with the non-isotropicity of the pumping on the Zeeman sublevels or with the difference in circular anisotropy of the resonator [1].

Thus, from the presented experimental results it is obvious that increasing the pressure has qualitatively the same effect on the interaction of the σ-modes of the laser both in small and in large magnetic fields.

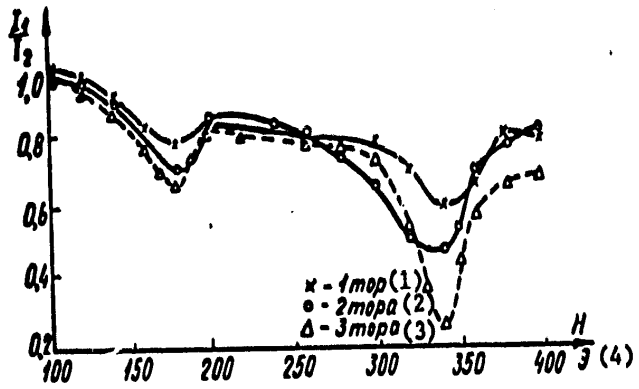

Figure 2

Key:
1. 1 torr
2. 2 torr
3. 3 torr
4. oersteds

BIBLIOGRAPHY

1. Fork, R. L.; Tomlinson, W. J. PHYS. REV., No 164, 1967, p 466.

2. Fork, R. L.; Tomlinson, W. J.; Heilos, L. J. PHYS REV., No 8, 1966, p 162.

3. Andreyeva, Ye. Yu.; Gulyayev, S. N.; Terekhin, D. K. OPTIKA I SPEKTROSKOPIYA [Optics and Spectroscopy], No 2, 1974.

4. Andreyeva, Ye. Yu.; Terekhin, D. K.; Fridrikhov, S. A. TRUDY LPI [Works of the Leningrad Polytechnical Institute], No 328, Izd. Leningr. Politekhn. in-ta imeni M. I. Kalinina, 1973.

5. Mensies, R. T. PHYS. LETT., No 43A, 1973, p 3.

6. Ladygin, M. V.; Tsar'kov, V. A. OPTIKA I SPEKTROSKOPIYA, No 30, 1971.

7. Sargent, M.; Lamb, W. E.; Fork, R. L. PHYS. REV., No 164, 1967, p 450.

8. Lamb, W. E. PHYS. REV., No 134, 1964, p 1229.

STABILIZATION OF THE FREQUENCY SPECTRUM OF A CONTINUOUS Ar^+ LASER BY A LONGITUDINAL MAGNETIC FIELD

[Article by A. E. Fotiadi]

[Text] It is well known [1-6] that the frequency spectrum of the radiation of an Ar^+ laser has a number of specific peculiarities connected with the great width of the radiation line of the argon ions. Basically these peculiarities reduce to the following.

1. For the average excitation levels, the spectrum of the Ar^+ laser is stable and is characterized by an increase in the interval between the general frequencies which amounts to several frequency intervals of the resonator c/2L.

2. The spectrum of the ion laser is extremely unstable for the excitation level exceeding some physical value. Generation occurs randomly on all of the resonance frequencies of the resonator.

3. As a rule, the axial magnetic field shifts the upper bound of the region of stable generation in the direction of larger excitation levels. The broadening of the stable generation range on application of the longitudinal magnetic field was connected with broadening of the uniform line [6, 7] and with general broadening of the contour of the radiation line [7].

In this paper a study was made of the spectrum of the longitudinal types of oscillations of the continuous Ar^+ laser (λ=4880 A) as a function of the discharge current and the intensity of the longitudinal magnetic field. In this paper a study was made of the frequency spectrum of lasers of two types: with internal mirrors and with Brewster windows. The length of the discharge tubes and the resonator in both lasers was identical; c/2L=240 megahertz. Just as in the papers by other authors, the spectrum of the longitudinal types of oscillations of both types of lasers was stable until the radiation intensity exceeded a defined value. As soon as it exceeds this critical value, the spectrum will immediately become unstable and will contain a large number of fluctuating modes. The longitudinal magnetic field has a different effect on the frequency spectrum of the

laser emission with internal mirrors and with Brewster windows. The series of oscillograms of the radiation spectrum of the laser with internal mirrors is presented in Fig 1 for various values of the magnetic field intensity. As is obvious from this figure, the spectrum remains invariant to fields of approximately 150 oersteds (see Fig 1, b).

With an increase in the magnetic field intensity, the spectrum varies discontinuously (Fig 1, c): the frequency distance between the two generating modes is 480 megahertz (2c/2L). Here the frequency distance between the centers of the Zeeman σ-contours is 560 megahertz. A further increase in the field led to an increase proportionally to the magnetic field of the distance between the generating modes (Fig 1, d). The analysis of the radiation polarization using the λ/4 plate demonstrated that each mode corresponds to its Zeeman σ-component. It must be noted that when obtaining these oscillograms, the intensity of the emission was maintained approximately on the same level (using the discharge current). This was a forced measure inasmuch as for a magnetic field intensity of more than 160 oersteds, a sharp increase in intensity of the laser emission with the field started, which led to instability of the frequency spectrum. The maximum intensity for which a stable radiation spectrum was maintained for the laser with internal mirrors, in the absence of the magnetic field exceeded the critical intensity in the absence of the field by a total of 15%.

Another picture was observed in a laser with Brewster windows. Fig 2 shows a series of oscillograms obtained for this type of laser for various values of the magnetic field intensity. As is obvious from the figure, the radiation spectrum of the laser did not change to a field with an intensity of 360 oersteds (Fig 2, a, b). For a field intensity of 360 oersteds two stable modes appeared in the spectrum. The intensity of the laser radiation increased in this case by 4 times. These two modes were retained in the generation on variation of the field to 600 oersteds. The spacing between them did not change, it remained constant, and the radiation increased by 1.5 times (Fig 2, d). For a field intensity of 600 oersteds, a spectrum discontinuously transfers to multimode, nonstable, although it has two characteristic frequencies (Fig 2, e). Finally, for a field intensity of 800 oersteds the spectrum becomes stable, and the generation occurs on the individual σ-components. With a further increase in the field, the spacing between these modes increases proportionally to the field (Fig 2, f).

Thus, it is possible to draw the conclusion that basically it is not simply the superposition of the longitudinal magnetic field in itself that leads to increased stabilization of the radiation spectrum of the Ar^+ laser, but the presence of a window at the Brewster angle in the laser resonator. Apparently, the presence of a window at the Brewster angle in the laser resonator intensifies the competition of the longitudinal types of oscillations. Actually, the losses introduced by the Brewster window are different for circular Zeeman components and the overlap zone of them inasmuch as the radiation polarization in the overlap zone of the contours

is linear. The growth of the population inversion in the magnetic field leads to an increase in the overlap zone, and the modes located in it have lower losses than the modes outside this zone. Inasmuch as the overlap zone of the σ-contours is more constricted than the entire amplification circuit, the competition occurs between a smaller number of modes, and therefore generation is possible on one or two stable frequencies. On achievement of this inversion when the amplification on each circular σ-component is greater than the losses determined by the Brewster window, the spectrum becomes unstable (the generation jumps from individual σ-components to their overlap zone and back). Finally, for a field intensity where the amount that the amplification exceeds the losses in the overlap zone is less than the amount that the amplification in each circular σ-loop exceeds the losses in the Brewster resonator, generation again becomes stable, and each mode generates on its own σ-circuit. With an increase in the pumping power so much that the amplification coefficient on each individual σ-component is so large that generation is possible on several modes in each circular component, generation again will be characterized by a nonstable spectrum for all values of H. This was actually observed in the experiment. Thus, in the present paper it was discovered that through a stabilization of the spectrum of the Ar^+ laser in a longitudinal magnetic field is caused not by magnetic field itself, but it is connected with the presence in the resonator of a window at the Brewster angle.

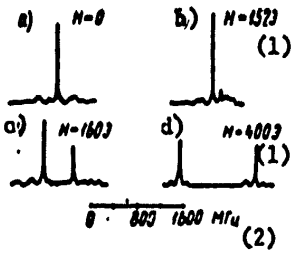

Figure 1

Key:
1. oersteds
2. megahertz

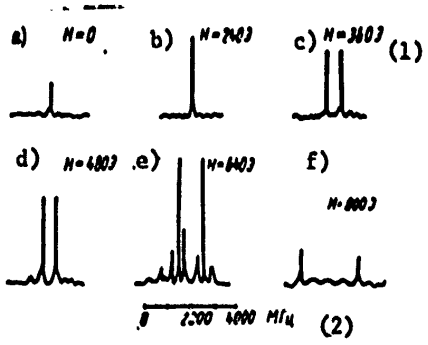

Figure 2

Key:
1. oersteds
2. megahertz

BIBLIOGRAPHY

1. Bridges, W.; Rigrod, W. W. IEEE J. OF QUANTUM ELECTRONICS, QE-1, No 7, 1965.

2. Borisova, M. S.; Pyndik, A. M. RADIOTEKHNIKA I ELEKTRONIKA [Radioengineering and Electronics], No 13, 1968, p 754.

3. Lebedeva, V. V.; Odintsov, A. I.; Solimov, V. M. ZHTF [Journal of Technical Physics], No 38, 1968, p 1373.

4. Statz, H.; Bass, de Mars. APPL. PHYS. LETT., Vol 12, No 1, 1968, p 17.

5. Gorod, I.; Spong, F. W. IEEE OF QUANTUM ELECTRONICS, QE-3, No 12, 1967.

6. Borisova, M. S. RADIOTEKHNIKA I ELEKTRONIKA, No 16, 1971, p 4.

7. Kitayeva, V. F.; Odintsov, A. I.; Sobolev, N. N. UFN [Progress in the Physical Sciences], Vol 99, No 3, 1969, p 361.

SINGLE-FREQUENCY Nd: YAG LASER

[Article by V. N. Arzumanov, G. F. Zaytsev, S. V. Kruzhalov, L. N. Pakhomov]

[Text] The Nd:YAG lasers are some of the most prospective solid state quantum lasers for various applications [1]. The basic problem on the path of broad utilization of such lasers is obtaining the single-frequency operating mode. In comparatively few publications on this subject, an inclined Fabry-Perot interferometer was used as the longitudinal mode selectors [2, 3]. The authors of [2, 3] noted that on realization of the single-mode regime in a broad pumping range the Q-factor of the inclined interferometer must be quite high. However, the losses introduced into the resonator by the inclined interferometer increase sharply in this case, the requirement on the precision of the manufacture, its installation in the resonator, and so on are higher. The deficiencies of the inclined interferometer as a selector of longitudinal modes must also be considered to include the difficulty of tuning the frequency corresponding to the maximum transmission factor, the resonator mode frequency during operation in the laser frequency stabilization regime with respect to an external standard.

The multimirror systems of selectors developed and successfully used in gas lasers are to a significant degree free of these deficiencies.

The operating principle of such devices consists in the fact that one of the resonator mirrors is replaced by a complex multimirror reflector having a sharp dependence of the reflection coefficient on the frequency. For selection of longitudinal modes in the Nd:YAG laser in the given paper perhaps the most successful system proposed in reference [4] was used.

The schematic of the experimental device is illustrated in the figure. The laser resonator is formed by the mirrors 1-4. The Nd:YAG crystal 3 mm in diameter by 45 mm was used as the active medium. A transparent coating was applied to the ends of the crystal, and one of the ends was beveled at an angle of 1.5°. The pumping was realized by a high-pressure DKRTV-1500 krypton lamp. The diaphragm D 1.7 mm in diameter was placed in the resonator for operation on one transverse mode.

As was demonstrated in reference [4], the T-type resonator made up of the mirrors 1-4 can be considered as a two-mirror resonator with length $\ell=\ell_1+\ell_2$ formed by the mirror 1 and the reflector, the reflection coefficient of which varies as a function of frequency according to the following law:

where R_2, R_3, R_4 are the reflection coefficients with respect to the field of the mirrors 2-4 respectively; T_4 is the transmission coefficient with respect to the field of the dividing mirror 4; k is the wave number.

Selecting the transmission coefficient of the dividing mirror 4, it is possible to achieve a situation in which the losses for the mode adjacent to the selected mode will exceed the amplification of the active medium. In our case the indicated losses amounted to approximately 8%. The power reflection coefficients of the mirrors were equal to the following: $R_2^2=R_3^2=99.5\%$, $R_1^2=96.5\%$, $R_4^2=65\%$.

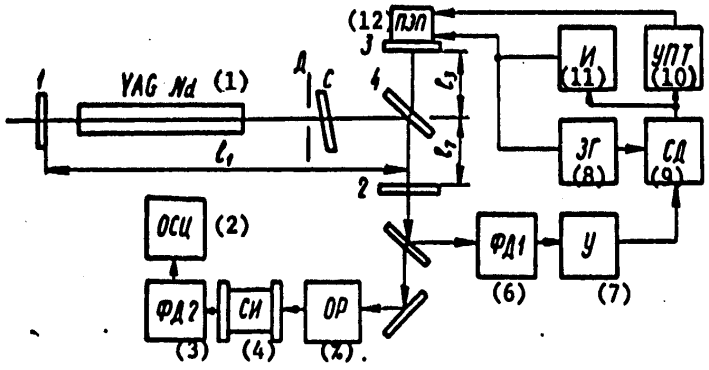

Key:

1. YAG Nd
2. OSTs -- oscillograph
3. FD2 -- photo diode 2
4. SI -- Fabry-Perot scanning interferometer
5. OR -- optical decoupling
6. FD1 -- photo diode 1
7. U -- amplifier
8. ZG -- sound generator
9. SD -- synchronous detector
10. UPT -- DC amplifier
11. I -- integrator
12. PEP -- piezoelectric converter

In order to decrease the losses introduced by the complex reflector, the second surface of the dividing mirror was transilluminated. The length of the active resonator was equal to $\ell_1+\ell_2=80$ cm, and the length of the passive resonator, $\ell_2+\ell_3=8$ cm.

Inasmuch as the amplification line width of the Nd:YAG laser was about 150 gigahertz, the generation could occur on several frequencies corresponding to the peaks of the reflection coefficient of the multimirror selector. In order to obtain generation on one longitudinal mode, an auxiliary selector S was placed in the resonator which is in the form of an inclined Fabry-Perot interferometer. In connection with the fact that the peaks of the reflection coefficient of the complex reflector are quite sharply separated with respect to frequency ($c/2(\ell_2+\ell_3)\approx 2\cdot 10^9$ hertz), the Q-factor of the auxiliary selector can be made low. This leads to a minimum in the losses introduced by them into the resonator, and it insures ease and noncriticalness of its tuning.

The interferometer used in this experiment C was a plane-parallel quartz plate 2 mm thick with interference coatings applied to its surface. The reflection coefficient of the coatings was on the order of 23%.

The selection mode was maintained using the electronic automatic frequency control system. For this purpose, the modulating voltage of 5 kilohertz frequency was fed from the sound generator (ZG) to one of the sides of the two-section piezoelectric converter (PEP). The signal generator using the photodiode (FD1), went from the amplifier (U) and then to the synchronous detector (SD). The error signal from the output of the synchronous detector was amplified in the DC amplifier and fed to the second section of the PEP for tuning the peak of the reflection coefficient of the selecting reflector to the generation frequency. In order to eliminate the residual error, the integrator (I) of the error signal was introduced into the automatic frequency control system, the output of which was connected to the first section of the PEP.

The described system made it possible to realize long-term stable single-frequency generation, exceeding the pumping threshold by more than 30%. The maximum obtained radiation power in the single-frequency mode was 300 milliwatts. The spectrum of the longitudinal modes was controlled using the Fabry-Perot scanning interferometer (SI) with a base of 100 mm and mirror reflection coefficients of about 99%, the radiation to which was fed through the optical decoupling (OR). The transverse distribution was recorded on the screen of an image converter. On disconnection of the automatic frequency control system, the time of existence of the single-frequency generation mode did not exceed 15 minutes, and it jumps from mode to mode or generation on several modes directly were observed. The power fluctuations of the output emission increased significantly simultaneously.

An experimental check of the investigated system makes it possible to consider it highly prospective for obtaining stable single-frequency generation in the Nd:YAG lasers. The optimization of the parameters of

the complex reflector and the resonator should, in our opinion, make it possible to realize single-frequency generation with a power to 1 watt.

In conclusion, let us note that the investigated system permits us to proceed with the solution of the problem of stabilizing the radiation frequency of the Nd:YAG laser.

BIBLIOGRAPHY

1. Lindgren, N. TIIER, No 58, 1970, p 7.

2. Gerhardt, H.; Bödecker, W.; Welling, H. Z. F. ANGEW PHYSIK, No 31, 1971, p 11.

3. Danielmeyer, H. G.; Nilsen, W. G. APPL. PHYS. LETTERS, No 16, 1970, p 124.

4. Petrun'kin, V. Yu.; Vysotskiy, M. G.; Okunev, R. I. ZHTF [Journal of Technical Physics], No 38, 1968, p 1983.

OPTICAL BAND FREQUENCY DISCRIMINATOR BASED ON AN ANISOTROPIC RESONATOR

[Article by V. N. Arzumanov, S. V. Kruzhalov, L. N. Pakhomov, V. Yu. Petrun'kin]

[Text] A study was made in this report of the frequency discriminator designed for laser frequency stabilization systems based on passive interferometers. The method of obtaining the error signal in it permits us to do away with the scanning of the interferometer base and offers the possibility of significantly increasing the rigidity of the structural design, thus eliminating significant deficiencies characteristic of the known systems: disturbance of the adjustment of the mirrors during the process of their movement, sensitivity to vibrations, and so on.

The block diagram of the discriminator, the basic element of which is the anisotropic Fabry-Perot standard is presented in Fig 1. The emission of the laser through the optical decoupling 1 made up of the polaroid a and the quarter-wave plate b is sent to the interferometer 2, the backings of the mirrors 3 and 4 of which are executed from anisotropic material and are phase plates. The reflecting coatings are applied to the outside surfaces of the plates at the same time as their insides are transparent in order to reduce losses.

As is known, the circularly polarized light formed at the outset of the optical decoupling can be represented in the form of the sum of two orthogonal linearly polarized components 90° out of phase. The transmission coefficient T of an anisotropic interferometer will depend on the mutual orientation of the optical axes of the backings of the mirror 3 and 4.

Thus, for parallel arrangement of the axes, the curves for the transmission coefficient as a function of frequency for orthogonal, linearly polarized components of light turn out to be shifted relative to each other. This shift is explained by the fact that each of the light components has a different length of optical path, differing by the amount equal to the total difference in path created by the phase plates. For perpendicular arrangement of the optical axes of the backings, the two curves merge, for the phase plate of one of the mirrors causes lag, and the other, lead of the

orthogonal components of the light by the same amount. The rotation of the optical axes of the substrates for which the transmission curves intersect at the point ν_0 is normal (see Fig 2).

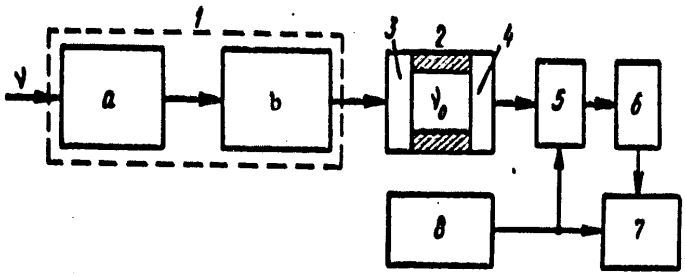

Figure 1

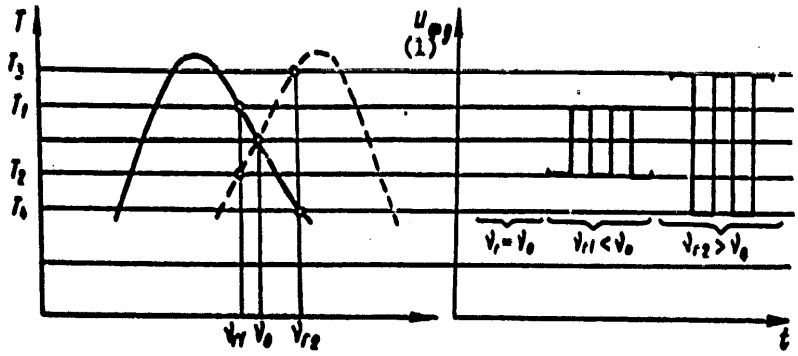

Key: 1. U_{pd}

Figure 2

The error signal U_D is generated in the load of the synchronous detector 7 (see Fig 1). For this purpose the polarization switch 5 alternately with the generator frequency 8 transmits orthogonal linearly polarized light components to the photoreceiver 6. The amplitude and phase of the signal u_{pd} formed at the output of the photoreceiver will depend on the generation frequency difference of the laser ν_g with respect to the standard frequency ν_0. For example, for $\nu_{g1}<\nu_0$ the voltage amplitude is determined by the difference in the transmission coefficient T_1 and T_2, and for $\nu_{g2}>\nu_0$, by the difference T_3 and T_4 respectively (see Fig 2).

Let us consider the discriminator characteristic. In accordance with what has been discussed

$$U_д = k\Phi[T_1(\nu) - T_3(\nu)].$$

where $T_1(\nu)$ and $T_2(\nu)$ are the transmission coefficients of the anisotropic interferometer respectively for each of the orthogonally polarized components of the light; k is the proportionality factor determined by the efficiency of the transformations of the photoreceiver and the synchronous detector; Φ is the light flux at the input of the interferometer.

In accordance with the paper by G. Hird[1], for mirrors with identical reflection coefficients R and in accordance with the notation assumed in Fig 2, we have

$$T_1(\Delta\nu) = \frac{(1-R)^2}{1-2R\cos\frac{4\pi n_1 l}{c}(\nu_{10}-\Delta\nu_{10}+\Delta\nu)+R^2};$$

$$T_2(\Delta\nu) = \frac{(1-R)^2}{1-2R\cos\frac{4\pi n_2 l}{c}(\nu_{20}-\Delta\nu_{20}+\Delta\nu)+R^2}.$$

Here $n_1\ell$ and $n_2\ell$ are the lengths of the optical paths for both components of the light; $\Delta\nu=\nu-\nu_0$ is the current mismatch; c is the speed of light.

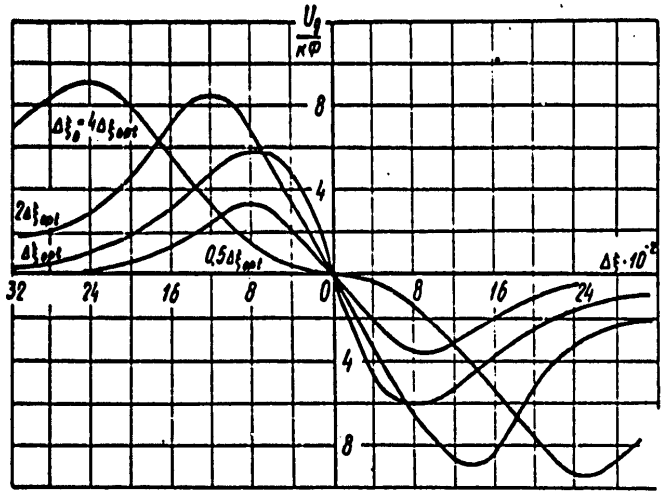

Figure 3

Considering that at the points ν_{10} and ν_{20} the functions $T_1(\Delta\nu)$ and $T_2(\Delta\nu)$ are maximal and, consequently,

$$\frac{4\pi n_1 l}{c}\nu_{10} = \frac{4\pi n_2 l}{c}\nu_{20} = 2m\pi.$$

[1] G. Hird, IZMERENIYE LAZERNYKH PARAMETROV [Measuring Laser Parameters], Mir, 1970.

where m is an integer, setting $\nu_{10} \approx \nu_{20} \approx 0$ and introducing the notation $\Delta\xi = 2m\pi\Delta\nu/\nu_0$, we obtain

$$U_A = k\Phi\left[\frac{(1-R)^2}{1-2R\cos(\Delta\xi_{10}+\Delta\xi)+R^2} - \frac{(1-R)^2}{1-2R\cos(\Delta\xi_{20}-\Delta\xi)+R^2}\right]. \quad (1)$$

The characteristics of the discriminator instructed according to formula (1) for symmetric mismatches $\Delta\xi_{10} = \Delta\xi_{20} = \Delta\xi_0$ and R=0,9 are presented in Fig 3. For optimal mismatch $\Delta\xi_0 = \Delta\xi_{opt}$ the steepness of the initial section of the discriminator characteristic is maximal. The optimal mismatch can be determined from (1). For R close to 1, $\Delta\xi_{opt} \approx \pm(1-R)/\sqrt{3}$.

It is possible to show that $\Delta\xi_{opt}$ corresponds to the rotation of the interferometer mirror backings for which the curves of the transmission coefficients $T_1(\nu)$ and $T_2(\nu)$ intersect at the points of maximum steepness. Let us note that the realization of the maximum steepness of the discriminator is not always expedient. As follows from the curves in Fig 3, by selecting $\Delta\xi_0 > \Delta\xi_{opt}$ with an insignificant reduction in steepness it is possible to obtain a greater region of the operating section of the discriminator characteristic. Such important parameters as the delay band of the automatic frequency control system are increased in this case.

PULSE POLARIMETER FOR LASER RESEARCH

[Article by N. M. Kozhevnikov, S. V. Kruzhalov, L. N. Pakhomov]

[Text] At the present time the most complete study has been made of the polarization characteristics of the quantum generator with the form of the polarization and intensity of the emission (for example, of gas lasers), slowly varying in time, for the polarization analysis in this case is based on the well-known methods. The polarization properties of the emission of the pulsed solid-state lasers have been less investigated due to the fact that the pulse polarimeters required for this purpose have essentially greater complexity. The latter is connected with the necessity for determining with high time resolution both the ellipticity and the azimuth of the completely polarized part of the emission and the degree of polarization of the emission, the intensity of which is of a clearly expressed nonsteady state nature.

At the same time, the study of the polarization properties of the emission of solid state lasers is becoming more and more urgent, for an entire series of problems connected with the broad introduction of these devices in science and engineering will require the use of polarization-anisotropic elements in the composition of the laser. It is also known that the anisotropy of some of the resonator elements, in particular, the active body of the laser, essentially depends on the operating conditions of the generator, and the polarization properties of the emission obviously are interconnected with the remaining output characteristics of the laser. Thus, the complex study of the polarization of the laser emission is required which would make it possible to solve the problem of its relation to the other radiation characteristics and to the operating conditions of the generator which, in turn, would promote more successful operation in the area of improving the output characteristics of the quantum devices.

Operating Principle of the Pulsed Polarimeter

As has already been noted above, the polarization analysis of the pulse characteristics of a laser is connected with the determination of the basic polarization characteristics of the emission in a time less than the time of significant variation of the radiation intensity. For the solution of this problem it is necessary with the corresponding time resolution to measure four independent variables, for example, the Stokes parameters

of the electromagnetic emission. The measurement of the Stokes parameters appears to be the most convenient, which is connected with simplicity of determination and interpretation of the values.

The determination of the Stokes parameters directly connected with the method of experimental location of them consists in the following [1]. Let us consider four filters, each of which transmits the intensity of the unpolarized light. The first filter is isotropic. The second filter is a complete polarizer with horizontal transmission axis, and the third is a complete polarizer with the transmission axis rotated by 45° with respect to the second, and the fourth completely transmits only the right-circular polarized light. If the investigated light beam is split into four parts and is fed to these four filters, then after the filters the intensities will be V_1, V_2, V_3, V_4. The desired Stokes parameters are defined in terms of these values in the following way:

$$I=2V_1;\quad M=2(V_2-V_1);\quad C=2(V_3-V_1);\quad S=2(V_4-V_1). \quad (1)$$

The parameters of the polarization ellipse and the degree of polarization are related to the Stokes parameters by the following expressions:

$$\alpha=\frac{1}{2}\operatorname{arctg}\frac{C}{M};\qquad \frac{b}{a}=\operatorname{tg}|\beta|;$$

$$\beta=\frac{1}{2}\arcsin\frac{S}{(M^2+C^2+S^2)^{1/2}};\qquad P=\frac{(M^2+C^2+S^2)^{1/2}}{I},$$

where α is the polarization azimuth; b/a is the ellipicity (the ratio of the axis of the ellipse to the major axis); P is the degree of polarization; the direction of rotation of the electric field vector is left if S<0, and right if S>0.

All of the structural elements of the pulsed polarimeters known at the present time in one way or another realize the procedure for determining the Stokes parameters based on the expression (1).[1] In reference [2], the division of the investigated light beam was made using semitransparent silvered mirrors. The compensation for the variation of the form of the

[1] It must be noted that all of the known schematics for the polarization analysis and, in particular, those used for investigation of the stationary electromagnetic radiation are in one way or another connected with determination of the Stokes parameters. However, in a number of cases these parameters can be determined successively (under the assumption of stationarity of the degree and form of polarization), and in a number of cases, only some of them, if there is a priori information about the remaining parameters (for example, it is known that the light is completely linearly polarized). Thus, the above-described operating principle of the pulsed polarimeter differs from the previously known polarimeters only by simultaneous measurement of all four Stokes parameters.

polarization on reflection (transmission) of light from the mirror was achieved by the setup of them such that the light would be successively reflected (with pass) from the mirrors, the planes of incidence on which were orthogonal. A large number of mirrors required for this purpose complicated the structural design of the instrument and made it inconvenient for operation.

Reference [3] contains a report on the structural design of the pulsed polarimeters differing advantageously from that investigated in [2] by combination of the light divider and polarizer functions in one element -- the Brewster plate. The instrument manufactured by us, the description of which is presented below, is analogous to that proposed in reference [3].

Structural Design of the Pulse Polarimeter

The optical system of the polarimeter is presented in Fig 1, a. The device is made up of three pairs of Brewster plates. The planes of incidence of the light on the plates in each pair are orthogonal, which permits us to have emission after each pair with the initial form and degree of polarization. The plane of incidence of the light on the first plate of the second pair is rotated by 45° with respect to the plane of incidence of the light on the first plate of the first pair. Before the third pair of plates there is a linear quarter-wave phase plate, the axis of the highest velocity of which is rotated with respect to the plane of incidence of the light on the first plate of the third pair by 45°. This mutual position of the elements of the device will permit performance of four independent measurements of the intensities which are directly related to the parameters of the Stokes electromagnetic radiation. In order to eliminate the effect of the selective properties of the Brewster plates on the readings of the device, the plates are made with a wedge angle of ~10'. The quarter-wave plate was a plane-parallel substrate made of K-8 glass and a plate made of crystal quartz in optical contact with it, the optical axis of which was located in the plane of the input face. The thickness of the quartz plate was 30.1 μ, which corresponds to the phase lead of $\lambda/4$ between the orthogonal components of the electric field (λ=1.06μ).

The light reflection from the Brewster plates was incident on the interference filters (λ=1.06μ, $\Delta\lambda$=200 Å), and then it was focused by the lenses (f~20 mm) on the FD-7K photodiodes which were used as radiation receivers. The pass band of the photodiodes was sufficient for resolution of the individual peaks of free generation of the laser on Nd^{3+} glass. The signals from the photodiodes were incident on the inputs of the five-beam S1-33 oscillograph.

The instrument was tuned with respect to the gas laser beam and after mutual orientation of the Brewster and quarter-wave plates it was reduced to matching of the gas laser beam with the axis of the device (using the diaphragms installed at the input and output of the device with small aperture). The calibration required for operation with the polarimeter was realized using a neodymium laser, in the resonator of which a complete polarizer was placed (a stack of 18 Brewster plates). The calibration

consisted in finding the coefficient by which the readings of the channels were multiplied during the further processing of the results.

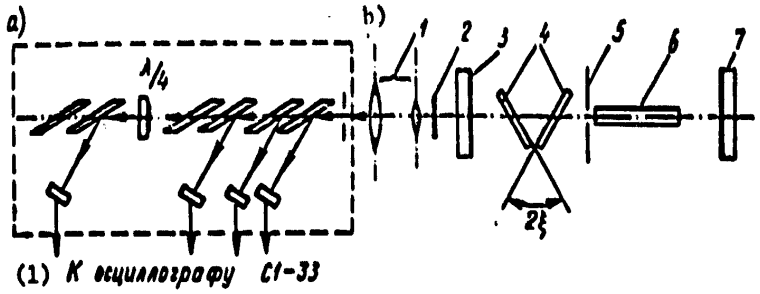

Figure 1

Key:
1. to the S1-33 oscillograph

After calibration, the device had a precision of measurement of the degree of polarization of ~1%, azimuth ~2° and ellipticity within the limits of 10%. The large error when determining the ellipticity obviously was connected with inaccuracy of manufacture of the quarter-wave plate.

Experimental Determination of the Polarization Characteristics of an Anisotropic Neodymium Glass Laser

The above-described pulsed polarimeter was used to investigate a neodymium glass laser, the resonator of which had circular phase and linear amplitude anisotropy.

The laser (see Fig 1, b) was made up of two plane mirrors 3 and 7 with reflection coefficients of 60% for the first and 99% for the second, an active element 6 20 mm in diameter X 260 mm made of KGSS-7 glass pumped by two spiral IFK-15000 pumping tubes, the diaphragm 5, 7 mm in diameter and the partial polarizer 4 formed by two plane-parallel plates inclined to the axis of the resonator. The output emission of this laser was attenuated by isotropic filters 2, and it was fed through the telescopic system 1 to the polarimeter input. An experimental determination was made of the polarization characteristics of the emission for series and counter inclusion of the pumping tubes. The amplitude anisotropy of the resonator was given by the slope ξ of the plane-parallel plates with respect to the resonator axis.

Let us first consider the case of counter inclusion of the pumping tubes (magnetooptical rotation of the direction of polarization in the active body [4] is absent). The performed investigation demonstrated that the state of polarization of the laser emission is determined by the magnitude of the amplitude anisotropy of the resonator. For low anisotropy the

polarization characteristics of the emission varied randomly from peak to peak in the free generation pulse process. With an increase in the anisotropy of the resonator, the initial section of the generation pulse became almost completely linearly polarized. The polarization azimuth in this case experienced oscillations around the position corresponding to the direction of the axis of greatest transmission of the partial polarizer (Fig 2, line 1). On rotation of the plane-parallel plate by an angle close to the Brewster angle (ξ=57°, p=0.52), the emission was found to be almost completely polarized during the entire generation pulse.

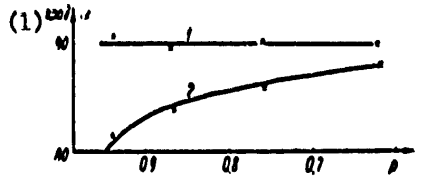

Figure 2

Key:
1. degrees

These results are easy to understand if we consider that in a resonator with amplitude anisotropy two orthogonal linear polarizations oriented with respect to the natural axes of transmission of the partial polarizer are self-reproducing. Inasmuch as the losses for the natural polarization are different, the polarization, the azimuth of which coincides with the axis of greatest transmission of the partial polarizer has an advantage. However, under defined conditions (low magnitude of the anisotropy, high pumping level), considering the weakness of the mechanisms of energy exchange with respect to polarization, the generation conditions can be executed also for emission with polarization having greater losses. This problem was investigated theoretically in reference [5], with the outputs of which our results agree well.

In the case of successive inclusion of the pumping tubes in the obtained experimental relations two regions were clearly observed. A region p>~0.94 (the angle of inclination of the plates ξ<20°) was characterized by high dispersion in the values of the degree of polarization (from 0 to 100%), ellipticity (from 0 to 1) and polarization azimuth (0°-360°) from peak to peak. In the region p>~0.94, noticeable ordering of the polarization characteristics of the emission occurred. The magnitude of the ellipticity and the dispersion of the values in it decreased sharply, and the form of the polarization approached linear. On variation of the parameter p from 0.94 to 0.62, the polarization azimuth varied smoothly from ~81 to ~88°, approaching the direction coinciding with the axis of greatest transmission of the partial polarizer (Fig 2, curve 2).

In order to explain the results obtained, let us use the conclusions of reference [6], where by using the Jones method a study was made of the natural states of polarization of the analogous resonator. A characteristic feature of the investigated system is the existence of the limiting angle of rotation of the direction of polarization by a nonmutual rotator $\phi_{1im}(p)$ which depends on the parameter p:

$$\varphi_{np}(p) = \arccos\left(\frac{2\sqrt{p}}{p+1}\right). \quad (1)$$

Key:
1. lim

In the range of angle $|\varphi| \leqslant \varphi_{np}(p)$ where $\varphi = 2\psi$, two different polarizations are reproduced in the resonator with azimuths and losses which depend on ϕ. In the region $|\varphi| > \varphi_{np}(p)$ two elliptical polarizations are reproduced with identical losses which do not depend on ϕ, identical azimuths and ellipticities, but different with respect to direction of rotation of the electric vector.

This behavior of the polarization characteristics of the resonator makes the presence of two regions in the experimental functions understandable. Actually, inasmuch as for large values of the parameter p two ellipses with identical losses and opposite directions of rotation of the field vector are reproduced, it is entirely natural (considering the fluctuation processes in real lasers) that the output emission is found to be non-polarized during the free generation pulse. Beginning with the time when $p \simeq 0.94$ is satisfied, the emission becomes polarized to a significant degree, for out of the two natural linear polarizations of the resonator possible in this case, the generation conditions are satisfied (for small excesses of the pumping over the threshold realized in our experiments) only for one having smaller losses. The comparison of the experimental and calculated behavior of the emission polarization azimuth as a function of the amplitude anisotropy parameter permits highly precise determination of the angle of rotation of the direction of polarization in the active body which turned out to be equal to $\sim 1.5°$. This value of the angle agrees well with the value obtained in reference [4].

The results of this paper demonstrated the prospectiveness of using the created polarimeter to study the characteristics of the pulse lasers.

BIBLIOGRAPHY

1. W. Shercliff. POLYARIZOVANNYY SVET [Polarized Light], Mir, 1965.

2. Sun Lu; Rabson, T. A. APPL. OPT., No 5, 1966, p 1293.

3. Chartier, G.; Aninat, Ch. COMPT. REND., No 265, 1967, p B-815.

4. Petrun'kin, V. Yu.; Pakhomov, L. N.; Kruzhalov, S. V.; Kozhevnikov, N. M. ZHTF [Journal of Technical Physics], No 42, 1972, p 1531.

5. Ratner, A. M. SB. KVANTOVAYA ELEKTRONIKA [Quantum Electronics], Kiev, Naukova dumka, 1967, p 91.

6. Kruzhalov, S. V.; Kozhevnikov, N. M. ZHTF, No 42, 1972, p 1452.

MULTICHANNEL LIQUID ULTRASONIC LIGHT MODULATORS

[Article by V. S. Bondarenko, N. A. Bukharin, V. A. Grigor'yev, N. A. Yesepkina, N. V. Kuznetsov, S. V. Pruss-Zhukovskiy, V. V. Chkalova]

[Text] As the data input devices to the coherent optical system for processing radio signals it is possible to use diffraction ultrasonic light modulators operating in real time. These single-channel and spatial-multichannel modulators find application in the optical systems realizing spectral analysis and correlation processing of the signals, scanning of the laser beam with a large number of resolved points and also in the systems for optical processing of the signals of antenna arrays [1-6].

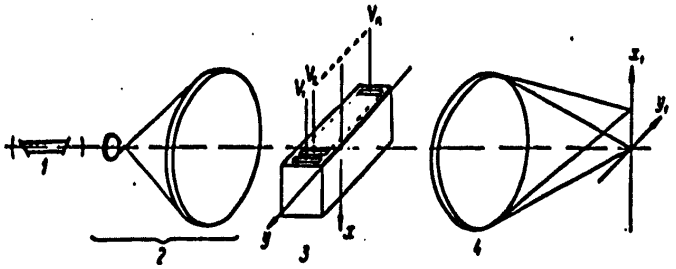

Figure 1

The diffraction ultrasonic light modulators can be liquid or solid-state. In the liquid modulators usually distilled water which has high diffraction activity is used as the sound guide. However, as a result of the high attenuation of ultrasound the operating frequencies of liquid modulators are limited and do not exceed ~30 megahertz.

In this article a study is made of some of the problems of the optical processing of signals using multichannel liquid ultrasonic light modulators operating in the Raman-Nutt diffraction mode (Debye-Sears modulators) and the Bragg diffraction mode [7]. A discussion is presented of the peculiarities of the manufacture of such multichannel modulators, and experimental results are presented with respect to optical processing of the radio signals.

Optical Processing of Radio Signals Using Ultrasonic Light Modulators

Let us consider the optical signal processing system, the modulation of the light flux in which is realized by the ultrasonic Debye-Sears or Bragg light modulators. A schematic of such a device is presented in Fig 1 where 1 is a laser, 2 is a collimator, 3 is a multichannel ultrasonic light modulator, 4 is an integrating lens.

It is possible to demonstrate [4] that on excitation of the Debye-Sears modulator by a harmonic signal with angular frequency $\Omega=2\pi F$ and an initial phase α

$$V(t) = V_0 \cos 2\pi(Ft \pm \alpha)$$

the amplitude distributions and intensities of the light field in the diffraction spectra of $\pm$1st order in the output focal plane of the optical system are determined by the expressions:

$$\left.\begin{aligned} \frac{E_{\pm 1}(u, v)}{E_a} &= jJ_1(\psi)\frac{\sin\left[\pi\left(\frac{1}{\Lambda}\mp u\right)D\right]}{\pi\left(\frac{1}{\Lambda}\mp u\right)D}\frac{\sin(\pi Wv)}{\pi Wv}\times \\ &\times \exp j2\pi[(\nu \pm F)t \pm \alpha]; \\ \frac{I_{\pm 1}(u, v)}{I_a} &= J_1^2(\psi)\frac{\sin^2\left[\pi\left(\frac{1}{\Lambda}\mp u\right)D\right]}{\left[\pi\left(\frac{1}{\Lambda}\mp u\right)D\right]^2}\frac{\sin^2(\pi Wv)}{(\pi Wv)^2}, \end{aligned}\right\} \quad (1)$$

where $E_a = E_0\frac{n_0 DW}{\lambda f}$.

The following notation has been introduced: E_0 and I_0 are the amplitude and intensity of the light beam incident on the modulators; $J_1(\psi)$ is a Bessel function, and ψ is the modulation index proportional to the amplitude of the input signal; $\Lambda=S/F$ is the wave length; S, F is the propagation velocity and frequency of the ultrasonic oscillations; W, D are the width and length of the ultrasonic channel; $u=x_1/\lambda f$, $v=y_1/\lambda f$ are the normalized coordinates in the output focal plane; ν, λ are the frequency and wave length of the light oscillations; n_0 is the index of refraction of the medium of the sound guides; f is the focal length of the lens.

From expression (1) it is obvious that the amplitude of the light field in the diffraction lobe of the first order for small modulation indexes is proportional to the amplitude of the input signal V(t).[1] The position of the diffraction peak of the 1st order in the focal plane (u, v) corresponds to the coordinates

[1] It is possible to consider the light distribution also in the diffraction lobe of the 1st order. Here and hereafter we shall consider that the operating region is located near the diffraction lobe of +1st order and we shall consider the light distribution only in this lobe.

$$u = x_1/\lambda f = 1/\Lambda = F/S, \quad v = 0.$$

On variation of the frequency of the input signal, the peak shifts along the u axis. Consequently, if a signal of the type

$$V(t) = a(t)\cos 2\pi[Ft + \varphi(t)],$$

reaches the input of the modulator, then the light intensity distribution in the output focal plane with respect to the u-axis will correspond to the energy spectrum of the signal.

According to the estimates presented in references [8, 9], the optical processing system with ultrasonic Debye-Sears light modulator insures a dynamic range of about 40 decibels.

In order to perform a spectral analysis of the set of signals $V_n(t)$, a multichannel modulator can be used with independent channels [1]. In this case, it is necessary to use a cylindrical optical system realizing Fourier transformations only with respect to one coordinate.

As follows from expressions (1), the ultrasonic light modulator retains the input signal phase; therefore it can be used as an element of the multichannel modulator for the system for optical processing of the antenna array signals [4-6]. If the modulator parameters are selected so that the divergence of the ultrasonic beams is insignificant and the adjacent channels of the modulator are nonoverlapping beams, then the light modulation is realized by the ultrasonic waves in the near zone of each radiator

$$D \leq W^2/2 \text{ to } 4\Lambda.$$

In this case the light intensity distribution in the diffraction spectrum of the first order in the output focal plane on excitation of the channels of the modulator by harmonic signals of equal amplitude and with linear variation of the phase from channel to channel by $2\pi\alpha$ corresponds to the radiation pattern of the linear antenna array and is determined by the expression:

$$\frac{I_1}{I_0} = J_1^2(\psi)\left\{\frac{\sin\left[\pi\left(\frac{1}{\Lambda}-u\right)D\right]}{\pi\left(\frac{1}{\Lambda}-u\right)D}\right\}^2\left[\frac{\sin\pi Wv}{\pi Wv}\right]^2\left\{\frac{\sin[\pi N(vl+\alpha)]}{\sin[\pi(vl+\alpha)]}\right\}^2. \quad (2)$$

Here ℓ is the spacing between the ultrasonic channels; N is the number of channels in the light modulator equal to the number of elements in the array.

The position of the peak intensity in the focal plane (u, v) corresponds to the coordinates

$$u = \frac{x_1}{Nf} = \frac{1}{\Lambda} = \frac{F}{S}, \quad v = \frac{y_1}{Nf} = -\frac{a}{l}.$$

Measuring the position of the peak along the v-axis, it is possible to determine the phase shift between the signals $2\pi a$. Setting $a=(d/\lambda_p)\sin\phi$, where λ_p is the radial wave length; d is the distance between the elements of the antenna array; ϕ is the angle reckoned from the normal to the array, we find that

$$v = -\frac{d}{\lambda_p l}\sin\varphi. \qquad (3)$$

Each point source of radio emission located in a sector of the field of view corresponds to its own light spot with its center at the point v. As follows from expressions (2) and (3), the width of the light spot

$$\Delta v_{0,5} \approx 1/Nl.$$

This value corresponds to the angle

$$\Delta\varphi_{0,5} \simeq 1/Nd\cos\varphi,$$

determining the width of the radiation pattern of the antenna with respect to the half-power level. Consequently, the resolution of the optical processing system coincides with the resolution of the antenna array.

On frequencies

$$F \geqslant \left(\frac{n\Lambda^2}{\lambda H}\right)^{1/2},$$

where H is the dimensionless modulator in the direction of propagation of the light (the thickness of the modulator), the ultrasonic modulators operate in the Bragg diffraction mode. Here only one of the diffraction spectra of the 1st order is observed. For liquid ultrasonic modulators at H=10 mm the Bragg diffraction mode is observed on frequencies of 25 to 30 megahertz. In this case the distribution of the light intensity in the focal plane (u, v) on excitation of the channels of the modulator by signals of equal amplitude and with linear variation of the phase from channel to channel by $2\pi a$ is defined by the expression [10]:

$$\frac{I_1(u, v)}{I_0} = \sin^2\frac{\psi}{2}\left\{\frac{\sin\left[\pi d\left(u - u_B - \frac{1}{\Lambda}\right)\right]}{\pi d\left(u - u_B - \frac{1}{\Lambda}\right)}\right\}^2\left[\frac{\sin \pi W(v)}{\pi W v}\right]^2 \times$$

$$\times\left\{\frac{\sin[\pi N(vl + a)]}{\pi(vl + a)}\right\}^2\left\{\frac{\sin\left[\frac{\pi\lambda H}{2n_0}(u^2 - u_B^2)\right]}{\frac{\pi\lambda H}{2n_0}(u^2 - u_B^2)}\right\}^2. \qquad (4)$$

Here the notation corresponds to that introduced earlier, and

$$u_B \approx \frac{\theta_B}{\Lambda}; \qquad \sin\theta_B \approx \theta_B = \frac{\lambda}{2\Lambda_B};$$

θ_B is the Bragg diffraction angle.

The presence in expression (4) of the last cofactor is connected with consideration of finite thickness of the modulator H which also leads to selective volumetric reflection and observation of one diffraction order.

The light intensity distribution with respect to the v-coordinate is determined by third and fourth cofactors in expression (4) and coincides with the distribution (2) obtained for the Debye-Sears modulator. The maximum in the light intensity distribution (4) corresponds to the coordinates

$$u = \frac{x_1}{\lambda f} = u_B + \frac{1}{\Lambda}, \qquad v = \frac{y_1}{\lambda f} = -\frac{a}{l}.$$

A comparison of the characteristics of ultrasonic modulators of both types indicates that the Bragg modulators are energy-wise more inefficient than the Debye-Sears modulators, and they are wider-band [11].

The possibilities of the optical signal processing system with ultrasonic light modulator and an input device are most completely realized for a large number of channels. For the development of the modulator with a large number of channels it is necessary to determine the maximum possible density of the arrangement of the channels, for the total size of its useful aperture is limited by the optical system. This is connected with the fact that for large apertures the optical system itself begins to introduce phase distortions which essentially worsens the characteristics of the processing system. The density of the arrangement of the ultrasonic channels in the modulator can be increased by several procedures.

1. As was proposed in reference [12], use a multichannel sound guide system permitting spatial separation of the ultrasonic channels.

2. Raise the operating frequency of the modulator and, consequently, decrease the divergence of the ultrasonic nodes. However, for liquid

modulators raising the operating frequency is limited by the large amount of attenuation of the ultrasound.

3. Increase the density of the arrangement of the channels by using a multichannel modulator in which the ultrasonic nodes overlap.

The modulators with overlapping nodes can be used for optical processing of the antenna array signals. The investigation of the operation of the modulator indicates that on variation of the angle of incidence of the radial wave on the antenna array, the maximum distribution of the light field will be shifted in the focal plane around the circle with radius $k=2\pi/\Lambda$ with its center on the optical axis of the system [13]. The signals with different frequencies F_i will correspond to circles with radii $k_i=2\pi/\Lambda_i$, that is, the radial distribution of the light intensity will correspond to the power spectrum of the input signal. With this processing procedure, the maximum density of the arrangement of the channels will be limited by the admissible magnitude of the electroacoustic interaction between the electrodes of the piezoconverter.

It is possible to show [13] that on satisfaction of the condition

$$D < \frac{f\lambda_p^2}{v\Lambda d^2}$$

the distribution of the light field in the diffraction spectrum of the 1st order in the region defined by the zone of the field of view $|v| \leq d/\lambda_p f$ coincides with the expression (1). Consequently, in this case it is possible in general to neglect the divergence of the ultrasonic nodes.

Experimental Study of Multichannel Ultrasonic Light Modulators

The development of the structural design and the process for the manufacture of multichannel liquid modulators was initially carried out on models of 8-channel modulators. On the basis of the results of these studies, models of multichannel modulators (40 to 50 channels) were built with a sound guide system and with overlapping channels operating in the Raman-Nutt and Bragg diffraction nodes. As the electroacoustic converters, the TsTS-23 piezoceramic plates were used.

The first of the investigated models had 8 channels. The modulator was made up of a holder for the piezoconverters, couvettes made up of fused quartz filled with distilled water and methyl holders for the couvette. Eight palladium electrodes were applied to the converter plate 18X10 mm in size and 110 microns thick ($F_{cut} \approx 20$ megahertz) on one side, and it was completely metal plated on the other side. The electrodes were arranged with a repetition period of $l=1.5$ mm, and their dimensions were $W=0.75$ mm and $H=8$mm. The holder of the piezoconverter was designed in such a way that in the operating position the plate of the converter was completely submerged in water. The ultrasonic waves emitted from one side of the piezoconverter were absorbed by a rubber insert fastened to the holder.

On the other side of the converter the waves were emitted into the operating aperture of the modulator and they were used for modulation of the light beam. On the bottom of the couvette there was an absorbing rubber insert which insured the traveling wave regime. The multichannel sound guide system was made up of a number of opaque glass partitions 0.3 mm thick attached with the same repetition period in a special frame which was inserted in the couvette. When necessary the modulator could be used without the sound guide system. The couvette was rigidly fastened in the metal frame in which provision was made for the possibility of adjusting the converter with respect to the sound guide system.

The modulators were investigated in an optical device made up of OSK-2 elements with focal length of the integrating lense of 1600 mm.

The frequency characteristics of the modulator were measured by the light intensity in the diffraction spectrum of the 1st order. As the measurements demonstrated, the resonance frequencies of the modulator channels differed insignificantly, and the operating frequency band with respect to the 3 decibel level was about 10%. The required values of the modulation index $\psi=0.3$ was reached for an amplitude of the input signal of 0.5 volts. The magnitude of the acoustic interaction between adjacent channels was estimated in the following way: one of the modulator channels was excited, and the intensity of the diffracted light was measured. It turned out that this intensity caused by penetration of the ultrasound from the adjacent channel was 20 decibels less than the intensity of the light diffracted on the ultrasonic waves of the excited channel. For parallel excitation of the modulator channel, the dispersion in the intensity of the ultrasound in the channel did not exceed 1 decibel.

The distribution of the light intensity in the diffraction spectrum of the 1st order with cophasal excitation of the modulator channels was measured. As the photometric measurements demonstrated, this distribution basically corresponds to expression (2). On excitation of the channels by signals with linear phase lead from channel to channel by $\pm 90°$ the shift of the principal peak of the light intensity in the diffraction spectrum of the 1st order corresponds to the calculated value of ± 168 microns.

A study is made of the possibility of decreasing the level of the side lobes for which amplitude weighting of the signals exciting the modulator by the following law was introduced:

$$V_n = V_0 \left[\frac{1}{3} + \frac{2}{3}\cos\pi\left(\frac{n}{N} - \frac{1}{2}\right)\right].$$

With this distribution, the signal amplitude of the edge channels of the modulator drops to $V_0/3$. As the measurements demonstrated, the side lobe level in this case was 19 decibels, and the width of the main peak increased by approximately 1.6 times.

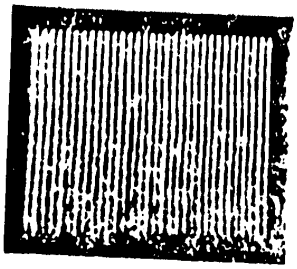

Figure 2

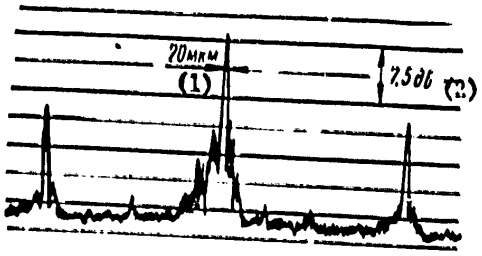

Figure 3

Key:
1. microns 2. decibels

The structural design of the model of the Debye-Sears multichannel liquid light modulator (≈40 channels) with the sound guide system is analogous to the one investigated above. The size of the operating aperture of this modulator was 60X50 mm. The distribution of the ultrasound intensity in the modulator channels is presented in Fig 2. The remaining characteristics of the modulator are the same as in the preceding case. The multichannel (≈50 channels) light modulator with overlapping channels operated in the Bragg fraction regime on a frequency of 27 megahertz. The spacing between the electrodes of the converter in this case was 1 mm.

In Fig 3 we see the light intensity distribution in the diffraction spectrum of the 1st order for cophasal excitation of all the channels by signals of equal amplitude. The width of the principal peak of this distribution with respect to the halfpower level will be ≈20 microns. On excitation of the modulator channels by signals of equal amplitude but with linear phase leads from channel to channel by $\pm 135°$, the displacement of the principal peak corresponded to the calculated value and was ± 375 microns. Incidentally, this modulator can be used in the system for optical processing of the antenna array signals.

The performed studies indicate the possibility of creating sufficiently complex multichannel ultrasonic light modulators suitable as the information input devices to the optical signal processing systems for various purposes.

BIBLIOGRAPHY

1. Lambert, L. B. IRE INTERN. CONV. REC., No 6, 1962, p 69.

2. Arm, et al. TIIER, Vol 52, No 17, 1964, p 897.

3. Mustel', Ye. R.; Parygin, V. N. METODY MODULYATSII I SKANIROVANIYA SVETA [Methods of Light Modulation and Scanning], Nauka, 1970.

4. Lambert, Arm, Aymet. ZARUBEZHNAYA RADIOELEKTRONIKA [Foreign Radio-electronics], No 8, 1968, p 3.

5. Bakhrakh, L. D., et al. VOPROSY RADIOELEKTRONIKI [Problems of Radioelectronics], OT Series, No 1, 1972, p 36.

6. Stark. TIIER, Vol 60, No 8, 1972, p 104.

7. Rytov, S. M. IZV. AN SSSR. SER. FIZICH. [News of the USSR Academy of Sciences, Physics Series], No 2, 1973, p 223.

8. Preston, K. ELEKTRONIKA [Electronics], No 18, 1965, p 12.

9. Lambert, L. SOVREMENNAYA RADIOLOKATSIYA [Modern Radar], Sovetskoye radio, 1969, p 245.

10. Aksenov, Ye. T., et al. VOPROSY RADIOELEKTRONIKI [Problems of Radioelectroni s], Ser. OT, No 5, 1973, p 8.

11. Grigor'yev, V. A.; Rogov, S. A. See the present collection, p 56.

12. Andreyev, V. A., et al. "Multichannel Ultrasonic Light Modulator," USSR Author's Certificate No 393791.

13. Aksenov, Ye. T.; Bukharin, N. A.; Grigor'yev, V. A.; Pruss-Zhukovskiy, S.V. See present collection, p 52.

SOLID STATE ULTRASONIC LIGHT MODULATORS WITH LIGHT GUIDES MADE OF HEAVY FLINTS

[Article by Ye. T. Aksenov, N. A. Yesepkina, V. A. Markov, V. P. Pikarnikov, S. V. Pruss-Zhukovskiy]

[Text] Ultrasonic light modulators are being successfully used in the systems for optical data processing for input and analysis of signals. In these modulators the sound guides can be liquids (to frequencies of ~30 megahertz), optically transparent solid states -- crystals (α- HIO_3, $PbMoO_4$, $LiNbO_3$, α - SiO_2) and also certain varieties of glass).

In a number of cases (vibration, large temperature gradient, and so on) the application of the liquids can turn out to be complicated. On the other hand the crystals which could be used in this case are at the present time comparatively expensive and have certain technological deficiencies. Therefore, the special glass, the acoustooptical quality of which is relatively high is of definite interest for the manufacture of the sound guides for ultrasonic modulators. The data on measuring the acoutooptical parameters of glass of the heavy flint type [1] indicate that for comparatively small damping of the ultrasound (from 0.1 to 2 decibels/cm on a frequency of ~40 megahertz) the coefficient of their acoustooptical quality $M_2=n^6p^2/\rho S^3$ is 4-6 times greater than fused quartz. In the presented formula n is the index of refraction of the material; p is the photoelastic constant; ρ is the density of the material; S is the speed of the ultrasonic oscillations. From the point of view of acoustooptical qualities and also considering that optically uniform samples of large size can be made from the glass, the heavy flints are highly prospective for the manufacture of sound guides of ultrasonic light modulators in the frequency band to 100 megahertz.

According to the process described in [2], several single-channel and multi-channel models of modulators made of flints of the TF-10, TF-3, TF-1 types in the frequency band of 20 to 40 megahertz were manufactured and investigated. Half-wave plates of TsTS-23 ceramic and $LiNbO_3$ Y+36° cut were used as the piezoconverter. In order to obtain the traveling ultrasonic wave regime, the end of the modulator opposite the piezoconverter was beveled at an angle of ~10°.

On the basis of the single-channel ultrasonic modulator operating in the Raman-Nutt diffraction mode at a frequency of 36 megahertz, a model of an acoustooptical spectral analyzer was developed, the schematic of which is presented in Fig 1. Its band with respect to level of relative intensity equal to 0.5 was 26 megahertz. The sound guide of the modulator 20X25X65 mm^3 was made of TF-3 glass. The halfwave plate of $LiNbO_3$ Y+36° cut was used as the piezoconverter. The dimensions of the operating electrodes determining the region of interaction of the light with sound are 3X20 mm^2. For the input signal $v(t)=a\cos[\Omega t+\phi(t)]$ the amplitude and intensity distribution of the light diffracted on the ultrasonic wave in the 1st order spectrum in the output focal plane of the acoustooptical spectral analyzer is defined by the expressions [3, 4]:

$$\frac{E_1(u)}{E_\pi} \sim J_1(\psi)\frac{\sin\pi\left(\frac{1}{\Lambda}-u\right)D}{\pi\left(\frac{1}{\Lambda}-u\right)D}\exp j[(\omega\pm\Omega)t+\varphi(t)]; \qquad (1)$$

$$\frac{I_1(u)}{I_\pi} \sim J_1^2(\psi)\frac{\sin^2\pi\left(\frac{1}{\Lambda}-u\right)D}{\left[\pi\left(\frac{1}{\Lambda}-u\right)D\right]^2}, \qquad (2)$$

where E_π, I_π are the amplitude and intensity of the incident light waves; $J_1(\psi)$ is the 1st-order Bessel function; Λ is the wave length of the sound oscillations; $u=x_1/\lambda f$ is the reduced coordinate in the output focal plane; f is the focal length of the lens; λ is the light wave length; D is the sound guide length; ω is the angular frequency of the light; Ω is the angular frequency of the sound vibration; $\psi=2\pi\ell\Delta n/\lambda$ is the phase modulation index of the light wave; Δn is the variation of the index of refraction of the medium of the sound guide under the effect of an elastic wave; $\phi(t)$ is the initial phase of the signal fed to the piezoconverter. From the presented expressions it follows that the distribution of the light intensity in the output focal plane represents the energy spectrum of the signal hitting the piezoconverter of the ultrasonic modulator and also that the position of the diffraction peak depends on the frequency of the input signal, and is defined by ratio $u=1/\Lambda$. For small angles of diffraction, the direction of the 1st-order diffraction peak is defined by the expression

$$\theta \simeq \frac{x_1}{f} = \frac{\lambda}{\Lambda} = \frac{\lambda F}{S}. \qquad (3)$$

A characteristic feature of the acoustooptical spectral analyzer is the fact that the amplitudes and frequencies of the entire analyzed spectrum are recorded simultaneously at the output and not on the individual frequency components. Its operation is analogous to the operation of the multichannel electronic spectral analyzer. The number of channels is determined by the number of resolved points.

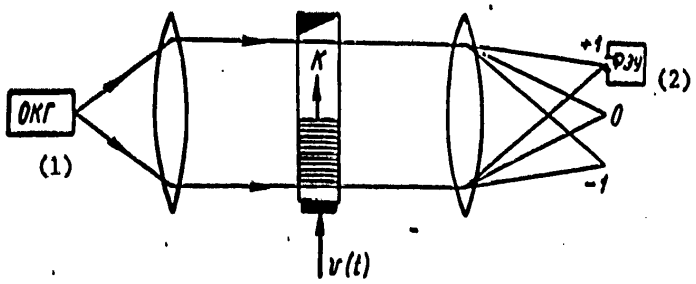

Figure 1

Key: 1. laser; 2. photomultiplier

The basic parameters with respect to analyzer is the frequency resolution. In the case of the acoustooptical analyzer it depends on the diffraction divergence of the light beam connected with the restriction of the light wave incident on the modulator by the modulator aperture. The angular divergence data with respect to halfintensity level is

$$\beta = \lambda/D, \tag{4}$$

where D is the width of the collimated light beam which in our case is determined by the length of the modulator light guide. The minimum frequency interval ΔF_{min} which can be resolved is defined as the integral for which the angle of deflection of the light beam $\Delta\theta=\lambda/S$ (ΔF_{min}) is equal to its angular divergence. From (3) and (4) we have

$$\Delta F_{min} = S/D. \tag{5}$$

The number of resolved points N of the acoustooptical spectral analyzer is

$$N = \frac{\Delta F}{\Delta F_{\text{мин}}} \overset{(1)}{=} \frac{D}{S}\Delta F.$$

Key:
1. min

As has already been indicated N defines the number of channels of the equivalent multichannel spectral analyzer. It is necessary to note that the band of the acoustooptical spectral analyzer ΔF, the ultrasonic modulator of which operates in the Raman-Nutt diffraction mode cannot exceed ~70% of the basic frequency [3].

By using the developed spectral analyzer, a study was made of the spectra of several signals. On feeding the signal to the piezoconverter of the ultrasonic modulator in the focal plane of an integrating lens, the spectrum of the signal was recorded. The intensity distribution of the light field was recorded on photographic film. In addition, it was recorded using a moving slit diaphragm after which there was an FEU-27 photomultiplier.

The signal from the photomultiplier passed through the U1-7 electrometric amplifier to the N-110 pen recorder. For monitoring the operation of the acoustooptical spectral analyzer, the electronic spectral analysis circuit was introduced which was included in parallel to the piezoconverter. The shape and spectrum of the investigated signals were recorded by the S1-31 oscillograph and the S4-25 spectral analyzer.

One of the investigated signals was an amplitude-modulated oscillation with a carrier frequency of 36 megahertz, a modulation frequency of 1.5 megahertz and a modulation depth of 100%. The spectrum of the signal photographed from the screen of the S4-25 device and a photograph of the light intensity distribution in the focal plane, respectively, were presented in Fig 2, a, b. The measured frequency resolution for the given model was ~130 kilohertz. The calculated value obtained from expression (5) is 110 kilohertz. The number of resolved points in our case was ~200.

By using the acoustooptical analyzer it is possible also to perform a successive analysis of the spectrum. In this case, a moving light spot will be observed in the focal plane, the instantaneous position of which corresponds to the frequency of the signal propagated in the light guide. The effect of the movement of the light beam can be used to create deflectors in the information readout systems, for the creation of the deflection device and the system for formation of the television image, and so on.

If it is necessary to analyze the spectrum of several signals simultaneously, then by using the two-dimensionality of the optical system it is possible to create a spatial-multichannel spectral analyzer [3], the integrating lens of which must be cylindrical. In the spatial-multichannel ultrasonic modulator used in this analyzer, the relation between the channels must be absent. Each channel of this device can have its own operating frequency. The condition that the channels of the multichannel spectral analyzer be decoupled imposes defined requirements on the structural design of the ultrasonic modulator. If the sound guide of the modulator is a monolithic unit, then the admissible channel density is determined by the diffraction divergence of the ultrasonic wave. In the case where great density of the channels is necessary, it is possible to use a sound guide with mechanically separated channels [5].

The distribution of the sound field of the eight-channel modulator with distributed channels is presented in Fig 3. From the figure it is obvious that the relation between the channels was in practice absent.

The multichannel ultrasonic light modulators in the systems for coherent optical data processing can be used not only for analysis of the spectrum of the input signals, but also for the solution of a number of other problems, for example, for processing the antenna array signals [6]. As was demonstrated in [7], when processing the antenna array signals it is possible to use multichannel ultrasonic modulators with overlapping

channels. We manufactured several models of such modulators with from 10 to 40 channels and frequencies from 20 to 40 megahertz. The sound guides of these models were made of TF-10, TF-3, TF-1 glass. In the majority of models the converters were attached to the sound guides using indium binding layers by the method of thermal compression.

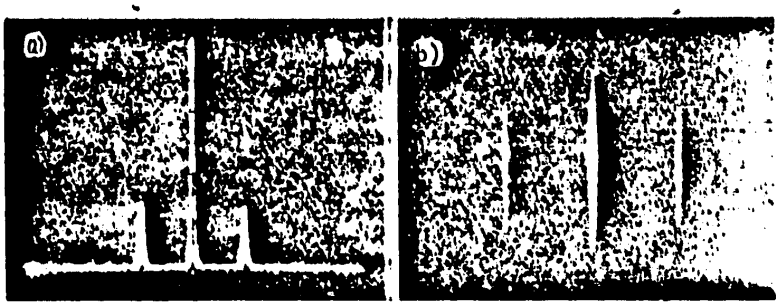

Figure 2

The resonance frequencies and bands of all of the channels were in practice identical. The input impedances had scattering not exceeding 10%. In practice there was no relation between the channels through the plate of the piezoconverter. In the case of cophasal excitation of all of the channels and also for linear phase lead (the case where the phase difference between the excitation signals of adjacent channels was 60° was considered) the light intensity distribution at the 1st-order diffraction peak coincided well with the calculated value. The distribution diagram of the light field at the 1st-order diffraction peak was presented for cophasal equal-amplitude excitation of the channels of the 13-channel ultrasonic modulator on the central frequency of F=23 megahertz. The upper electrodes were deposited with spacing of 1.5 mm, and their dimensions were 0.7X20 mm. The converter was made of $LiNbO_3$ Y+36° cut. For the signal amplitude on the converter equal to 80 MV, the signal/noise ratio was $I_{+1}/I_{noise}=1$.

Figure 3

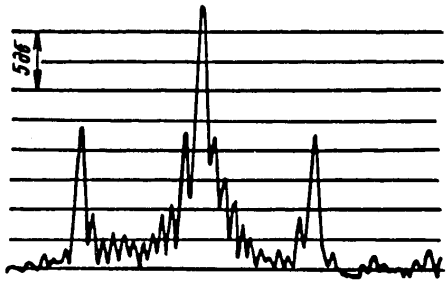

Figure 4

Thus, the performed experiments indicate that the ultrasonic light modulators with sound guides made of glass of the heavy flint type have parameters permitting successful application of them in the system for coherent optical data processing.

BIBLIOGRAPHY

1. Kludzin, V. V. OPTIKO-MEKHANICHESKAYA PROMYSHLENNOST' [Optical-Mechanical Industry], No 1, 1972.

2. Aksenov, Ye. T., et al. ZHTF [Journal of Technical Physics], No 42, 1972, p 11.

3. Lambert, L. B. IRE CONVENTIONS RECORD, Vol 6, No 10, 1962.

4. Mustel', Ye. R.; Parygin, V. N. METODY MODULYATSII I SKANIROVANIYA SVETA [Methods of Light Modulation and Scanning], Nauka, 1970.

5. Aksenov, Ye. T., et al. VOPROSY RADIOELEKTRONIKI [Problems of Radioelectronics], Ser. OT, No 3, 1973.

6. Lambert, L. ZARUBEZHNAYA RADIOELEKTRONIKA [Foreign Radioelectronics], No 8, 1968.

7. Aksenov, Ye. T.; Bukharin, N. A.; Grigor'yev, V. A.; Pruss-Zhukovskiy, S. V. See the present collection, p 52.

HIGH-FREQUENCY SOLID-STATE ULTRASONIC LIGHT MODULATORS

[Article by Ye. T. Aksenov, N. A. Yesepkina, V. A. Markov, V. P. Pikarnikov]

[Text] The ultrasonic diffraction light modulators are prospective devices for signal input to the optical data processing system. The ultrasonic modulators operate in real time and can be both single-channel and multichannel. An important parameter of such modulators is the frequency band, and in the case of the multichannel modulators, the admissible density of the arrangement of the ultrasonic channel with given magnitude of the coupling between them.

It is possible to expand the frequency band and increase the density of the placement of the channels by increasing the operating frequency of the modulator to frequencies of hundreds of megahertz. On such frequencies the Bragg diffraction regime is realized which has a number of advantages by comparison with the Raman-Nutt regimes: greater efficiency, greater dynamic range, and so on.

In this article the results are presented from studying multichannel solid state ultrasonic light modulators on frequencies above 100 megahertz.

In the high-frequency ultrasonic light modulators spin-film and plate half-wave piezoconverters are used. In the investigated models of the modulators, the half-wave plate made of lithium niobate Y+36° cut 1, fastened to the sound guides 3 made of fused quartz using indium binding layer 2 (see Fig 1) were used as the piezoconverters. On frequencies above 100 megahertz the thickness of this layer is comparable to the sound wave length, and therefore its effect must be considered when finding the input impedance of the piezoconverter.

Before making the transition to a discussion of the experimental results, let us determine the input impedance of piezoconverter. The knowledge of the magnitude of the input impedance permits us to estimate the conversion losses and their dependence on the frequency, and to find the conditions of matching the piezoconverter to the generator, and so on.

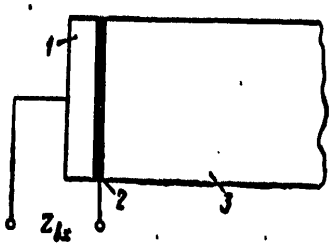

Figure 1

As was demonstrated in references [1, 2], the input impedance of the converter loaded on the active acoustic load is defined by the following expression:

$$Z_{\text{вх}(1)} = \frac{1}{j\omega C_0} + \frac{K^2}{\omega C_0 \gamma} \frac{2W(1-\cos\gamma)+j\sin\gamma}{jW\sin\gamma-\cos\gamma}, \qquad (1)$$

Key:
1. inp

where ω is the angular frequency of the sound; C_0 is the static capacitance of the converter; K is the coefficient of electromechanical coupling of the selected longitudinal mode of the oscillations; $\gamma=\omega\ell/Y$; ℓ is the thickness of the converter; $W=Z_п/Z_3$ is the ratio of the wave acoustic impedances of the materials of the converter $Z_п$ and the sound guide Z_3 for longitudinal waves.

Separating the real and imaginary parts in expression (1), we obtain

$$Z_{\text{вх}} = \frac{1}{j\omega C_0} - \frac{1}{j\omega C_0}\frac{K^2}{\gamma}\frac{\sin\gamma\left[2W^2-(2W^2-1)\cos\gamma\right]}{W^2\sin^2\gamma+\cos^2\gamma} + \\ + \frac{1}{\omega C_0}\frac{K^2}{\gamma}\frac{2W(1-\cos\gamma)}{\cos^2\gamma+W^2\sin^2\gamma}. \qquad (2)$$

The first term of expression (2) is the impedance of the static capacitance of the converter, and the second is the reactive mechanical resistance X_a; the third is the purely active impedance of the emission R_a.

Expression (1) was obtained under the condition that the thickness of the transmission layer between the converter and sound guide is small by comparison with the wave length, and its effect can be neglected. This expression easily is reduced to the form taking into account the effect of the transition layer. For this purpose we must consider that the converter is loaded on the medium with complex acoustic impedance which depends on the parameters of the binding layer. The magnitude of this acoustic impedance can be determined by using the formulas presented in reference [3] where a study is made of the characteristics of the multi-layer systems.

If the converter with wave acoustic impedance $Z_п$ is noted on a sound guide with the impedance Z_a, and the resistance of the binding layer Z_c, then the magnitude of W in formula (1) can be replaced by the value of Z_{ac} determined by the formula:

$$Z_{ac} = W_c \frac{W_c \cos\varphi + jW \sin\varphi}{W \cos\varphi + jW_c \sin\varphi}, \qquad (3)$$

(1)

Key:
1. ac

where $W_c = Z_п/Z_c$; $W = Z_п/Z_a$; $\varphi = \omega h/V_c$; h is the thickness of the transition layer; V_c is the speed of sound in the material of the transition layer.

Considering (3) and the effect of the transition layer, for the input acoustic impedance of the converter we obtain

$$Z_{ak} = \frac{1}{j\omega C_0} + \frac{K^2}{\omega C_0 \gamma} \frac{2Z_{ak}(1 - \cos\gamma) + j\sin\gamma}{jZ_{ak}\sin\gamma - \cos\gamma}. \qquad (4)$$

The conversion losses П are the ratio of the power P_c picked up from the generator for the matched load to the power P_a which is generated on the radiation impedance. The expressions for these powers are as follows:

$$P_a = \frac{E^2 \operatorname{Re} Z_н}{|Z_н + Z_г|^2}; \qquad P_c = \frac{E^2}{4 \operatorname{Re} Z_г}. \qquad (5)$$

Here E is the generated emf; Z_H and $Z_Г$ are the input impedance of the converter and the generator.

The expression for the conversion losses can be presented in the form:

$$П = 10\lg \frac{|Z_н + Z_г|}{4 \operatorname{Re} Z_н \operatorname{Re} Z_г}. \qquad (6)$$

According to formula (6), considering (4) the series of amplitude-frequency characteristics was calculated for the converters made of lithium niobate Y+36° cut loaded on the sound guide made of fused quartz for various thicknesses of the indium binding layer. For the calculations the resistance of the generator was considered purely active and equal to 75 ohms. The static capacitance of the converter for the selected configuration of the electrodes of 0.75X5 mm was 60 picofarads.

The analysis of the calculated frequency-amplitude characteristics demonstrated that the optimal thickness of the layer for which the minimum losses were reached on the 50% band is 6 microns. The electrodes of the

indicated configuration and the layer of the mentioned thickness were used in our models of the modulator.

The experimentally measured frequency-amplitude characteristics agree well with the calculated ones.

In the investigated models of the multichannel (the number of channels from 20 to 30) modulators lithium niobate Y+36° cut plates were used as the piezoconverters operating on the basic resonance frequency of ~200 megahertz. The sound guides were monolithic units of fused quartz 15X45X75 mm^3. Their operating faces were made by the method of precision optical grinding and polishing with a precision on the order of $\lambda/6$. The converter plates were fastened to the sound guides through the indium binding layers approximately 6 microns thick using the process discussed in [4]. The traveling sound wave in the sound guide was created by beveling the end opposite to the one on which the piezoconverter was located at an angle of ~5° to the direction of propagation of the sound. The electrodes 0.7X5 mm^2 with spacing of 1.5 mm were deposited on the converter plate.

The excitation voltage was fed to the modulator channel from the G4-5 generator through the strip exponential power divider [5]. Using this divider it was possible simultaneously to excite 14 channels. When measuring the optoacoustic parameters of the modulator, it was illuminated by the light of the LG-36 optical generator through the collimating system of lenses. The distribution of the diffracted light intensity was observed in the focal plane of the output lens located beyond the modulator. The frequency functions for the intensity of the diffracted light were picked up with constant excitation voltage of 1 volt on the piezoconverter. The frequency characteristics of the modulator channels were in practice identical. The standard characteristics are presented in Fig 2. Curve 1 was recorded with tuning on each frequency of the angle of incidence of the light on the modulator so that the intensity of the diffracted light will be maximal. Curve 2 was recorded with invariant orientation of the modulator with respect to the incident light. The Bragg angle was in this case set for a frequency of 210 megahertz. It is obvious that the pass band with respect to the half-intensity level is approximately 40 megahertz. The measured frequency characteristics are in qualitative accordance with the calculated ones. A study was made of the operation of the model for cophasal equal amplitude excitation of its 14 channels. The shadow distribution pattern of the sound field in the modulator was measured which indicated that the sound beams of the individual channels almost do not overlap with respect to the entire modulator aperture.

The distribution of the light field at the diffraction peak of the 1st order and the diagram of this distribution obtained in the focal plane of the output lens are presented in Fig 3, a, b. The diagram of the light field distribution was obtained using a moving slit diaphragm behind which the FEU-27 photomultiplier was located. The signal from the photomultiplier passed through the U1-7 amplifier to the N-110 pen recorder.

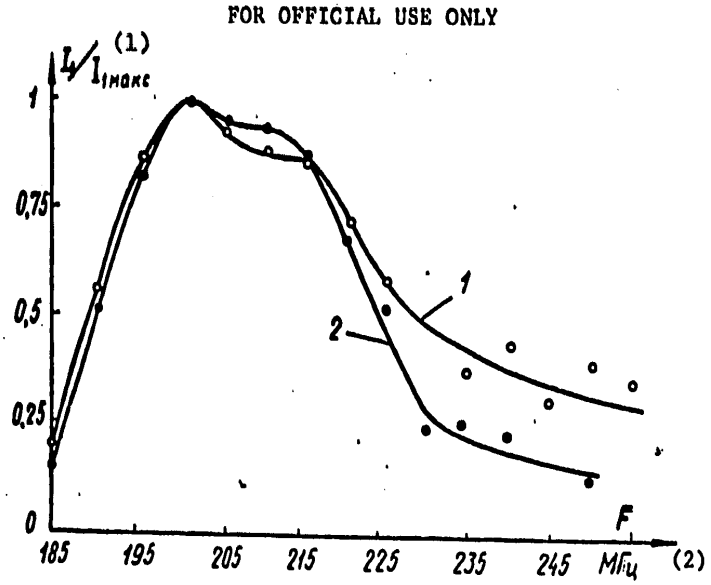

Figure 2

Key:
1. $L_i/I_{i\,max}$
2. megahertz

Thus, the performed studies of the operation of the models of multichannel solid-state high-frequency ultrasonic light modulators indicate that the modulators manufactured by the described process can be used in the systems for optical processing of radio signals.

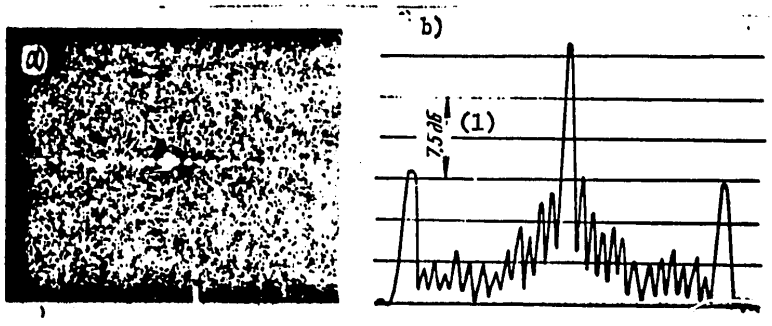

Figure 3

Key:
1. decibels

BIBLIOGRAPHY

1. Reder T. M.; Winslow, D. K. IEEE TRANSACTIONS, MTT-17, No 11, November 1969.

2. Brekhovskikh, L. M. VOLNY V SLOISTYKH SREDAKH [Waves in Layered Media], Nauka, 1973.

3. Foster, N. F. JOURNAL OF APPL. PHYS., No 38, 1967, p 149.

4. Aksenov, Ye. T., et al. ZHTF [Journal of Technical Physics], No 42, 1972, p 11.

5. Yesepkina, N. A.; Pavlov, B. Ya.; Petrun'kin, V. Yu. TRUDY LPI [Works of the Leningrad Polytechnical Institute], No 255, Energiya, 1965.

MULTICHANNEL ACOUSTOOPTICAL MODULATOR WITH OVERLAPPING ULTRASONIC BEAMS

[Article by Ye. T. Aksenov, N. A. Bukharin, V. A. Grigor'yev, S. V. Pruss-Zhukovskiy]

[Text] In the system for optical processing of antenna array signals investigated in reference [1], the light flux modulation is realized by a multichannel acoustooptical modulator.

The dimensions of the modulator converter electrodes, their repetition period, the size of the modulator with respect to the direction of propagation of the ultrasonic waves and the operating frequency were selected in such a way that the waves propagated from the adjacent converters are nonoverlapping ultrasonic means. Here, ultrasonic waves in the near zone of each emitter are used for light modulation so that in each beam the modulation is realized independently of the others.

Let us investigate the possibility of optical processing of the signals of a multielement antenna where the field in the far zone of an individual emitter of ultrasonic waves within the near zone of the entire array of emitters as a whole is used for the light modulation. Here the ultrasonic waves corresponding to the individual elements of the piezoconverter can overlap.

Let us consider the light diffraction on ultrasonic waves generated by an electroacoustic converter of finite dimensions for arbitrary ratio between its size W and the ultrasonic wave length Λ, Fig 1. Let us give the excitation function of the ultrasonic wave emitter

$$F(y)=\begin{cases} 1, & |y|\leqslant W/2; \\ 0, & |y|>W/2. \end{cases}$$

The distribution of the ultrasonic wave field in the region $x\geqslant 0$ can be represented in the form of the superposition of plane waves [2]:

$$\left.\begin{aligned} F(x, y) &= \int_{-\infty}^{\infty} \Phi_w(k_y) \exp\left[i\left(k_y y + \sqrt{k^2 - k_y^2}\, x\right)\right] dk_y, \\ F(x, y)\big|_{x=0} &= F(y) = \int_{-\infty}^{\infty} \Phi_w(k_y) \exp\left(ik_y y\right) dk_y, \end{aligned}\right\} \quad (1)$$

where

$$\Phi_w(k_y) = \frac{1}{2\pi} \int_{-\infty}^{\infty} F(y) \exp\left(-ik_y y\right) dy = \frac{\sin\left(k_y \frac{W}{2}\right)}{\pi k_y}, \quad (2)$$

$$k = 2\pi/\Lambda.$$

In expression (1) the term under the integral sign

$$\exp\left[i\left(k_y y + \sqrt{k^2 - k_y^2}\, x\right)\right]$$

corresponds to a plane wave propagated at an angle of $\theta = \arcsin(k_y/k)$ to the x-axis.

The variation of the index of refraction of the sound conducting medium caused by the ultrasonic wave in it is proportional to the field distribution F(x,y). We shall show that under the effect of the ultrasonic wave the light beam is modulated only with respect to phase, that is, the condition of Raman-Nutt diffraction is satisfied [1]. The distribution of the light amplitude in the output focal plane of the lens located behind the modulator, the size of the eliminated aperture of which D with respect to the amplitude of the light beam incident on the modulator will be equal to the following with a precision to the constant factor:

$$\frac{E(\omega_x, \omega_y)}{E_\pi} = \int_0^D \int_{-\infty}^{\infty} \exp\left[i\psi F(x, y)\right] \exp\left[-i(\omega_x x + \omega_y y)\right] dy dx \simeq$$
$$\simeq \int_0^D \int_{-\infty}^{\infty} \left[1 + i\psi F(x, y)\right] \exp\left[-i(\omega_x x + \omega_y y)\right] dy dx.$$

Here E_π is the amplitude of the light beam incident on the modulator; $\omega_x = -2\pi x/\lambda f$ and $\omega_y = -2\pi y/\lambda f$ are the normalized coordinates in the output focal plane of the lens with the focal length f; λ is the light wave length; ψ is the modulation index where $\psi << 1$ rad. The light amplitude distribution in the diffraction spectra of $\pm$1st order

$$\frac{E_{\pm 1}}{E_\pi} = \int_0^D \int_{-\infty}^{\infty} F(x, y) \exp\left[-i(\omega_x x + \omega_y y)\right] dy dx =$$
$$= \int_{-\infty}^{\infty} \Phi_w(k_y) \left\{ \int_0^D \int_{-\infty}^{\infty} \exp\left[i\left(k_y y + \sqrt{k^2 - k_y^2}\, x\right)\right] \times \right.$$
$$\left. \times \exp\left[-i(\omega_x x + \omega_y y)\right] dy dx \right\} dk_y. \quad (3)$$

Using expression (2) and integrating, we find that with a precision to a constant factor[1]

---

[1] This expression pertains to the modulator operating in the Raman-Nutt diffraction regime. It is possible to obtain an analogous expression for the Bragg diffraction regime.

$$\frac{E_{+1}}{E_0} = \exp\left[i\left(\sqrt{k^2-\omega_y^2}-\omega_x\right)\frac{D}{2}\right]\frac{\sin\left[\left(\sqrt{k^2-\omega_y^2}-\omega_x\right)\frac{D}{2}\right]}{\left(\sqrt{k^2-\omega_y^2}-\omega_x\right)\frac{D}{2}}\cdot\frac{\sin\left[\left(\frac{W}{2}\right)\omega_y\right]}{\left(\frac{W}{2}\right)\omega_y}. \quad (4)$$

On satisfaction of the condition

$$k\left(\frac{\omega_y}{k}\right)^2\frac{D}{2} < 1, \quad (5)$$

the last two cofactors in (4) can be represented with sufficient precision in the form

$$\frac{\sin\left(\frac{W}{2}\omega_y\right)}{\frac{W}{2}\omega_y}\cdot\frac{\sin\left[\left(\omega_x \pm k\right)\frac{D}{2}\right]}{\left(\omega_x \pm k\right)\frac{D}{2}}. \quad (6)$$

As follows from (5) and (6) for

$$D \leqslant W^2/n^2\pi\lambda$$

expression (6) quite precisely determines the light amplitude distribution in the diffraction spectra of the ±1st order to the n-th null with respect to the ω_y coordinate.

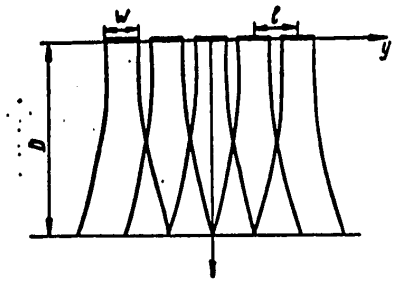

Figure 1

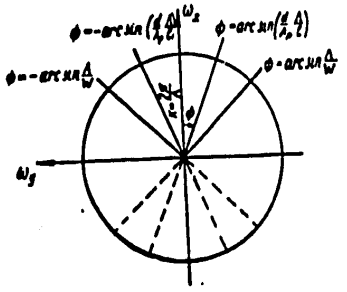

Figure 2

Let us introduce the polar coordinates $\omega_x=\omega\cos\Phi$, $\omega_y=\omega\sin\Phi$ and let us consider the distribution of the diffracted light on the circle $\omega=k=2\pi/\Lambda$. The first two cofactors in expression (4) are in this case equal to one, and the function

$$\frac{\sin\left(\frac{W}{2}k\sin\Phi\right)}{\frac{W}{2}k\sin\Phi}$$

for

$$\frac{W}{2}k\sin\Phi_n = n\pi;\ \Phi_n = \arcsin\left(n\frac{\Lambda}{W}\right);\quad n = \pm1, \pm2\ldots$$

has zeros (see Fig 2).

The distribution of the light intensity in the focal length of the optical system on excitation of one of the channels of the liquid light modulator by the harmonic signal with frequency of 10 megahertz is presented in Fig 3. The size of the converter electrode is 0.75 mm, the size of the sound guide is 50 mm, and the wave length of the ultrasonic modulations in the water on this frequency was 0.15 mm. It is obvious that the light intensity in the diffraction spectra of $\pm$1st order is distributed around the circle of radius $\omega=2\pi/\Lambda$.

From expression (3) and (4) it follows that the distribution of the light intensity in the focal plane of the optical system in the diffraction spectra of $\pm$1st order is determined only by the size of the illuminated aperture, that is, the size of the illuminated section of the diverging ultrasonic beam and not by its position along the x axis.

Now let us consider the light diffraction on the ultrasonic wave stimulated by the array of M acoustic radiators located along the y axis with repetition period ℓ. Let us represent the excitation function of the array in the form

$$F(x, y)\big|_{x=0} = F_1(y) = \sum_{m=-(M-1)/2}^{(M-1)/2} F(y - ml)\exp(-2\pi i m\alpha),$$

where $2\pi\alpha$ is the phase shift between the signals of the adjacent elements of the antenna array, and

$$F(y - ml) = \begin{cases} 1, & |y - ml| \leqslant W/2; \\ 0, & |y - ml| > W/2. \end{cases}$$

Then, as can be demonstrated

$$\Phi_{MW}(k_y) = \frac{11}{2\pi}\int_{-\infty}^{\infty} F(y)\exp(-ik_y y)\,dy = \Phi_W(k_y)\frac{\sin\left[\pi M\left(\frac{k_y l}{2\pi}+\alpha\right)\right]}{\sin\left[\pi\left(\frac{k_y l}{2\pi}+\alpha\right)\right]}. \quad (7)$$

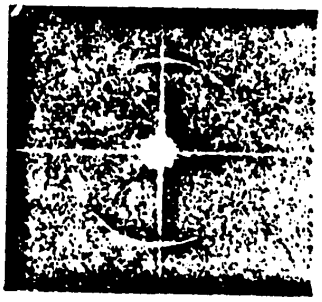

Figure 3

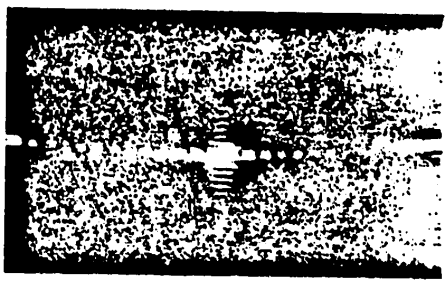

Figure 4

Substituting expression (7) in formula (3), we find that the light amplitude distribution in the diffraction spectra of ±1st order is

$$\frac{E_{\pm 1}}{E_0} = \exp\left[i\left(\sqrt{k^2-\omega_y^2}-\omega_x\right)\frac{D}{2}\right]\frac{\sin\left[\left(\sqrt{k^2-\omega_y^2}-\omega_x\right)\frac{D}{2}\right]}{\left(\sqrt{k^2-\omega_y^2}-\omega_x\right)\frac{D}{2}}\times$$

$$\times\frac{\sin\left(\frac{W}{2}\omega_y\right)}{\frac{W}{2}\omega_y}\frac{\sin\left[\pi M\left(\frac{\omega_y l}{2\pi}+\alpha\right)\right]}{\sin\left[\pi\left(\frac{\omega_y l}{2\pi}+\alpha\right)\right]}. \qquad (8)$$

In the polar coordinates introduced above, for $\omega=k=2\pi/\Lambda$ the first two cofactors in expression (8) are equal to one, and, consequently,

$$\frac{E_{\pm 1}}{E_0} = \frac{\sin\left(\frac{W}{2}k\sin\Phi\right)}{\frac{W}{2}k\sin\Phi}\frac{\sin\left[\pi M\left(\frac{kl}{2\pi}\sin\Phi+\alpha\right)\right]}{\sin\left[\pi\left(\frac{kl}{2\pi}\sin\Phi+\alpha\right)\right]}. \qquad (9)$$

The second cofactor in expression (9) has a peak for

$$\frac{kl}{2\pi}\sin\Phi = -\alpha.$$

If we set

$$\alpha = \frac{d}{\lambda_p}\sin\varphi, \qquad (10)$$

where d is the distance between the elements of the antenna array; λ_p is the radial wave length; ϕ is the angle of incidence of the radial wave on the antenna array reckoned with respect to the normal to it, then

$$\sin\Phi = -\frac{\Lambda}{l}\frac{d}{\lambda_p}\sin\varphi.$$

Consequently, on variation of the angle of incidence of the radial wave on the antenna array ϕ the maximum light field distribution in the focal plane will be shifted along the circle of radius $k=2\pi/\Lambda$ with the center on the optical axis of the system. Since $|\phi|\leq 90°$, the zone of the field of view in the focal plane with respect to the angle Φ will be defined by the expression (see Fig 2).

$$|\Phi| < \arcsin\left(\frac{\Lambda}{l}\frac{d}{\lambda_p}\right).$$

The solid-state 13-channel modulator with the sound guide made of TF-3 type glass with D=50 mm size operated on a frequency of 25 megahertz. The electrodes of the piezoconverter with dimensions of W=0.75 mm were arranged with a repetition period of ℓ=1.5 mm. The wave length of the ultrasonic oscillations in the glass on this frequency was $\Lambda\approx$0.15 mm. The light intensity distribution in the output focal plane of the optical system in the region of one of the 1st order diffraction spectra for cophasal equal amplitude excitation of the modulator channels is presented in Fig 4. This light distribution, in accordance with the expression (9) is formed on a circle of radius $\omega=2\pi/\Lambda$.

Consequently, the acoustooptical modulators with overlapping ultrasonic beams can be used as the system for optical processing of the signals of a multielement antenna which will permit significant increase in density of arrangement of the channels.

BIBLIOGRAPHY

1. Lambert, L.; Arm, M.; Aymet, A. ZARUBEZHNAYA RADIOELEKTRONIKA [Foreign Radioelectronics], No 8, 1968, p 3.

2. Morse, F. M.; Fishbach, G. METODY TEORETICHESKOY FIZIKI [Methods of Theoretical Physics], Vol II, IL, 1964.

FREQUENCY CHARACTERISTICS OF ULTRASONIC LIGHT MODULATORS OPERATING IN THE BRAGG DIFFRACTION MODE

[Article by V. A. Grigor'yev, S. A. Rogov]

[Text] The diffraction ultrasonic light modulators are finding broad application in various systems for optical signal processing as the data input device in real time and also in the laser beam scanning systems with high resolution. The achievements in the field of obtaining wide band, high-frequency piezoconverters [1-3] and also the appearance of new single crystals having small acoustic losses and large diffraction activity [4] made it possible to create ultrasonic light modulators for frequencies above 100 megahertz operating in the Bragg diffraction mode [5, 6].

The frequency band of the ultrasonic light modulator is defined by the pass band of the piezoconverter with an electric cycle and the effective optical acoustic interaction band. Here a study is made of the effective optical acoustic interaction band for modulators operating in the Bragg diffraction regime.

It is known that for light diffraction on ultrasound, the region of propagation of which is limited to the dimensions D, H and W (Fig 1), in the case where the thickness of the modulator H is appreciably greater than the length of the ultrasonic wave, the light intensity distribution in the diffraction spectra of $\pm$1st order with respect to the intensity of the incident light beam is defined by the expression [7, 8]

$$\frac{I_{\pm 1}}{I_n} = \sin^2\frac{\psi}{2}\left(\frac{\sin\xi}{\xi}\right)^2\left(\frac{\sin\eta}{\eta}\right)^2\left(\frac{\sin\zeta}{\zeta}\right)^2, \qquad (1)$$

where

$$\xi = \pi D\left(\frac{\theta-\theta_0}{\lambda} \mp \frac{1}{\Lambda}\right); \quad \eta = \frac{\pi H}{2n_0\lambda}(\theta^2-\theta_0^2); \quad \zeta = \frac{\pi W}{\lambda}\Phi,$$

ψ is the modulation index equal to [9]

$$\psi = \frac{2\pi n_1 H}{\lambda} = \pi\left[\frac{2}{\lambda^2}\left(\frac{H}{W}\right)\left(\frac{n_0^6 p^2}{\rho S^3}\right)P_a\right]^{1/2};$$

θ_0 is the angle of incidence of the light beam; θ and Φ are the angles characterizing the observation point (see Fig 1); λ is the wave length of the light vibrations; Λ is the wave length of the ultrasonic oscillations; n_0 is the index of refraction of the light guide medium; n_1 is the maximum variation of the index of refraction of the medium caused by the ultrasonic wave; ρ is the density of the medium; S is the propagation rate of the ultrasonic oscillations; p is the photoelasticity constant; P_a is the acoustic power.

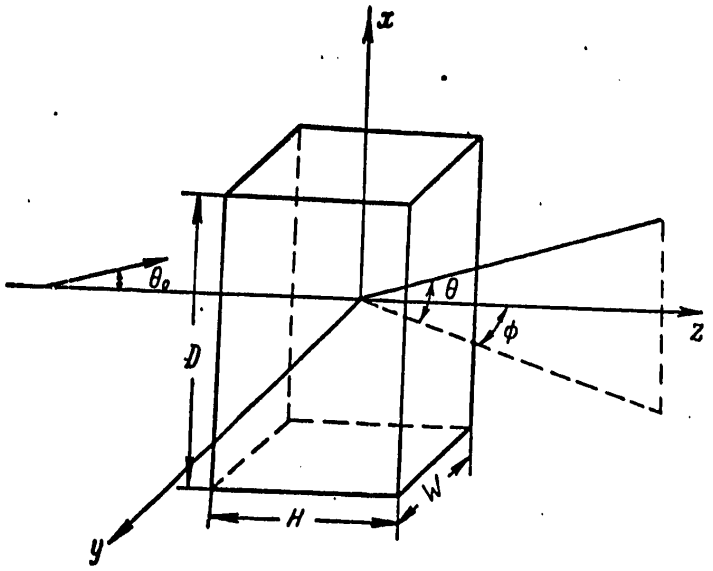

Figure 1

The distribution of the light intensity in the diffraction spectra of the $\pm$1st order (1) has two peaks differing with respect to intensity and corresponding to the conditions: $\theta_{\pm}=\theta_0\pm\lambda/\Lambda$; $\Phi=0$. As follows from (1), on satisfaction of the condition

$$\lambda H/n_0\Lambda^2 \geqslant 1 \qquad (2)$$

jointly with the requirement of equality of the angle of incidence to the Bragg angle

$$\theta_0=\theta_{\text{Б}}=\mp\frac{\lambda}{2\Lambda} \qquad (3)$$

the intensity of one of the diffraction spectra of $\pm$1st order is maximal, and the other does not exceed 5% of this maximum. Consequently, the conditions (4) and (3) are the conditions of observation of one diffraction spectrum, that is, the Bragg diffraction conditions.

The angular position of the diffraction peaks of ±1st order depends on the ultrasonic wave length. Here the light intensity in them varies in accordance with

$$\left(\frac{\sin\eta}{\eta}\right)^2_{\pm} = \frac{\sin^2\left[\frac{\pi H}{2n_0\lambda}\left(\frac{\lambda}{\Lambda}\pm 2\theta_0\right)\right]}{\left[\frac{\pi H}{2n_0\lambda}\left(\frac{\lambda}{\Lambda}\pm 2\theta_0\right)\right]^2}. \qquad (4)$$

Let us determine the effective optical acoustic interaction band with respect to the level of 0.5 of the maximum value of the intensity in one of the diffraction orders. Let the angle of incidence of the light beam be equal to the Bragg angle $\theta_0=\theta_B=+\lambda/2\Lambda_B$, where $\Lambda_B=S/F_B$, and F is the frequency of the ultrasonic oscillations. Let us rewrite expression (4) for the predominant diffraction spectrum of the 1st order in the following form:

$$\left(\frac{\sin\eta}{\eta}\right)^2_{-} = \frac{\sin^2\left[\frac{\pi\lambda H}{2n_0S^2}F_B^2\left(\frac{F^2}{F_B^2}-\frac{F}{F_B}\right)\right]}{\left[\frac{\pi\lambda H}{2n_0S^2}F_B^2\left(\frac{F^2}{F_B^2}-\frac{F}{F_B}\right)\right]^2}. \qquad (5)$$

Expression $(\sin\eta/\eta)^{-2}$ has two principal peaks, the position of which is determined by the Bragg angles $\theta=\pm\theta_0=\pm\lambda/2\Lambda_B$ which, according to (5) corresponds to the frequencies of F =0 and $F=F_B$.

The higher F_B, the greater the angular distance between the principal peaks of the function $(\sin\eta/\eta)^{-2}$ which is determined by the magnitude of $2\theta_0=\lambda/\Lambda_B$. The mutual arrangement of the principal peaks for the values of $F_B=2\sqrt{2}F_{B\min}$; $1{,}88\,F_{B\min}$ is shown in Fig 2, where $F_{B\min}=(n_0S^2/\lambda H)^{1/2}$ is determined from condition (3) of the observation of one diffraction order.

From Fig 2, a it is obvious that the range of frequencies in which the intensity of the diffracted light is less than half of its maximum peak in the case where $F_B>1.88\,F_{B\,min}$ is made up of two parts. In practice only the part determined by the width of the main lobe of the functions $(\sin\eta/\eta)^{-2}$ with the center at $\theta=-\theta_0$, $F=F_B$ is of interest. Let us find this pass band as a function of the Bragg frequency for a fixed value of H. Let the condition of Bragg diffraction (3) be satisfied on the central frequency, and let the frequencies F_1 and F_2 correspond to the edges of the pass band.

Beginning with the condition

$$\left|\frac{\sin\eta}{\eta}\,\frac{\sin\xi}{\xi}\right| = \frac{1}{\sqrt{2}},$$

setting $\sin\xi/\xi=1$, we find the angles corresponding to the edges of the pass band:

$$\left.\begin{aligned}\theta_1 &= \theta_0 - \frac{\lambda}{\Lambda_1} = -\sqrt{\theta_0^2 - \frac{0{,}89 n_0 \lambda}{H}};\\ \theta_2 &= \theta_0 - \frac{\lambda}{\Lambda_2} = -\sqrt{\theta_0^2 + \frac{0{,}89 n_0 \lambda}{H}}.\end{aligned}\right\} \qquad (6)$$

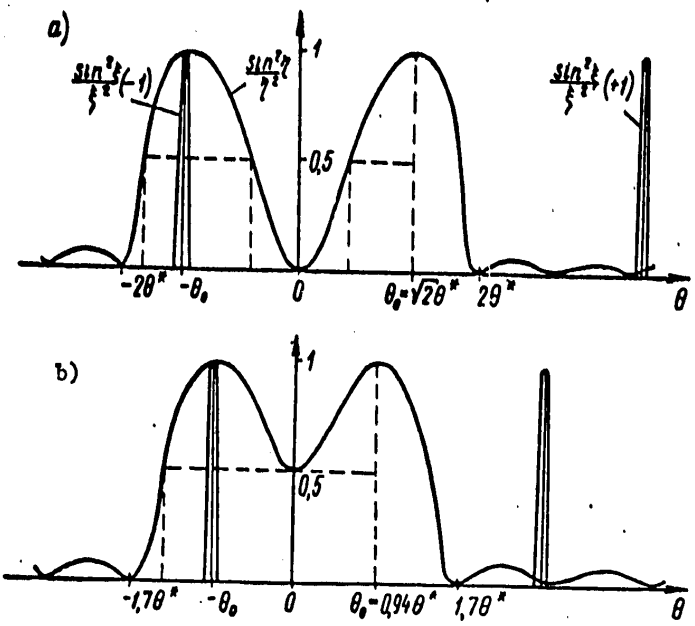

Figure 2

The shift of the diffracted light peak is

$$\theta_2 - \theta_1 = -\lambda\left(\frac{1}{\Lambda_2} - \frac{1}{\Lambda_1}\right) = -\frac{\lambda}{S}(F_2 - F_1) =$$
$$= -\left(\sqrt{\theta_0^2 + 0{,}89\theta^{*2}} - \sqrt{\theta_0^2 - 0{,}89\theta^{*2}}\right),$$

where $\theta^{*2}=n_0\lambda/H$.

For the pass band we have the following expression:

$$\Delta F = F_2 - F_1 = \frac{F_{\text{Б min}}}{2}\left[\sqrt{\left(\frac{F_\text{Б}}{F_{\text{Б min}}}\right)^2 + (1{,}88)^2} - \right.$$
$$\left. - \sqrt{\left(\frac{F_\text{Б}}{F_{\text{Б min}}}\right)^2 - (1{,}88)^2}\right], \qquad (7)$$
$$F_\text{Б} > 1{,}88 F_{\text{Б min}}.$$

On high frequencies F_B where $F_B \gg F_{B_{min}}$, from formula (7) we find

$$\Delta F = 1{,}77 \frac{F_{Б\min}}{F_Б} = \frac{1{,}77 n_m S^2}{\lambda H F_Б},$$

which coincides with the one obtained by Gordon [6].

From formula (7) it is obvious that in order to obtain the maximum pass band it is necessary to satisfy the following condition:

$$F_Б \geqslant 1{,}88 F_{Б\min} = 1{,}88 \sqrt{\frac{n_m S^2}{\lambda H}}.$$

For the given F_B, this can be done by selecting H. Then

$$(\Delta F)_{max} \simeq 0{,}707 F_Б, \quad F_Б \geqslant 1{,}88 F_{Б\min}.$$

In the case where $F_B \leqslant 1.88 F_{B_{min}}$ (see Fig 2, b), that is where the trough between the principal peaks of the function $(\sin \eta/\eta)^{-2}$ is no lower than the 0.5 level, it is meaningful to indicate only the upper cutoff frequency $F_{cut}=F_2$. Taking this into account, from expressions (6) we obtain

$$F_{Б\,ср} = \frac{F_{Б\min}}{2}\left[\sqrt{\left(\frac{F_Б}{F_{Б\min}}\right)^2 + (1{,}88)^2} + \frac{F_Б}{F_{Б\min}}\right]; \quad F_Б < 1{,}88 F_{Б\min}. \tag{8}$$

(1)

Key: 1. cut

The maximum value of $F_{B\ cut}$ is achieved for $F_B = 1{,}88 F_{B_{min}}$ and it is equal to 1.2 F_B. The relation for the pass band (7) and the cutoff frequency (8) as a function of the Bragg frequency is presented in Fig 3.

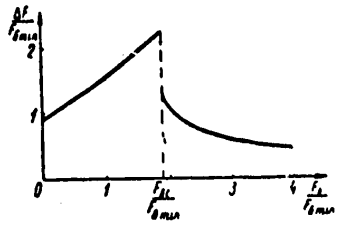

Figure 3

With an increase in this frequency the pass band initially increases in accordance with (8) as a result of expansion of the function $(\sin \eta/\eta)^{-2}$. When a frequency of $F_B = F_{B_c} = 1.88 F_{B_{min}}$ the trough between the principal

peaks of the function $(\sin \eta/\eta)^2$ reaches the 0,5 level (Fig 2, b), and the pass band decreases discontinuously. With a further increase in the frequency F_B, the band is already determined by the width of one lobe of the indicated function and, as follows from expression (7), it decreases.

Let us compare the frequency band for the optical-acoustic interaction of the ultrasonic Bragg and Debye-Sears modulators.

In the Bragg modulators in the case of a sound guide made of fused quartz with an ultrasonic beam 5 mm thick on a frequency of 240 megahertz (which corresponds to $F_B \geq 1.88F_{B_{min}}$) the pass band $\Delta F = 0.7F_B \approx 170$ megahertz. On frequencies of $F_B \leq 1.88F_{B_{min}}$, the upper cutoff frequency determined by expression (8) for the sound guide made of fused quartz on a frequency of 240 megahertz is 290 megahertz, and for the sound guide made of water 10 mm thick on a frequency of 30 megahertz it is $\approx$40 megahertz. As is known, for the Debye-Sears modulators the upper cutoff frequency does not exceed 20 megahertz for a sound guide made of water and 100 megahertz for sound guide made of fused quartz.

Thus, the Bragg ultrasonic light modulators operating at higher frequencies than ultrasonic the Debye-Sears modulators have essentially greater absolute frequency band in which the optical-acoustic interaction is observed.

BIBLIOGRAPHY

1. Foster, N. F. J. APPL. PHYS., No 38, 1967, p 149.

2. Zittig, Kun. TIIER, Vol 56, No 8, 1968, p 124.

3. Aksenov, Ye. T., et al. ZHTF [Journal of Technical Physics], No 17, 1972, p 2432.

4. Dixon, R. W. J. APPL. PHYS., No 38, 1967, p 5149.

5. Pinnow, D., et al. APPL. PHYS. LETT., Vol 15, No 3, 1969, p 83.

6. Parks. ZARUBEZHNAYA RADIOELEKTRONIKA [Foreign Radioelectronics], No 12, 1970, p 3.

7. Rytov, S. M. IZV. AN SSSR. SER. FIZICHESKAYA [News of the USSR Academy of Sciences, Physics Series], No 2, 1937, p 233.

8. Born, M.; Wolf, E. OSNOVY OPTIKI [Fundamentals of Optics], Nauka, 1970.

9. Gordon. TIIER, Vol 54, No 10, 1966, p 181.

EFFECT OF MANUFACTURING AND ADJUSTMENT IMPRECISION ON THE OPERATION OF AN OPTICAL DATA PROCESSING SYSTEM

[Article by M. G. Vysotskiy]

[Text] When designing an optical data processing system it is possible to consider the imprecision occurring in the process of manufacturing and adjusting its elements. The consideration of the effect of the imprecision permits first of all determination of the admissible deviations of the parameters of the elements from the calculated values and, secondly, estimation of the difficulties and the theoretical possibility of implementing the system.

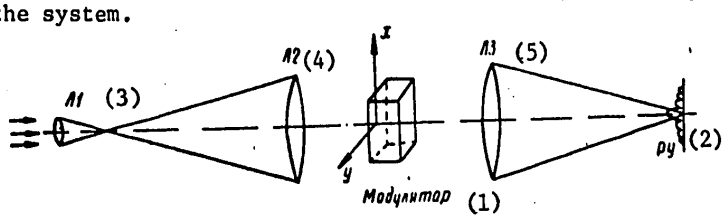

Figure 1

Key:
1. Modulator
2. Recorder
3. L1
4. L2
5. L3

In this article a theoretical and experimental study is made of the effect of imprecision on the operation of an optical data processing system which is made up (see Fig 1) of a source of coherent optical emission, a telescopic system that expands the light beam (the lenses L1 and L2), a light modulator or a data input device, the integrating lens L3 and the recorder (PY). In the case of experimental investigation, the LG-36 type laser was used as the coherent light source; two collimator tubes of the OSK-2 optical bench were used for expansion of the beam and integration of the image. The multichannel diffraction type water modulator was used in the model [1, 2]. Structurally, it was in the form of a couvette filled with distilled water in which ultrasonic oscillations were excited by using piezoelectric converters.

The light distribution in the focal plane of the integrating lens bearing information on the signals coming to the modulator was recorded by a photoreceiver (FEU [photomultiplier]). The radiation was incident on the cathode of the FEU through a narrow slit, and after detection and amplification, the signal was recorded on the pen recorder tape (type N110).

The results are presented below from the calculations and the experimental investigation of imprecision which can occur during the manufacture and adjustment of the elements entering into the system (the lens, the recorder, modulator), and the effect of these imprecisions on its operation. The basic quality criterion of the operation of the system was the form of the diffraction spot recorded by the pen recorder.

Collimator Lenses

The lenses L1 and L2 of the eyepiece and the objective of the first collimator tube are used for creation of the quite broad coherent light beam with a flat phase front. For normal operation it is important that these lenses be precisely cofocal. If the lens L1 is shifted toward the lens L2 by the interval δ with respect to the cofocal position, then the radius of curvature of the phase front of the light emitting from the lens L2 will be $r_0=F_2^2/\delta$, and on the edge of the modulator of size D a phase error appears

$$\Delta\varphi = 1/8\,(D/F_2)^2\delta k, \qquad (1)$$

where F_2 is the focal length of the lens L2; k is the wave number of the optical oscillation.

The field distribution in the focal plane of the integrating lens L3 can be found by calculating the integral

$$E_1(u, v) = \int\int E(x, y)\, T_c(x, y) \exp\left[-2\pi j\,(u_x + v_y)\right] dxdy, \qquad (2)$$

where $u=x_1/\lambda F_3$; $v=y_1/\lambda F_3$; x_1, y_1 are the coordinates in the focal plane of the collecting lens; λ is the wave length of the light vibrations; E(x, y) is the distribution of the electric field incident on the light modulator equal to

$$E(x, y) = E_0 \exp\left[-j\,(\Delta^2 x^2 + \Delta^2 y^2)\right];$$

x,y are the coordinates in the plane of the modulator; $\Delta^2=k/2r_0$; E_0 is the amplitude of the incident light.

The transparency function of the modulator for the investigated structural design

$$T_c(x, y) = \sum_{n=-N/2}^{n=N/2} P_D(x)\, P_W(y - nl) \exp\left[j\psi_m \cos\left(2\pi\frac{v}{\Lambda} - n\pi\right)\right].$$

Here

$$P_D(x) = \begin{cases} 1 & |x| < D/2; \\ 0 & |x| > D/2; \end{cases}$$

$$P_W(y - nl) = \begin{cases} 1 & |y - (n - 1/2)l| \leq W/2; \\ 0 & |y - (n - 1/2)l| > W/2; \end{cases}$$

D is the length of the ultrasonic channel; W is the width of the channel; ℓ is the spacing between the centers of the channels; ψ_m is the light modulation index created by the ultrasound; α is the phase shift between the radial frequency signals incident on the piezoconverters of the adjacent channels; Λ is the ultrasonic wave length.

In the special case $\alpha=0$, calculation of the integral (2) gives the following expressions for the field distribution in the diffraction beams of $\pm$1st order:

$$E_1(u, v) = AE_1(u)E_1(v); \tag{3}$$

$$E_1(u) = \exp\left[j\left(\frac{a_x}{2\Delta}\right)^2\right]\frac{1}{\Delta}\left\{\left[C\left(\frac{a_x}{2\Delta} + \Delta\frac{D}{2}\right) - C\left(\frac{a_x}{2\Delta} - \Delta\frac{D}{2}\right)\right] - j\left[S\left(\frac{a_x}{2\Delta} - \Delta\frac{D}{2}\right) - S\left(\frac{a_x}{2\Delta} + \Delta\frac{D}{2}\right)\right]; \tag{4}$$

$$E_1(v) = \exp\left[j\left(\frac{a_y}{2\Delta}\right)^2\right]\frac{1}{\Delta}\left\{\left[C\left(\frac{a_y}{2\Delta} + \Delta\frac{Nl}{2}\right) - C\left(\frac{a_y}{2\Delta} - \Delta\frac{Nl}{2}\right)\right] - j\left[S\left(\frac{a_y}{2\Delta} - \Delta\frac{Nl}{2}\right) - S\left(\frac{a_y}{2\Delta} - \Delta\frac{Nl}{2}\right)\right], \tag{5}$$

where C and S are the cosine and sine Fresnel integral; A is the constant which depends on the parameters of the ultrasonic converter; a_x for +1st and -1st order and a_y are determined by the expressions:

$$a_x = 2\pi\left(u \pm \frac{1}{\Lambda}\right); \quad a_y = 2\pi v.$$

When calculating expression (5) it was proposed that the number of channels N of the modulator is quite large and the summation with respect to the index n will be replaced by integration.

The results of the numerical calculations performed according to formula (3)-(5) give a picture of the field distribution in the presence of quadratic phase errors (see Fig 2). For the calculated curves 1-5, the magnitude of the phase error is 0; $\pi/8$; $\pi/4$; $\pi/2$; π, respectively. It is easy to see that the maladjustment of the lenses L1 and L2 accompanied by the appearance of a quadratic phase error causes "blurring" of the zeros and also a decrease in the principal peak of the field distribution.

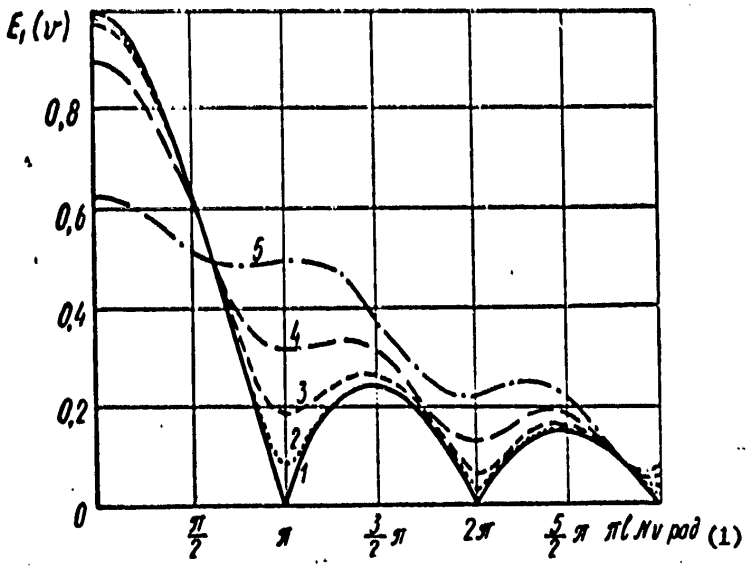

Figure 2

Key:
1. rad

Being given the maximum admissible error at the edge of the modulator $\Delta\phi=\Delta\phi_{max}$, from expression (1) it is possible to find the required precision of setting the lenses L1 and L2. For example, from the calculation it follows that for F_2=1600 mm, D=60 mm, λ=0.63 microns, the precision of the setting must be no worse than 0.18 and 0.36 mm for $\Delta\phi_{max}$ equal to $\pi/4$ and $\pi/2$ respectively.

The nature of the field distribution at the output is influenced in exactly the same way by the change in mutual position of the integrating lens L3 and the recording device; therefore the requirements on the precision of their setting are the same as for the lenses L1 and L2.

The effect of the precision with which the collimator lenses are set on the operation of the system was checked experimentally. For this purpose, a rectangular shaped diaphragm (emitting aperture) was placed at the location of the modulator, and the diffraction distribution of the field in the zero order at the output was recorded for various distances between the lens L3 and the photoreceiver. Fig 3 shows the diagrams obtained from the horizontally oriented emitting aperture 40X5 mm for three positions of the recorder. The right diagram was recorded with the position of the receiving slit closest to the focal plane L3, and the left, with a shift of 1 mm (this corresponds to $\Delta\phi_{max}=\pi/4$). The central diagram is for a shift of 3 mm ($\Delta\phi_{max}=3\pi/4$). For comparison, the points which indicate the calculated level of the first minimum are plotted on the left diagram.

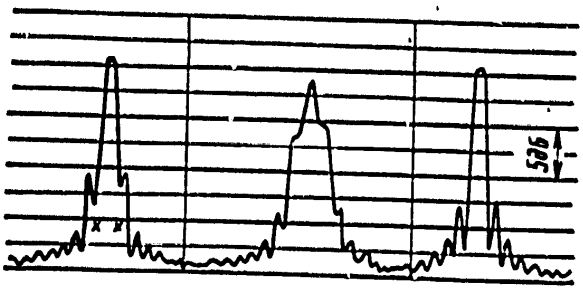

(1)

Figure 3

Key:
1. 5 decibels

A study was also made of the quality of the collimator lenses. For this purpose, the diaphragms of various sizes were placed in the vertical plane between the objectives L2 and L3 so that the light passing through the various sections of the lenses was diffracted. The diaphragms 50X5 and 75X5 mm and also 100X10 and 140X20 mm were used. The experiment did not reveal any significant worsening of the diffraction pattern for shifting of the diaphragm to the edges of the lenses or increasing the dimensions of the diaphragm.

Recorder

The plane of the receiving slit of the device must coincide with the focal plane of the objective L3; otherwise the above-described distortions of the recorded signal occur. The distortion of the signal also occurs if the slit is displaced nonperpendicular to the optical axis, for during movement the receiving slit leaves the focal plane of the objective L3.

Another source of the signal distortions is connected with the finiteness of the width of the receiving slit. In the case of finite width of the slit, the intensity distribution at the output will be expressed by the integral

$$F(\xi_0) = \int_{\xi_0-a}^{\xi_0+a} f(\xi)\, d\xi, \qquad (6)$$

where $f(\xi)$ is the true distribution of the intensity in the plane of the receiving set; ξ_0, ξ are the normalized coordinates; a is the normalized halfwidth of the slit. Using the results of calculating the integral (6), it is possible to find the maximum slit width not distorting the output signal significantly. The calculation shows that the slit width must be no more than 20% of the width of the main lobe of the diffraction distribution with respect to the zero level. For F=1600 mm, D=60 mm, λ=0.63 microns, a slit width of no more than 3 microns is required. In order to enlarge the diffraction pattern, it is possible to use an additional lens. As it is easy to show, in this case the increase in size of the image in

the plane of the receiving slit by n times will be accompanied by an increase in the depth of the image by n^2 times. The requirements on adjustment of the recorder will be lessened by as many times. However, the auxiliary lens must be installed with the same precision with which the recorder is installed in the system without the auxiliary lens.

The experiments confirmed the calculated data pertaining to the selection of the receiving slit width and the effectiveness of using an additional lens to enlarge the diffraction pattern.

Ultrasonic Modulator

Phase distortions of the light wave front connected with defects in the processing and gluing of the couvette and nonuniformities of the water medium and also amplitude and phase distortions caused by dispersion of the voltages which excite the ultrasonic oscillations can arise in the modulator of the given type.

The quality of the couvette used was investigated by recording the diffraction pattern from the light passing through its various sections. The measurements performed both for an empty couvette and for a couvette filled with water demonstrated that the quality of the diagrams remains good to apertures of 50X55 and 60X55 mm (Fig 4, a and b respectively).

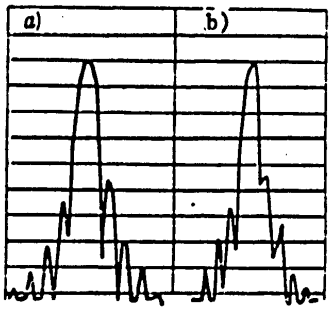

Figure 4

Calculations were also performed pertaining to bending of the plate with piezoconverters which leads to two effects: a change in direction of propagation of the ultrasonic waves and an additional phase shift of them. It is demonstrated that for the case of modulators with a large number of elements the first effect can be neglected, and the additional phase shift turns out to be on the first and higher orders of the diffraction pattern just as the quadratic error in the light distribution. Hence, it follows that for an admissible phase shift of $\pi/2$ and $\pi/4$ the bending of the plate does not exceed a quarter or an eighth of the wave length of the ultrasonic oscillation respectively. If the deflection exceeds the

admissible value, then it is necessary to introduce compensating phase shift into the excitation channels of the piezoconverter.

As a result of the investigation, the requirements on the adjustment and manufacture of the elements of an optical data processing system have been defined. It is demonstrated that the equipment used in this model is suitable for the creation of a practical version of the system. The results of the calculations and the experiments pertaining to the lenses and the recorder are also valid for systems of other types, for example, using electrooptical modulators.

BIBLIOGRAPHY

1. Bondarenko, V. S., et al. See this collection, p 38.

2. Lambert, L. B.; Arm, M.; Aymet, A. ZARUBEZHNAYA RADIOELEKTRONIKA [Foreign Radioelectronics], No 8, 1968, p 3.

CALCULATION OF THE INTENSITY OF LIGHT SCATTERED BY ACOUSTIC WAVES IN AN $LiNbO_3$ CRYSTAL

[Article by B. S. Abesgauz, V. I. Yevdokimov, A. G. Kuzin, V. V. Soroka, A. S. Shcherbakov]

[Text] The interest in the acoustooptical modulators and deflectors using the phenomenon of light diffraction on ultrasonic waves in crystals is growing with every year. From the point of view of practical applications the high-frequency acoustooptical devices are especially prospective, for the transition to high frequencies will permit significant improvement of the parameters of the modulators and deflectors, for example, it will make it possible to obtain large scanning angles of the laser light beam, to process complex signals with a large product of the frequency band times the duration, and so on.

However, the transition to high frequencies imposes rigid requirements on the materials used in the optical-acoustic devices which must have large photoelastic coefficients, low damping of the sound and have good optical uniformity and transparency.

An important factor is also the degree of perfection of the process of obtaining materials. Out of all the admissible materials known at the present time, the most prospective for the high-frequency acoustooptical devices is the $LiNbO_3$ crystal in which a very low attenuation of the hypersound with high optical and photoelastic properties are combined successfully.

In addition, at the present time the industrial production of quite large lithium-niobate crystals has been mastered. Therefore, a detailed quantitative analysis of the various aspects of the interaction of light and sound waves with different propagation directions and polarizations in $LiNbO_3$ crystals is of interest.

In the present paper a study is made of the results of the numerical calculations of the intensity of the light scattered by sound waves in the crystals. As was demonstrated by one of the authors [1], the general

expression for the intensity of the scattered light during Bragg diffraction of the light on ultrasound in an arbitrary anisotropic medium has the form

$$J_1 = J_0 \frac{k_p^2 L^2}{16} \left(\frac{N_d b N_p}{N_d B^0 N_d} \right)^2. \qquad (1)$$

Here J_1 is the intensity of the diffracted light in the first diffraction order; J_0 is the intensity of the light in the zero order, $k_d = k_d n_d$ and $k_p = k_p n_p$ are the wave vectors of the diffracted and incident light waves; L is the width of the acoustic beam; N_p and N_d are the unit vectors of the polarization of the incident and diffracted light; B^0 is the undisturbed tensor B which is the inverse of the tensor of the relative dielectric constant; b is the second class tensor describing the disturbance of the tensor B caused by deformation of the medium on propagation of the sound wave in it. The components of the perturbation tensor are as follows:

$$b_{jk} = ip_{jklm} q_e U_m^0.$$

Here j, k, ℓ, m = 1, 2, 3; p_{jklm} is the photoelastic tensor of the crystals; q and U^0 are the wave vector and the vector of the sound wave displacement amplitude; i is an imaginary unit.

Formula (1) is valid when the angle of incidence of the light is equal to the Bragg angle, the intensity of the sound wave is small, the angles of incidence and diffraction of the light are small.

Thus, in order to find the intensity of the diffracted light for any directions and polarizations of the light and sound waves it is necessary to know the magnitudes and directions of the vectors q, U^0, k_p and k_d which we shall find by solving the Christoffel [2] and Fresnel [3] equations for the corresponding directions of propagation of sound and light waves. In the general case the solutions of these equations and the calculations by formula (1) present an extraordinarily complex and difficult problem. However, if we are dealing with a specific crystal, with known acoustic and optical properties, then it is expedient to perform the same calculations on a computer as for the $LiNbO_3$ crystal.

We shall give the directions of the wave vector q of the sound wave by the spherical angular coordinates θ (the angle between the optical axis c and q) and ϕ (the azimuthal angle). Considering that the photoelastic properties of lithium niobate are characterized by the 3d-order axis of symmetry coinciding with the optical axis c, the calculations were performed for the angles θ from 0 to 180° and ϕ from 0 to 120° with a step of 10°.

In the calculations it was proposed that the angles of incidence and scattering of the light are so small that the incident and scattered light beams can be considered colinear and perpendicular to the vector q. This condition is quite well satisfied for all of the real sound frequencies if the diffraction is not accompanied by rotation of the light polarization plane.

In the case of anisotropic diffraction [4] of the light on the ultrasound accompanied by rotation of the light polarization plane, the condition of smallness of the angles of incidence and diffraction occur only in the weakly anisotropic media in some sound frequency range. Therefore the results presented below from calculating the intensity of the diffracted light for anisotropic diffraction in $LiNbO_3$ are of an approximate nature, for the optical anisotropy of the lithium niobate is quite large. Nevertheless, these calculations are of definite interest, for they permit at least qualitative solution of the problem of the optimal configuration of the anisotropic Bragg diffraction for which the intensity of the diffracted light is the greatest.

The values of the elastic moduli of $LiNbO_3$ for the calculations were taken equal to the following in 10^{11} dynes/cm^2 [5]: C_{11}=20.16; C_{12}=5.67; C_{13}=7.50; C_{14}=0.93; C_{33}=24.50; C_{44}=6.01.

The $LiNbO_3$ crystal is a strong piezoelectric; therefore for calculations of q and U^0 it is necessary to consider the piezo effect. In particular, these vectors for any given direction of the sound wave with a unit vector of the wave normal n were determined by solving the following tensor equations [6]:

$$\left(q^2\Lambda - \omega^2 + \frac{4\pi q^2}{\rho}\frac{nf\cdot nf}{\varepsilon_n}\right)U^0 = 0; \qquad (2)$$

$$\left|q^2\Lambda - \omega^2 + \frac{4\pi q^2}{\rho}\frac{nf\cdot nf}{\varepsilon_n}\right| = 0, \qquad (3)$$

where ω is the frequency of sound, ρ is the density of the medium, Λ is the symmetric tensor of the second class with the components $\Lambda_{ik} = \frac{1}{\rho}\lambda_{iklm}n_in_m$, λ_{iklm} is the elastic tensor, f is the 2d class tensor with the component $f_{ik}=\beta_{ik\ell}n_\ell$, $\beta_{ik\ell}$ is a piezoelectric tensor, $\varepsilon_n=n\varepsilon n$ is the value of the low-frequency relative dielectric constant in the direction of propagation of the sound wave, nf·nf is the tensor-dyad with the component $(nf\cdot nf)_{ik}=(nf)_i\cdot(nf)_k$. If we set the piezo moduli equal to 0 in (2) and (3) we obtain the ordinary Christoffel equations [2].

For the solution of these equations, independent tensor components of the low-frequency relative dielectric constant were used [7] ε_{11}=44.0 and ε_{33}=29.0 and the independent components of the piezoelectric tensor (in matrix notation) were taken as follows in 10^5 Cgs electrostatic units [7]: β_{33}=3.90; β_{31}=0.60; β_{15}=11.1; β_{16}=7.5.

For calculations of q and U^0, the density of $LiNbO_3$ was taken equal to 4.6444 g/cm^3 [5]. Finally, the values of the components of the photoelastic tensor were taken from reference [8]: p_{11}=0.025; p_{12}=0.079; p_{13}=0.089; p_{33}=0.086; p_{31}=0.168; p_{41}=0.158; p_{44}=0.019; p_{14}=0.100. In addition, B^0_{11}=0.1936 and B^0_{33}=0.230 [8].

The calculated angular relations for the intensity of the diffracted light in $LiNbO_3$ for the directions and polarizations of light and sound (quasilongitudinal L in Fig a and slow quasitransverse S_M in Fig b, c) most effective from the point of view of acoustooptical interaction are presented in the figure. The relative intensity of the diffracted light J_1/J_0 on the graphs is shown as a function of the angle α which determines the position of the light beams in the plane perpendicular to q for different angles θ: Δ — 31°; O — 61°; ● — 91°; ▲ — 121°. The angles α are reckoned clockwise from the normal to the plane formed by the vectors q and c. All of the calculations were performed for the light wave length in a vacuum λ_0=1 micron, the sound wave intensity P=1 watt/cm^2 (here the results of the calculations do not depend on the sound frequency) and L_{B3}=1 cm. On the graph the letters e and o denote the extraordinary and ordinary light beams respectively, and, for example, the case o-e indicates that the incident wave is ordinary, and the diffracted wave is extraordinary.

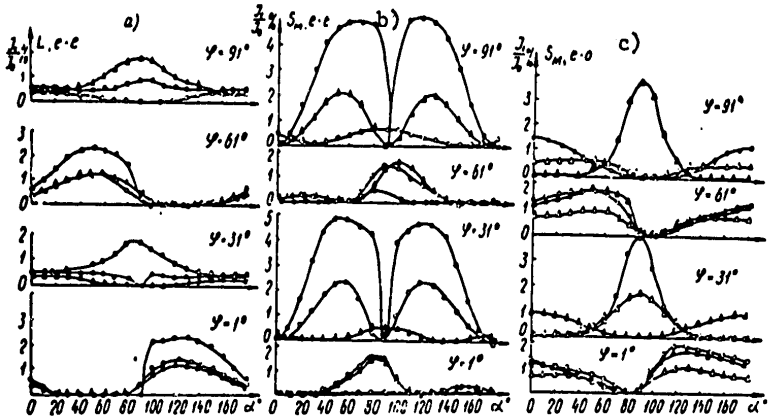

For the selected L_{B3}, P and λ, the values of J_1/J_0% coincide with an accuracy to the coefficient $2.12 \cdot 10^{-18}$ sec^3/g with the effective value of the acoustooptical Q-factor M_2. The calculations demonstrated that in $LiNbO_3$ effective (M_2~3) isotropic and anisotropic diffraction of the light on a fast quasi-shift wave is possible especially for θ equal to 30, 60 and 120°. The maximum values of M_2 are ~4.5 on a longitudinal wave, and ~10 on a slow shear wave.

The presented angular functions can be used when designing acoustooptical devices on the $LiNbO_3$ crystals.

In this case for $|U^0|$=1 it is necessary to know the velocities and polarizations of the sound waves in the corresponding directions (see the table).

ϑ°	φ°	Продольная волна (1)				Медленная сдвиговая волна (2)				Быстрая сдвиговая волна (3)			
		$V \cdot 10^5 \frac{см}{с}$	U_x°	U_y°	U_z°	$V \cdot 10^5 \frac{см}{с}$	U_x°	U_y°	U_z°	$V \cdot 10^5 \frac{см}{с}$	U_x°	U_y°	U_z°
30	0	7,28	0,444	0,002	0,896	3,68	0,424	−0,881	−0,208	3,98	0,789	0,473	−0,392
30	30	7,27	0,383	0,221	0,897	3,45	0,500	−0,866	0,000	4,00	0,776	0,448	−0,443
30	60	7,28	0,224	0,384	0,896	3,68	0,551	−0,808	0,208	3,98	0,804	0,447	−0,392
30	90	7,31	0,000	0,451	0,893	3,91	0,000	0,893	−0,451	3,92	1,000	0,000	0,000
60	0	7,00	0,795	−0,042	0,606	3,94	0,434	0,737	−0,518	4,40	0,425	−0,674	−0,604
60	30	6,88	0,700	0,104	0,589	3,64	0,510	0,295	−0,808	4,39	0,500	−0,866	0,000
60	60	7,00	0,361	0,709	0,606	3,94	0,555	0,006	−0,518	4,40	0,372	−0,705	0,604
60	90	7,42	0,000	0,820	0,573	4,06	0,000	0,573	−0,820	4,08	1,000	0,000	0,000
90	0	6,60	1,000	0,000	0,000	4,11	0,000	0,622	−0,783	5,04	0,000	0,783	0,622
90	30	6,82	0,860	0,497	−0,116	3,96	0,100	0,057	0,993	4,73	0,500	−0,866	0,000
90	60	6,60	0,500	0,866	0,000	4,11	0,539	−0,310	−0,783	5,04	0,678	−0,392	0,622
90	90	6,82	0,000	0,993	0,116	3,96	0,000	0,116	−0,993	4,73	1,000	0,000	0,000
120	0	7,00	0,795	0,042	−0,606	3,94	0,434	−0,737	0,518	4,40	0,425	0,674	0,604
120	30	7,43	0,710	0,410	−0,573	4,06	0,496	0,286	0,820	4,08	0,500	−0,866	0,000
120	60	7,00	0,434	0,667	−0,606	3,94	0,422	−0,744	−0,518	4,40	0,796	0,030	0,604
120	90	6,88	0,000	0,808	−0,589	3,64	0,000	0,000	0,000	4,39	0,000	0,589	0,808

Key:
1. Longitudinal wave
2. Slow shear wave
3. Fast shear wave

BIBLIOGRAPHY

1. Soroka, V. V. AKUSTICHESKIY ZHURNAL [Acoustics Journal], 19, 6, 8, 77, 1973.

2. Fedorov, F. I. TEORIYA UPRUGIKH VOLN V KRISTALLAKH [Theory of Elastic Waves in Crystals], Nauka, 1965.

3. Fedorov, F. I. OPTIKA ANIZOTROPNYKH SRED [Optics of Anisotropic Media], Izd. AN BSSR, Minsk, 1958.

4. Dixon, R. W. IEEE J. OF QUANTUM ELECTRONICS, QE-3, 1967, p 85.

5. Nassau, K.; Levinstein, H. J.; Goiacono, G. M. J. PHYS. CHEM. SOL., No 27, 1966, p 983.

6. Soroka, V. V. IZVESTIYA VUZOV. FIZIKA [News of the Institutions of Higher Learning. Physics], No 9, 1969, p 129.

7. Spencer, E. G. PROC. IEEE, No 12, 1964, p 2074.

8. Lemanov, V. V.; Shakin, O. V. FTT [Solid State Physics], No 14, 1972, p 229.

SOME CHARACTERISTICS OF THE ACOUSTOOPTICAL INTERACTION IN α-QUARTZ AND LITHIUM NIOBATE

[Article by V. V. Soroka, A. I. Shishkin, A. S. Shcherbakov]

[Text] The application of crystal sound guides in acoustooptical devices, for example, in deflectors is of great interest at the present time. A number of crystals are known with high efficiency of their acoustooptical interaction, but the most widespread materials are α-quartz (α-SiO_2) and lithium niobate.

The purpose of this paper was investigation of some of the characteristics of acoustooptical interaction in the indicated crystals, which is needed for optimization of the configuration of the scattering on creation of the acoustooptical devices.

For excitation of longitudinal elastic waves in α-quartz, a thin-film CdS-converter was applied to the z-cut of the crystal. In the $LiNbO_3$ sample, the longitudinal and slow transverse elastic waves propagated along the x-axis were excited as a result of the natural piezo effect. The type of elastic waves was controlled by the oscillograms of the echoes which demonstrated that there was no fast shear wave in the lithium niobate sample. The length of the acoustooptical interaction in the α-quartz was ~10^{-3} m, and in lithium niobate it was ~10^{-2} microns.

The experiment was performed by the setup in [1] in which the polarization of the incident and diffracted light was controlled. The light source was the He-Ne laser, λ_0=0.6328 microns. The range of operating frequencies of the coaxial-strip microwave channel was 0.5-0.9 gigahertz with a power of the signal source of about 1 watt.

In the experiments with lithium niobate, a study was made of the light diffraction both on the longitudinal elastic waves without rotation of polarization and on the slow shear wave with rotation of polarization. As is demonstrated, for example, in [2] the most convenient section of the angular frequency functions for use in the deflectors is the region near a frequency of

$$f_0 = \frac{V}{\lambda_0}\sqrt{|n_0^2 - n_e^2|}\sin|\varphi|.$$

Here V is the speed of sound; λ_0 is the wavelength of the light in a vacuum; n_0 and n_e are the principal indexes of refraction of the crystal; ϕ is the angle between the optical axis of the medium and the dispersion plane on which the wave vectors of the incident light and the elastic wave lie.

The selection of the orientation of the dispersion plane thus determines the value of f_0. The angle $\phi=-12°$ which corresponds to $f_0=0.82$ gigahertz.

The experiment was performed in the Bragg diffraction regime, for the condition indicated in [3] $\lambda_0 L/n\Lambda^2 \geq 1$ (L is the interaction length of the light with hypersound; Λ is the elastic wave length) jointly with the requirement of the quality of the angle of incidence to the Bragg angle were satisfied. The light scattering configuration on hypersound in the lithium niobate ($\phi=-12°$) and α-quartz ($\phi=0$) samples is presented in Fig 1, a and 1, b respectively.

The effective photoelastic constants corresponding to the dispersion configuration (Fig 1) and using natural polarizations of the incident light and also the acoustooptical interaction band pertain to the investigated characteristics of the acoustooptical interaction.

Photoelastic Constants

The values of the effective photoelastic constants for α-quartz and lithium niobate under the assumption of small angles of incidence θ_i and diffraction θ_d of light can be found by the results of reference [4]. The ratio of the intensities of the diffracted light J_1 to the intensity of the incident light J_0 is defined as:

$$\frac{J_1}{J_0} = \frac{k_i^2 L^2}{16}\left(\frac{N_d p \gamma N_i}{N_d \varepsilon^{-1} N_d}\right)^2, \qquad (1)$$

where $k_i=2\pi n_i/\lambda_0$; n_i is the index of refraction for the incident light; ε^{-1} is the tensor of the inverse of the tensor of the dielectric constant 2d class; p is the photoelastic tensor 4th class; γ is the deformation tensor; N_i and N_d are the polarizations of the incident and diffracted light.

Let us propose that the elastic wave is plane and the deformation tensor

$$\gamma = \frac{i}{2}\frac{2\pi f}{V} U(q\cdot n + n\cdot q).$$

Here f and V are the frequency and phase velocity of the elastic wave; $U=U_q$ is the shift vector in the elastic wave; n is the wave normal of the sound; the dot indicates the dyad product.

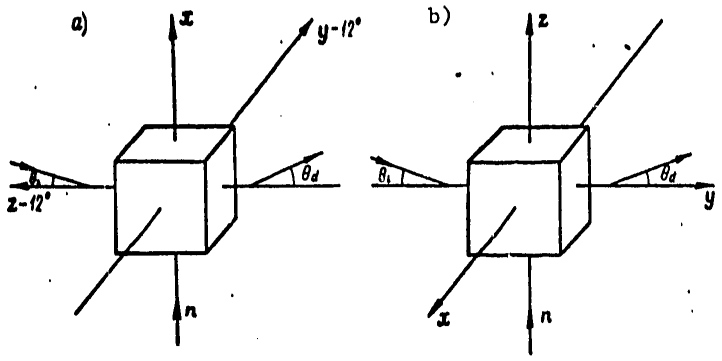

Figure 1

Then formula (1) is conveniently rewritten as:

$$\frac{J_1}{J_0} = \frac{\pi^4 L^2 n_i^2 n_d^4 U^2 f^2}{4\lambda_0^2 v^2} \{N_d p (\mathbf{n}\cdot\mathbf{q} + \mathbf{q}\cdot\mathbf{n}) N_i\}^2, \qquad (2)$$

where n_d is the index of refraction for diffracted light.

The expression for the effective photoelastic constant enters into (2) and has the form

$$p_{\text{эфф}} = \frac{1}{2} N_d p (\mathbf{n}\cdot\mathbf{q} + \mathbf{q}\cdot\mathbf{n}) N_i. \qquad (3)$$

(1)

Key:
1. eff

Let us determine the photoelastic constants in a lithium niobate sample of selected orientation (Fig 1, a). Let us introduce the polarization unit vectors:

$$\mathbf{t} = (\cos\theta_i, \sin\varphi \sin\theta_i, \sin\theta_i \cos\varphi);$$
$$\mathbf{r} = (\cos\theta_d, -\sin\theta_d \sin\varphi, -\sin\theta_d \cos\varphi);$$
$$\mathbf{s} = (0, \cos\varphi, \sin\varphi).$$

Then

$$\left.\begin{aligned} \mathbf{N}_i &= \mathbf{t}\sin\psi_i + \mathbf{s}\cos\psi_i; \\ \mathbf{N}_d &= \mathbf{r}\sin\psi_d + \mathbf{s}\cos\psi_d. \end{aligned}\right\} \qquad (4)$$

The values of ψ_i and ψ_d can assume only discrete values of $\pi m/2$, where m=... -2, -1, 0, 1, 2 ... This is caused by the necessity for investigating only the natural (ordinary and extraordinary) polarizations of the incident

and diffracted light for the given dispersion configuration. The angles ψ_d and ψ_i can be related by the expression: $\psi_d=\psi_i+\pi m/2$ where the even m corresponds to diffraction without polarization rotation, and odd m corresponds to diffraction with polarization rotation.

Substituting (4) in (3), we obtain the expressions for photoelastic constants p_{eff} for diffraction on longitudinal sound without polarization rotation for $N_i \| N_d \perp n$; $\psi_i=\psi_d=0$

$$p_{1\uparrow\uparrow\uparrow} = p_{12}\cos^2\varphi + p_{31}\sin^2\varphi - p_{41}\sin 2\varphi, \qquad (5)$$

for $N_i \| N_d \| n$; $\psi_i = \psi_d = \pi/2$

$$p_{2\uparrow\uparrow\uparrow} = p_{11}. \qquad (6)$$

Expressions (5) and (6) are found in accordance with the results of [5].

Using the numerical values of the components of the photoelastic tensor for lithium niobate from reference [5] in all of the calculations, we obtained: $p_{1eff}=0.149$; $p_{2eff}=0.025$. This leads to the ratio of the intensities of the corresponding light beams of order 10^{-2}. In the experiment, the diffracted light beam with photoelastic constant p_{2eff} was not detected. It is possible to demonstrate that p_{eff} for diffraction with polarization rotation on the longitudinal mode is approximately 15 times less than $p_{1\ eff}$ which corresponds to $\sim 10^{-2}$ with respect to intensity. The signals also were not detected experimentally.

On diffraction on an elastic shear wave with polarization rotation, we have:

$$p_{\underset{(1)}{\uparrow\uparrow\downarrow}} = p_{\underset{(2)}{\uparrow\downarrow\uparrow}} = \cos\varphi\,[p_{11}(qz) + p_{66}(qy)] - \sin\varphi\,[p_{41}(qz) + p_{14}(qy)].$$

Key:
1. $p_{3\ eff}$; 2. $p_{4\ eff}$

where $(qz)=\cos\alpha$; $(qy)=\sin\alpha$; α is the angle between the shift vector in the elastic wave and the axis. The solution of the elastic problems considering the piezo effect for the given case leads to a value of $\alpha=30°$, which agrees with the results of reference [6]. The numerical values are as follows: $p_{3\ eff}=p_{4\ eff}=0.053$. In our case, on diffraction of the light on the shear wave without polarization rotation $p_{eff}=0$.

Thus, from the calculation it follows that:

$$p_{3\ eff}/p_{4\ eff} = 1;\ p_{1\ eff}p_{3\ eff} = p_{1\ eff}/p_{4\ eff} = 2.81.$$

The ratios of the photoelastic constants obtained experimentally are as follows:

$$p_{3\ eff}/p_{4\ eff} = 1.02;\ p_{1\ eff}/p_{3\ eff} = 2.87;\ p_{1\ eff}/p_{4\ eff} = 2.97.$$

The photoelastic constants for α-quartz are calculated analogously. The polarization unit vectors

$$\mathbf{t} = (0,\ \sin\theta_i,\ \cos\theta_i);$$
$$\mathbf{r} = (0,\ -\sin\theta_d,\ \cos\theta_d);$$
$$\mathbf{s} = (1,\ 0,\ 0),$$

and the vectors

$$\mathbf{N}_i = \mathbf{t}\sin\psi_i + \mathbf{s}\cos\psi_i;$$
$$\mathbf{N}_d = \mathbf{t}\sin\psi_d + \mathbf{s}\cos\psi_d$$

It is possible to introduce the relation: $\psi_d = \psi_i + \pi m/2$.

Then for effective photoelastic constants for light diffraction without polarization rotation on the longitudinal mode, we obtain for $\mathbf{N}_i \| \mathbf{N}_d \| \mathbf{n}$

$$p_{5\ eff} = p_{33}\cos^2\theta - p_{13}\sin^2\theta,$$

for $\mathbf{N}_i \| \mathbf{N}_d \perp \mathbf{n}$

$$p_{6\ eff} = p_{13}.$$

The numerical values of photelastic components are presented in [7]; hence

$$p_{6\ eff}/p_{5\ eff} = 2.27,$$

and their experimentally measured ratio is 2.56.

The correspondence of the calculated and experimental data in the limits of 15% is satisfactory, for the magnitudes of the photoelastic constants with respect to different sources have dispersion of the same order.

Acoustooptical Interaction Band

The band of the acoustooptical device is determined by the band of the piezoconverter with the electric excitation system and the band of the effective acoustooptical interaction. It is known [8] that for hypersound frequencies exceeding the frequency

$$F_{\min} = \left(\frac{n v^3}{\lambda_0 L}\right)^{1/2},$$

the acoustooptical interaction band

$$\Delta f = \frac{1{,}77 n v^2}{\lambda_0 L f}. \qquad (7)$$

The investigation of the interaction band was performed in [9], where a lithium niobate sample was used, along the z-axis of which longitudinal sound was propagated. It is indicated here that the ratio (7) is valid for $\Delta f/f \ll 1$.

In this paper, the acoustooptical band was measured for the cases of the dispersion configuration in Fig 1. The electric feed circuits were tuned on each frequency in the operating band. On variation of the angle of incidence of the light on the sample in both directions from the optimal (Bragg) the intensity of the diffracted light diminished. In the experiment the values of the angles of incidence were recorded for which the intensity of the signal was cut in half along with the angle θ_1 corresponding to the maximal intensity in the diffracted light.

The results of the measurements and the calculation curves in the case of light diffraction on longitudinal elastic waves without polarization rotation in α-quartz and lithium niobate are presented in Figures 2, a and 2, b respectively. The notation is as follows: θ_1 -- solid line -- calculation, O - experiment; Δf -- dotted line -- calculation, X -- experiment.

The significant difference in magnitudes of the acoustooptical band in the investigated samples is connected with the fact that the interaction length L in the quartz was approximately 10 times less than in the lithium niobate.

An estimate was also made of the acoustooptical band on diffraction of the light with rotation of the polarization on a slow shear wave in lithium niobate. For a frequency of 0.82 gigahertz which is optimal for scanning, the acoustooptical band turned out to be equal to 150 megahertz. This exceeds by 5 times the same band in the same crystal and on the same frequency but without rotation of the polarization plane.

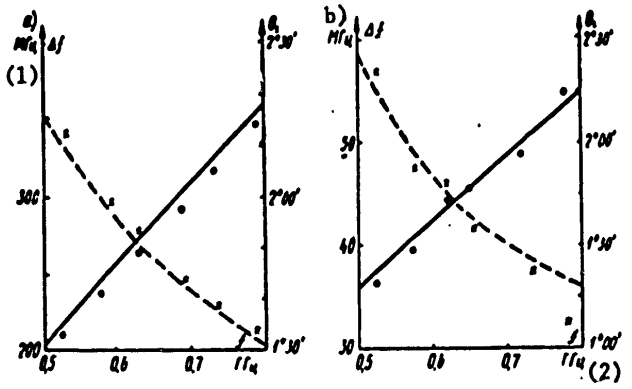

Figure 2

Key: 1. megahertz; 2. gigahertz

On the basis of the presented results it is possible to conclude that the procedure used in this paper for calculation and measurement is suitable for selecting the dispersion configuration on creation of the acousto-optical devices.

BIBLIOGRAPHY

1. Parks, J. K. IEEE TRANS., SOM-17, No 6, 1969, p 686.

2. Balakshiy, V. I.; Voloshinov, V. B.; Parygin, V. N. RADIOTEKHNIKA I ELEKTRONIKA [Radioengineering and Electronics], Vol 16, No 11, 1971, p 2226.

3. Rytov, S. M. IZV. AN SSSR. SER. FIZICH. [News of the USSR Academy of Sciences, Physics Series], No 2, 1937, p 223.

4. Soroka, V. V. AKUSTICHESKIY ZHURNAL [Acoustics Journal], Vol 19, No 6, 1973, p 877.

5. Lemanov, V.V. ; Shakin, O. V.; Smolenskiy, G. A. FTT [Solid State Physics], Vol 13, No 2, 1971, p 533.

6. Spencer, E. G.; Lenzo, P. V.; Ballman, A. A. PROC. IEEE, Vol 54, No 10, 1966, p 2074.

7. Reintjes, J.; Schulz, M. B. J. APPL. PHYS., No 39, 1968, p 5254.

8. Gordon. TIIER, Vol 54, No 10, 1966, p 181.

9. Brienza, M. J. IEEE TRANS.,IECT, No 1, 1969, p 62.

OPTICAL METHODS OF INVESTIGATING THE CHARACTERISTICS OF RADIOTELESCOPES

[Article by I. A. Vodovatov, G. K. Vinogradov, M. G. Vysotskiy, S. A. Rogov]

[Text] In recent times the optical methods of [1, 2] have become more and more widespread in antenna measurement engineering. As a result of the creation of coherent radiation sources (lasers), the possibility has occurred for the simulation of the antennas in the optical band which in a number of cases has simplified the investigation of their characteristics. Holography which permits simulation of antennas with different laws of variation of phase and amplitude in the aperture is opening up new possibilities in this area. The indicated methods are especially prospective for large antennas and antennas of complex configuration where obtaining the characteristics by direct measurement or by calculation is connected with significant difficulties.

This report contains a description of the procedure, and some of the experimental results are presented with respect to optical simulation of the antennas of radiotelescopes. In particular, a study was made of the radiation patterns and the frequency-space characteristics of the radiotelescopes with antennas of variable profile: the large Polkovo radiotelescope and the RATAN-600 radiotelescope [3]. The experiments were performed for uniform cophasal excitation and also for various laws of variation of phase amplitude of the field in the aperture which were given by especially manufactured holographic filters. In addition, by using the holographic method the study was made of the polarization characteristics of the antenna emission.

The schematic for measuring the radiation pattern is similar to that described in references [2, 4]. The beam of coherent light from the laser is expanded using a telescopic system and illuminates the optical model of the antenna. The diffraction pattern in the focal plane of the collecting lens corresponds to the radiation pattern of the antenna. The difference of the given system from the systems used by the authors of references [2, 4] consists in using the holographic filter in addition to the model of the antenna aperture. The filter is executed in the form of a nonuniform diffraction grating and permits simulation of the phase and polarization field distribution in the aperture. The radiation pattern is recorded in the case of noncophasal excitation in the first diffraction orders.

When checking the effectiveness of the method a study was made of the model of an antenna having rectangular aperture, the phase of which varied according to a quadratic law. The form of the diffraction spot in the first diffraction order corresponded to the radiation pattern of the antenna in the presence of quadratic phase errors. When the uniform diffraction grating was used as the holographic filter, the distributions in the first and null diffraction orders were analogous. The results obtained were compared with the data of reference [5] where a study was made of the effect of the quadratic phase errors on the operation of the optical data processing system.

In addition, by using special diffraction gratings, the distribution of the cross-polarization component of the field in the aperture of the symmetric antennas of the type of a paraboloid of rotation [6] and asymmetric antennas of the type of antennas of variable profile was simulated [7].

In order to investigate the space-frequency characteristics of the radiotelescope antennas, two methods were used. The first method was connected with mutual displacement of two identical apertures of the antenna models with the information on the phase and amplitude distribution and the antenna aperture recorded on them by the holographic procedure [8]. As is known [9], the space-frequency characteristic of the antenna in the case of operation with incoherent sources coincides with the autocorrelation function $R(x_0,y_0)$ of the field distribution $E(x,y)$ in the antenna aperture

$$R(x_0, y_0) = \iint E(x, y)\, E^*(x - x_0, y - y_0)\, dx\, dy,$$

where x,y are the coordinates in the plane of the antenna aperture; x_0,y_0 is the mutual displacement of two apertures. If we illuminate the apertures perpendicularly to the beam of coherent light incident on them with a plane phase front, then, depending on the experimental conditions in the zero or first orders of the diffraction, the energy will be proportional to the value of the autocorrelation function or the square of it.

Measurements were made of the space and the frequency characteristics for the antenna of the RATAN-600 radiotelescope on the optical models corresponding to operation on a wave length of λ=1.6 cm for angles of elevation of θ=0, 30, 90°. The measurements were made in the zero order for the cases of uniform field distribution in the aperture and the distribution of the field falling on the edges of the aperture. It was discovered, in particular, that a decrease in the field amplitude at the edges of the antenna is accompanied by a rise of the space-frequency characteristic on the average frequencies and a decrease of it on the high frequencies. As an example, Fig 1 shows the images of models of the antenna apertures of the RATAN-600 radiotelescope shifted by half the longitudinal dimension (antenna diameter 600 meters) corresponding to operation on λ=1.6 cm, θ=90°. The radius of the outside circle r≈12 mm, the thickness of the ring δ=0.25 mm, the angular dimension of the ring 110°.

In Fig 2 we have the normalized cross sections of the space-frequency characteristics for the given case with uniform distribution (curve 1) and amplitude distribution falling on the edges with respect to the cosinusoidal wall to a value equal to ~50% of maximum (see curve 2). The cross sections were obtained for the shift of the apertures along the x-axis.

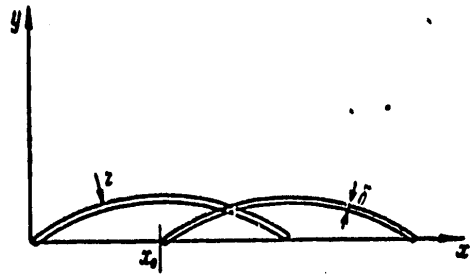

Figure 1

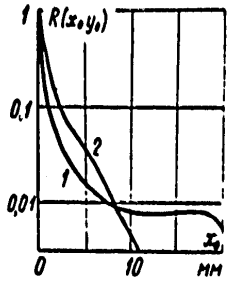

Figure 2

Experiments were also performed with respect to measuring the space-frequency characteristics for the noncophasal distribution. The first results indicating the effectiveness of the method were obtained.

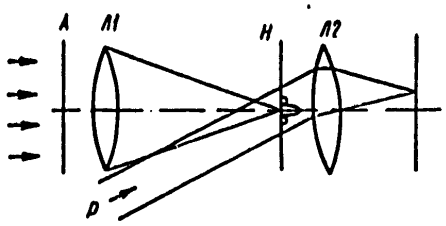

Figure 3

The second method of investigating the space-frequency characteristic is based on using the Van der Lugt filters [10]. The radiation pattern of the model of the antenna A is recorded holographically using the reference beam P on the photographic plate H placed in the focal plane o f the lens L1 (see Fig 3). After the corresponding photographic processing, the hologram which represents the Van der Lugt filter is illuminated through the same aperture. In this case the field distribution in the first diffraction order, that is, in the direction of reference beams when recording the hologram is proportional to the square of the modulus of the radiation pattern of the antenna. As is easy to show [9], the Fourier transformation from this distribution is proportional to the autocorrelation function of the distribution in the aperture

$$F\{|f(u, v)|^2\} \sim R(x_0, y_0),$$

where f(u,v) is the field distribution in the plane of the hologram from the aperture of the model of the antenna; realizing the Fourier transformation using the L2 lens, in its focal plane we obtain the autocorrelation distribution function in the aperture, that is, the space-frequency characteristic of the radiotelescope antenna.

The indicated procedure was used to investigate the models of the antennas of the RATAN-600 radiotelescope and the large Polkovo radiotelescope for different angles of elevation. The autocorrelation spots were photographed. The results obtained correspond to the calculation data.

The performed experiments demonstrated the efficiency of the methods of optical simulation for investigation of the characteristics of radiotelescopes.

BIBLIOGRAPHY

1. Wild, J. PROC. ROY. SOC. AUSTR., No 262, 1961, p 84.

2. Bakhrakh, L. D., et al. ANTENNY [Antennas], No 2, Svyaz', 1967, p 33.

3. Yesepkina, N. A.; Korol'kov, D. V.; Parnyskiy, Yu. N. RADIOTELESKOPY I RADIOMETRY [Radiotelescopes and Radiometers], Nauka, 1973.

4. Gel'freykh, G. B.; Korzhavin, A. N. RADIOTEKHNIKA I ELEKTRONIKA [Radioengineering and Electronics], Vol 13, No 7, 1968, p 1176.

5. Vysotskiy, M. G. See the present collection, p 61.

6. ANTENNY SANTIMETROVYKH VOLN. [Centimeter Wave Antennas], edited by Ya. N. Feld, Sovetskoye radio, 1950.

7. Yesepkina, N. A., et al. RADIOTEKHNIKA I ELEKTRONIKA, No 6, 1961, p 3.

8. Françon, M., et al. C. R. ACAD. SC., Paris, No 263, 1966, p 237.

9. Goodman, J. VVEDENIYE V FUR'YE-OPTIKU [Introduction to Fourier Optics], Mir, 1970.

10. Matsumoto, K. T. OSE. JAP. JOURN. APPL. PHYSICS, No 7, 1968, p 621.

INVESTIGATION OF SURFACE ROUGHNESS BY COHERENT OPTICAL METHODS

[Article by T. G. Alksis, M. M. Butusov, N. V. Yermakova]

[Text] The shape of the microunevennesses of the rough surfaces of the majority of actual objects is described by a random function of the coordinates $\zeta(x,y)$. One of the simplest characteristics of the random surface is the mean square deviation (dispersion) of the surface with respect to the average level

$$\sigma^2 = \int_{-\infty}^{\infty} \zeta^2 W(\zeta, x)\, d\zeta,$$

where $W(\zeta,x)$ is the distribution probability density of the surface altitudes. At the present time there is no solution to the general problem of the extraction of information on the structure of the statistically nonuniform surfaces from the light dispersion characteristics. Theoretically, this problem was investigated in [1] for two limiting cases.

The actual surface most frequently is multiparametric, that is, it is an intermediate type of surface between two calculated approximations. The theoretical analysis of the dispersion process is complicated in this respect. However, in order to develop the criteria for coherent-optical analysis of the quality of processing of the surfaces it is useful to find empirical relations between the characteristics of the scattered field and the surface characteristics (for example, the dispersion).

Determination of Roughness by the Scattering Index of Coherent Light

In order to record the scattering index, the samples were illuminated by the undiluted beam of the LG-36 laser. The special measurements and also the calculations [1] indicate that the variation of the illumination angle within the limits from 0 to 30° has no effect on the scattering index. In order to simplify the optical system, we used the illumination of the sample at an angle of 20°. The intensity of the scattered light was measured by the arc scanning photomultiplier, the output signal of which was fed to the vertical amplifier of the two-coordinate pen recording device. The movement of the photomultiplier was synchronized with the horizontal displacement of the pen recorder slide. Fig 1 shows the normalized scattering indexes of glass plates treated with standard

abrasive powder with an average grain size of 5, 7, 10, 14, 20 and 28 microns. The normalization was carried out by variation of the intensity of the incident light using a polaroid. From Fig 1, a clear trend is noted toward constriction of the index with a decrease in abrasive grain size, that is, with improvement of quality of treatment of the surface. This effect can be explained within the framework of the method of the tangential plane, according to the conclusions of which the index for the surface with normal distribution of slopes depends on the ratio of the correlation radius ℓ to the dispersion of the unevennesses σ. For example, for normal illumination

$$I(\theta) \sim \frac{1-\cos\theta}{\cos^3\theta}\exp-\left\{\frac{\cos^2\theta}{2\sin^2\theta\gamma^2}\right\}, \qquad (1)$$

where θ is the observation angle reckoned from the normal; $\gamma^{-2}=2\sigma^2/\ell^2$.

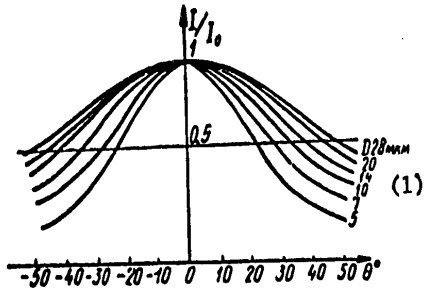

Key: 1. microns

Figure 1

The shape of the microprofilograms taken on the standard profilometer permits the proposition that as the abrasive grain size diminishes, a gradual "truncation" of the tips of the large-scale unevennesses takes place. Here the average correlation size of the surface (the large-scale nonuniformities are considered) varies little, and the altitude dispersion σ^2 decreases. According to formula (1), with a decrease in σ/ℓ the scattering index must become constricted. Obviously, the diffraction on the microunevennesses covering the large unevennesses has a smaller effect on the scattering index (as follows from the perturbation theory) than the processes of geometric reflection from the faces of these nonuniformities. Therefore, on the whole this decrease implies compression of the scattering index.

The analysis of indexes obtained demonstrated that their shape can be described with a sufficiently degree of accuracy by the following empirical formula:

$$\frac{I(\theta)}{I(0)}=\frac{1}{1+A\frac{\theta^2}{B^2}},$$

where A is the constant defined by the material of the sample and the experimental conditions (in our case A is 0.76); B is the halfwidth of the experimental curves obtained.

Thus, by the measured halfwidth of the scattering index it is possible to find the mean square deviations of the surface with respect to the average level which is the quality criterion of the processing of the surface.

Determination of Surface Roughness Using a Prism Interferometer

Another method for determining the degree of surface roughness is the use of an interferometer with a total internal reflection prism [2]. The optical diagram of the experiment is shown in Fig 2. The interferomter 1 with the sample 2 is illuminated by a collimated beam from the LG-36 laser. In the focal plane 4 of the lens 3 spatial separation of the light signals reflected from the hypotenuse of the prism I_0 and from the sample I takes place. The magnitude of these signals is measured by the photoreceivers 5 and 6.

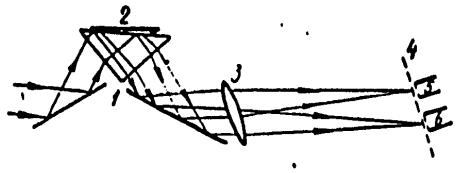

Figure 2

Using the expression for the reflection coefficient of the coherent component of the field for the surface with normal distribution of the heights of the unevennesses [1]

$$v(\psi) = \exp(-[2k^2\sigma^2\sin^2\psi), \qquad (2)$$

the ratio of the measured signals can be represented as follows:

$$I/I_0 = c(\psi)\exp(-2k^2\sigma^2\sin^2\psi), \qquad (3)$$

where k is the wave vector; ψ is the sliding angle of the light with respect to the sample; $c(\psi)$ is the constant for the given ψ.

Thus, by the measured ratio I/I_0, knowing the angle of incidence of the beam on the sample it is possible from expression (3) to determine σ^2.

In order to achieve satisfactory spatial separation of the signals from the face and sample the angle between the sample and the face must be on the order of a tenth of a degree if the focal length of the lens 3÷2 m. In the experiment the required angle between the sample and the face of the prism can be created if one edge of the sample is placed on a step about 50 to 100 microns high (depending on the sample size).

The dispersions of the heights σ_1^2 obtained by the given method are presented in the table. The light sliding angle $\psi=7°$. For comparison, values of σ^2_{lim} obtained from the microprofilograms are presented.

(1) Дисперсия высот, мкм²	Размер зерна, мкм (2)						
	3	5	7	10	14	20	28
σ_2^2	0,054	0,105	0,116	0,146	0,160	0,262	0,310
$\sigma_{пр}^2$ (3)	0,053	0,102	0,115	0,144	0,160	0,250	0,326
σ_1^2	0,059	0,093	0,110	0,144	0,181	0,245	—

Key:
1. Height dispersion, micron^2
2. Grain size, microns
3. σ^2_{lim}

The data in the table indicate good comparison of the results with respectto measurement of the reflection coefficient with the results obtained using the profilometer. This will permit the proposal of the given method for estimating the microrelief of rough surfaces.

The other path for estimating the quality of machining the rough surfaces using a prism interferometer lies through measuring the contrast of the interference bands on the interferograms obtained on this interferometer. For this purpose, a slope of the sample with respect to the face of the prism is created. If we denote by A_0 the wave field incident on the hypotenuse inside the prism and by A_1, the field of the wave reflected from the face, then by using (2) it is possible to record the expression for the contrast of the interference band in the following form:

$$K = \frac{2h(A_0 - A_1)}{A_1} \exp(-2k^2\sigma^2 \sin^2\psi) = P\exp(-2k^2\sigma^2\sin^2\psi).$$

Here h is the coefficient of reflection from the face of the air-glass interface for a wave returning to the prism after reflection from the sample; P is a constant determined by the experimental conditions.

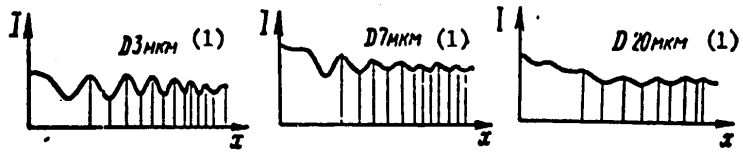

Figure 3

Key:
1. microns

Fig 3 shows examples of the photometric measurements of the interferograms of some samples, and the values of σ_2^2 obtained by the given method are presented in the table,

Good comparison of the results obtained with the data from the microprofilograms offers the possibility of using this method also for determining the height dispersion of the unevennesses of the rough surface.

Thus, the application of several coherent-optical methods of investigation of the rough surfaces is possible.

The methods making use of the prism interferometer offer the possibility of obtaining average information on the entire investigated surface quite rapidly. The deficiencies of these methods must include the effect of the nonplaneness of the samples and the inaccuracy of installation of them with respect to the illuminating beam.

The method of the dispersion indexes less critical with respect to the illumination angle, and its optical system is more compact. However, the time for obtaining the information is greater, and the information itself is of a local nature, for it pertains only to the illuminated section of the surface.

BIBLIOGRAPHY

1. Bass, F. G.; Fuks, I. M. RASSEYANIYE VOLN NA STATISTICHESKOY NEROVNOY POVERKHNOSTI [Wave Dispersion in a Statistical Uneven Surface], Nauka, 1972.

2. Yermakova, N. V.; Belogorodskiy, B. A.; Butusov, M. M. OPTICHESKAYA GOLOGRAFIYA I YEYE PRIMENENIYE [Optical Holography and Its Application], Leningrad, LDNTP, 1974, p 15.

HOLOGRAPHIC METHOD OF INVESTIGATING THE DISTORTION OF THE WAVE FRONT BY THE ACTIVE ELEMENTS OF A SOLID-STATE LASER DURING THE PUMPING PERIOD

[Article by A. A. Bugayev, M. M. Butusov]

[Text] The propagation of an electromagnetic wave in the direction perpendicular to which nonuniform distribution of the index of refraction occurs in the active elements of the solid state lasers and masers is accompanied by distortion of the wave front of the transmitted radiation. For the pumping period when the calculation of the nonuniform distribution of the index of refraction with respect to cross section of the active elements is complicated by the presence of energy transitions in the inverse medium [1] and also the temperature dependence of the coefficient of spectral absorption [2], preference is given to the experimental methods of investigating the distortions of the wave front. The methods used previously are as follows: recording of the radiation on the photographic plate [3], autocollimation [4] and measurement of the effective focal length [5] cannot exactly describe the wave front passing through the active element if the center and radius of curvature of the surface of this wave front are variable.

In this paper the distortions of the wave front by the active element during the pumping period were investigated by the holographic procedure [6] with respect to the Mach-Zender interferometer system. The subsequent reproduction of the subject wave F carried out with respect to the ordinary reproduction system [6] permits a detailed investigation of the profile of the distorted wave front in real time. For simplification of the experimental technique, a film of the KN-2 type was used as the recording medium, the sensitivity of which with an exposure time of 10^{-3} seconds offers the possibility of using the LG-75 operating in the single-mode regime in the role of the source. The recording of the hologram was made under the conditions where the carrier frequency of the interference grating $\alpha=\sin\theta/\lambda$ (θ is the angle between the reference and subject beam, λ is the wave length of the investigated emission) is close to 0.

As was stated above, the distortions of the plane wave passing through the active element are of a nature such that the reproduced subject wave R and its complex-conjugate R* form images of the source of spherical (bright point) or cylindrical (bright line) waves. Inasmuch as the carrier frequency of the interference grating is close to zero, the reproduced images of the

sources are located on the axis of the hologram [6] on both sides of it, and the image of one of them is always accompanied by the defocussed other one. However, as the experiments show, the real and imaginary images of the source are located at a significant distance from each other, and therefore they are easily distinguishable.

According to [6], it is also possible to state that in the case where one and the same collimated reference waves F is used on recording and reproduction of the hologram, and the coordinates of the image are x_0, y_0 and z_0, the coordinates of the reproduced imaginary and real images will be x_0, y_0, z_0 and x_0, y_0, $-z_0$, respectively. Thus, the application of the holographic procedure will permit performance not only of a qualitative analysis but also a quantitative analysis of the distortions of the wave front of the radiation passing through the active element.

In our paper studies are made of the distortions of the wave front of the radiation caused by the plane or cylindrical active elements during the pumping period. As the cylindrical rod, a rod made of GLS-1 type neodymium glass 8X130 mm was used. The pumping of the active elements was carried out by the IFP-1200 tube. The reflector was made in the form of a monolithic quartz block. The plane active element made of GLS-1 glass had dimensions of 8X20X120 mm. The pumping of it was realized by two IFP-1200 tubes through the side surface. The tubes were arranged along the optical axis of the active element. In both cases the pumping tubes and active element were cooled by running water through independent channels. The exposure of the negative took place 3 to 4 pumping periods after the time of switching on the tubes. The distortions of the wave front were investigated in the pumping energy range of 500-1000 joules for a cylindrical active element and 500-2000 joules for a plane active element.

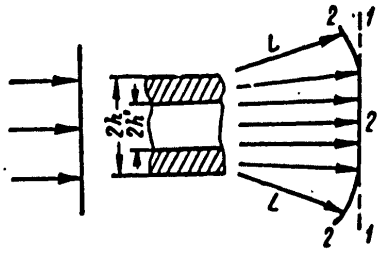

Figure 1

On the basis of the holograms obtained, it is possible to draw the conclusion that the wave front will become diverging after the active element. The reproduced image of the source of diverging waves for a flat active element is in the form of two bright horizontal lines. Consequently, the distortions of the wave front are caused only by peripheral sections of the transverse cross section of the active element, and the central sections

of the distortions are not introduced. Thus, the effect of the section of the plane element on the transmitted plane wave can be likened to the effect of the negative cylindrical lens with a focal length F which is split along its axis, and its halves are separated at a distance of 2h' from each other (see Fig 1).

As a result of the measurements it was established that wit' an increase in the pumping energy in the 500-800 joule range, a decrease in 2h' to a value equal to the halfthickness of the active element takes place. A further increase in the pumping energy does not change the value of 2h'. It is also necessary to note that the distance from the plane of the hologram to the real image of the source remains constant in the entire pumping energy range. Thus, the temperature profile occurring in the active element of a flat shape beginning approximately with 800 joules is stabilized with precision to a constant independently of the pumping energy.

In a cylindrical active element the reproduced image of the source of the diverging wave has the form of an irregular circle, for the pumping of the cylindrical active element has an explicitly expressed asymmetric nature. The increase in pumping energy in the case of a cylindrical element leads to the appearance of a trend toward insignificant decrease in the transverse dimensions (in the plane perpendicular to the direction of propagation of the radiation) of the reproduced image.

The fact that the reproduced images of the sources extend along the optical axis of the active element is significant for complete representation of the nature of the distortions. If this element is cylindrical, then beginning with the 800 joules, the transverse dimensions of the image along the optical axis decrease. This leads to pulling of the irregular circle toward the "point." (The diagrams of the most characteristic reproduced images of the source are presented in Fig 2.) The indicated phenomenon obviously is caused by distortion of the beam trajectory in the medium of the active element. Based on the results obtained it is possible to state that it is most expedient to realize correction of the thermal distortions of the resonator of the laser by the holographic method [7].

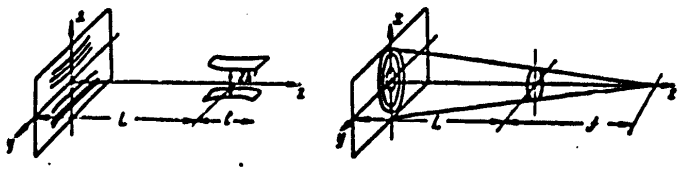

Figure 2

BIBLIOGRAPHY

1. Riedel, E.; Baldwin, G. D. J. APPL. PHYS., No 38, 1967, p 7.

2. Karapetyan, G. O.; Karris, Ya. Ye. ZHPS, No 1, 1964, p 3.

3. Koechner, W. APPL. OPT., No 9, 1970, p 11.

4. Bubnov, M. M.; Diyanov, Ye. M.; Prokhorov, A. M. DAN SSSR [Reports of the USSR Academy of Sciences], No 205, 1972, p 3.

5. Burnham, D. C. APPL. OPT., No 9, 1970, p 7.

6. Strowk, J. VVEDENIYE V KOGERENTNUYU OPTIKU I GOLOGRAFIYU Introduction to Coherent Optics and Holography], Mir, 1967.

7. Belokrinitskiy, N. S.; Gnatovskiy, A. V.; Danileyko, M. V. KVANTOVAYA ELEKTRONIKA [Quantum Electronics], Sovetskoye radio, No 2, 1973, p 118.

STUDY OF THE VARIOUS SYSTEMS FOR THE CONSTRUCTION OF AN AUTOMATED NUCLEAR MAGNETOMETER FOR PRECISE MEASUREMENT OF THE VARIATIONS OF THE NONUNIFORM MAGNETIC FIELDS

[Article by V. I. Dudkin, R. A. Zhitnikov, V. I. Filimonov]

[Text] In certain problems of physics engineering it is necessary to automatically measure the nonuniform magnetic fields with a high degree of accuracy. Out of all of the known methods for this purpose obviously the most suitable is the method of nuclear magnetic resonance in the current sample with the use of the nutation effect [1-3]. This permits the transfer of the observation of the nuclear magnetic resonance effect to a special magnet with high field uniformity in the clearance and thus, as a result of constriction of the nuclear magnetic resonance line and improvement of the signal/noise ratio, to insure high precision. The construction of the automatic magnetometer on this principle encounters a number of difficulties, the basic one of which is connected with the fact that the speed and dynamic error of the magnetometer are limited by the delay on transmission of the information from the measuring sensor to the analyzing unit. The magnitude of the delay $\tau=\ell/V$, where ℓ is the length of the connecting tube between the measuring sensor and the sensor of the analyzer; V is the speed with which the operating medium flows. From structural arguments usually it is difficult to make $\tau<0.1$ to 0.05 seconds. The presence of a delay imposes defined conditions on the construction of the tracking system of the magnetometer.

This paper is devoted to the creation of a nuclear magnetometer permitting automatic recording of the variations in intensity of a highly nonuniform magnetic field with high precision and sufficient speed for many circuits.

Block Diagram of the Magnetometer and Its Operating Principle

The principle of the use of nutation in a dynamic sample for measuring the magnetic field is described in [1-3]. Fig 1 shows the block diagram of a magnetometer. It is made up of four basic units: polarization and transporting of the working medium I, the measuring device II and the analyzer III and regulator IV.

The unit for polarization of the working medium includes the following elements: a permanent magnet 2 with field intensity in the gap of 4500 oersteds, the polarizer-vessel 3 100 cm^3 in volume and the centrifugal pump with the line 1. Distilled water was used as the working medium in the magnetometer. The length of the connecting tube 3 mm in diameter from the polarizer vessel to the sensor of the analyzer was 100 cm.

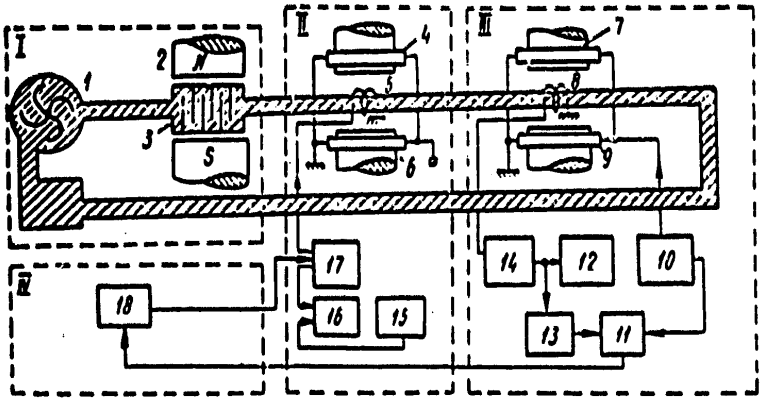

Figure 1

The measuring unit is made up of the sensor 5, the tunable radio frequency generator 17, the electronic counting frequency meter 16 and the highly stable sound frequency generator 15.

The analyzing unit contains a permanent magnet 7, $H_a \approx 1000$ oersteds with modulation coil 9, sensor 8, autodyne detector with quartz stabilization of the nuclear magnetic frequency 14, the low-frequency modulation generator 10, the selective amplifier 13, synchronous detector 11 and oscillograph 12.

The regulator 18 is executed on the basis of the decision elements of the MPT-9 series analog computer.

The magnetometer operates as follows. The water from the vessel of the centrifugal pump goes to the polarizer vessel placed in the gap of the permanent magnet. On passing through the labyrinth of the polarizer, it is magnetized, and it goes along the tube to the measuring sensor and the sensor of the analyzer where by using ordinary modulation procedures, the nuclear magnetic resonance signal is recorded in the field of the analyzer magnet. The field intensity of this magnet is selected from arguments of obtaining a quite high signal/noise ratio in the analyzer with a relative field gradient of 10^{-4} to 10^{-5} cm^{-1}. This ratio on the screen of the oscillograph is equal to 50-100, and on the output of the synchronous detector with a time constant of 0.5 seconds it is 400 to 800.

The measuring gauge is a coil connected to the generator 17. Under the effect of the pulse of radio frequency magnetic field (the generator

frequency is selected so that the nuclear magnetic resonance condition $\omega=\gamma H_{meas}$ in the measuring sensor will be satisfied) the magnification vector of the working medium is rotated by an angle from 0 to π.

The angle of rotation is determined by the amplitude of the radio frequency magnetic field and the degree of satisfaction of the resonance conditions in the measuring sensor. Far from the resonance in the sensor rotation of the magnetization vector does not take place, and the nuclear magnetic resonance absorption signal is observed in the analyzer. On satisfaction of the resonance conditions, the angle of rotation θ is equal to π, and the signal from the nuclear magnetic resonance emission is observed in the analyzer (the signal phase on the oscillograph screen and at the output of the synchronous detector varies by 180°). For the angle of rotation $\theta=\pi/2$ the signal in the analyzer is missing. If this condition is violated, then the signal appears in the analyzer, the amplitude and phase of which are defined by the angle θ.

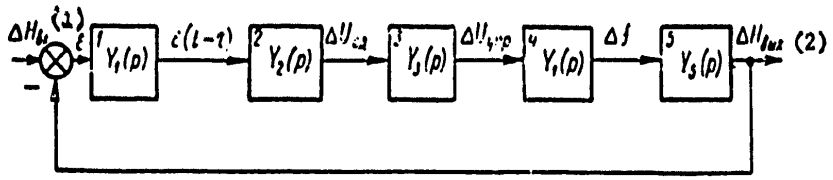

Figure 2

Key:
1. Input
2. Output

The regulator of the magnetometer generates a voltage which goes to the element controlling the frequency of the generator 17, which varies until the indicated condition is restored. Knowing the frequency difference for two cases in which $\theta=\pi/2$ and the gyromagnetic ratio of the proton, it is possible to calculate the variation of the measured magnetic field.

As the radio frequency generator, we used the G3-7A generator with changes in the system permitting tuning of its frequency by supplying the control voltage to the varicap. The indicator for the magnitude of the measured magnetic field was used as the ChZ-35 type electron calculating frequency meter operating in the "frequency ratio" mode. The voltage from the measuring generator 17 is fed to one of the inputs, and the voltage from the highly stable generator with a frequency equal with respect to magnitude to the gyromagnetic ratio of the proton in hertz/oersted, to the other. The value of the measured magnetic field in oersteds is observed on the display of the frequency meter.

The magnetometer is designed for measuring the variations of the average magnetic fields (H=800-1500 oersteds) with a relative gradient of $5 \cdot 10^3$ cm^{-1} and a variation range of $\pm 1\%$. The model of the magnetometer was tested with the permanent magnet 6 (H=1400 oersteds) equipped with the coil 4 (see Fig 1) by means of which the field variations were created, and studies were made of the dynamic characteristics of the magnetometer.

Peculiarities of the Automation of the Measurement Process and the Construction of the Regulator

The automation of the process of compensation of the external magnetic field is reduced to the construction of the automatic frequency control system of the generator 17 (see Fig 1). The structural diagram of this system can be represented in the form of the following links (Fig 2): delay 1, synchronous detector 2, regulator 3, high-frequency generator 4, converter 5 of the frequency to the magnetic field with the corresponding transfer functions $Y_1(p)$, $Y_2(p)$, $Y_3(p)$, $Y_4(p)$, and $Y_5(p)$. The converter 5 is an element taking into account the effect of the generator frequency on the variation of the field of the magnet.

In order to select the system and method of calculating the regulator parameters insuring the best static and dynamic characteristics of the automatic magnetometer, it is necessary to obtain a mathematical description of the elements 1, 2, 4 and 5. This was achieved by analyzing the reactions of these elements to the discontinuous input effect [4]. For small ranges of variation of the variables when the entire system can be considered as linear, the transfer functions of the mentioned elements were obtained in the form:

$$Y_1(p) = \exp(-p\tau); \quad Y_2(p) = \frac{K_2}{1+pT_2}; \quad Y_4(p) = \frac{K_4}{1+pT_4}; \quad Y_5 = K_5,$$

where

K_2=1.33 volts/oersteds; K_4=1.6 kilohertz/volts; $K_5=1/\gamma$=0.24 oersteds/kilohertz; T_2=0.48 sec; T_4=0.1 sec; τ=0.2 sec.

The presence in the mismatch circuit ε (see Fig 2) of a delay τ complicates regulation. This is expressed in the slow reaction of the system and in a tendency toward instability [6]. The analysis of the entire system when using the static $Y_3=K_3$, astatic $Y_3=K_3/p$ and isodromic

$$Y_3 = \frac{K_3(1+pT_3)}{p}$$

regulator indicates that the isodromic regulator which insures the best Q-factor with respect to velocity and null static error (in practice the static error is 30 hertz or $5 \cdot 10^{-6}$ with respect to H_{meas}) has the best characteristics.

For the given relative error $\delta=|\varepsilon|/\Delta H_{max}$ in processing the harmonic input signal $\Delta H=\Delta H_{max}\sin\omega_k t$ by a stable system it is sufficient that $A(\omega_k)>1/\delta$ be satisfied, where $A(\omega_k)$ is the value of the modulus of the frequency transfer function of the open system on the frequency of ω_k. The increase in this value of the modulus can take place as a result of an increase in K_3. For the isodromic regulator, the dependence of the critical value of K_3 for which the system is located on the stability boundary on T_3 has a maximum. For $\tau=0.2$ and $T_3=0.25$ we have $K_3=16$, which for $\omega_k=1.3$ gives $\delta\approx0.18$ (with respect to $H_{meas}=1400$ oersteds, $\delta_0=1.8\cdot10^{-3}$). The time of the transition process is units of seconds.

Thus, if the error in processing the signal statically for the given system can be theoretically found equal to zero for traditional regulators, the error dynamically and the time of the transition process are found to be unacceptably large as a result of the tendency toward instability with an increase in the amplification coefficient of the system. There are a number of methods of improving the precision under dynamic conditions for the systems with delay the basic ones of which are the following: the introduction of a nonlinearity into the control law, the introduction of the Smith predictor [5] and extrapolator [6] into the system.

Introduction of Nonlinearities into the Control Law

The width of the region in which the characteristic of the synchronous detector is close to linear is 2 oersteds. Inasmuch as the variation of the magnetic field can reach ±8 oersteds, the characteristic of the synchronous detector will be used in its essentially nonlinear part (in the saturation zone), and the time of the transition process will increase sharply. The decrease in this effect was realized by the regulator with an amplification coefficient which varies as a function of the magnitude of the mismatch, which was achieved by the application of the diode-resistive limiting circuits. The application of such a regulator, as the experiment demonstrated, made it possible to decrease the time of the transition process by 30%.

Smith Predictor

The application of the system with the Smith predictor[5] changes the structural diagram of the system somewhat (see Fig 3).

For $\tau_y=\tau$ and $Y_0(p)=Y_2(p)Y_4(p)Y_5(p)$ the transfer function of the closed system

$$Y_{замкн}(p)=\frac{\exp(-p\tau)\,Y_2(p)\,Y_3(p)\,Y_4(p)\,Y_5(p)}{1+Y_2(p)\,Y_3\cdot p)\,Y_4(p)\,Y_5\cdot p)}=Y(p)\exp(-p\tau),$$

where Y(p) is the transfer function of the closed system with the delay element included. In this case the stability of the entire system is determined by the stability of the subsystem described by the transfer function Y(p). The reaction of the system to the input effect will

correspond to the reaction of the system without delay, but shifted by the delay time.

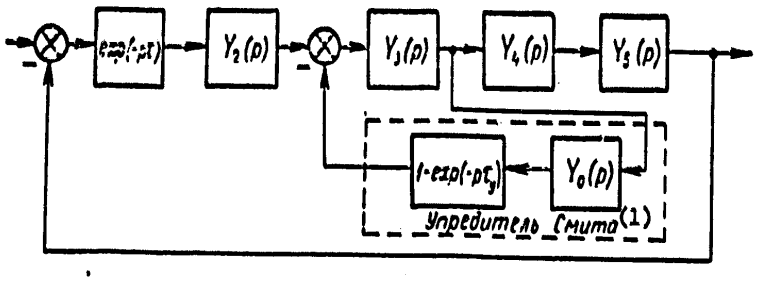

Figure 3

Key:
1. Smith predictor

The limits of stability of the system with the Smith predictor in the region of the parameters K_3 and T_3 can be found, for example, using the Naiquist criterion for the subsystem with the transfer function Y(p).

In the realized Smith predictor, the BPZ-2 constant delay unit and the decision elements of the MPT-9 analog computer were used.

The application of the Smith predictor permits a tenfold increase in the critical amplification coefficient of the system, which leads to smaller dynamic errors and decreases the time of the transient process by several times. The investigation of the system in the harmonic signal processing regime with an isodromic regulator demonstrated that with the introduction of the Smith predictor the processing error diminished by approximately an order: $\delta_0 \approx 10^{-4}$ with respect to H_{meas}=1400 oersteds.

Introduction to the Extrapolator Regulator

The extrapolator is included between the synchronous detector and the regulator (see Fig 2) and with an accuracy determined by the selected method of extrapolation reproduces the signal which must appear at the output of the synchronous detector after the time τ, thus excluding the delay from the operation of the system. The use of the Lagrange polynomial $L_n(t)$ for the construction of the extrapolator will permit estimation of the extrapolation error and for n=1, 2 sufficiently simple realization of linear and quadratic extrapolators on the analog computer.

The investigation of the system under the conditions of processing a harmonic signal with an isodromic regulator and linear extrapolator demonstrated that the increase in precision dynamically is approximately the same as with the Smith predictor. However, the system with the extrapolator has lower noiseproofness, which requires the use of filters at the system input.

Increasing the Stable Operating Zone of the Magnetometer

The sensitivity of the magnetomer is determined by the signal/noise ratio in the analyzer and the steepness of the slope of the nutation line at the operating point (see Fig 4, a). The smaller the segment AB (the width of the nutation line), the greater the steepness of the slope and the higher the sensitivity of the magnetometer. The width of the nutation line depends on many factors, but in our case, broadening connected with nonuniformity of the measured magnetic field will be predominant.

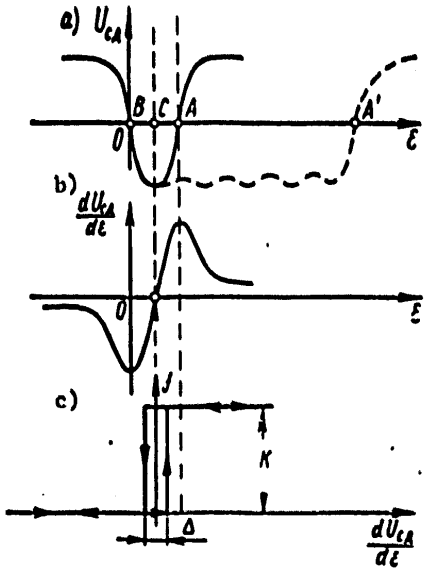

Figure 4

The narrow nutation line permits us to increase the sensitivity of the magnetometer, but it limits the range of rates of measureable variations of the magnetic field in the automatic measurement mode. On discontinuous variations of the magnetic field, their magnitude is limited by the width of the nutation line. In the automatic operating mode, the above-described zero measurement method is used, and the operation of the magnetometer takes place on one of the sections of the nutation line to the left of point A (see Fig 4, a). For variations with respect to magnitude greater than AB (Fig 4, a) and positive with respect to sign, the operating point of the magnetometer can be shifted beyond the point A, and the entire closed system falls into the unstable operating zone, for a positive feedback arises. The expansion of the zone of stable operations of the tracking system of the magnetometer can be achieved by two procedures.

By the first procedure, the broadening of the zone of stable operation of the magnetometer can be realized as a result of expansion of the nutation

line while retaining quite high steepness of its slopes. Inasmuch as the measured magnetic field is nonuniform, by locating one of the measuring sensors in the center of the magnet and several sensors alongside it, but shifting them closer to the edge of the magnet hole, it is possible to achieve the situation such that the conditions of nuclear magnetic resonance will be satisfied for each sensor on its own frequency. In our case in this way it was possible to expand the zone of stable operations of the magnetometer from +0.5 oersteds (for a single sensor) to +10 oersteds. Fig 4, a shows the boundary of the expanded zone by a dotted line.

By the second procedure the zone of stable operation of the magnetometer can be expanded in practice without limit by using the characteristic which is the derivative of the nutation line (Fig 4, b), that is, $dU_{shift}/d\varepsilon$. In this case, it is possible to feed the $U_{ind\ reg}$ effect of the following type to the input of the regulator (see Fig 2) instead of U_{shift}

$$\underset{(1)}{U_{\text{inp reg}}} = U_{\text{shift}}(t) - f\left(\frac{\underset{(2)}{dU_{\text{shift}}}}{dt}\right), \qquad (1)$$

Key:
1. $U_{inp\ reg}$
2. U_{shift}

where $f(dU_{shift}/d\varepsilon)$ is an ambiguous function of the argument detected in Fig 4, c where $|k|>|U_{shift}|_{max}$, and the width of the hysteresis loop Δ is less than the width of the nutation line. Whereas during operation of the system it will occur that $\varepsilon>c+\Delta/2$ (see Fig 4, a), the appearance of an additional signal in accordance with (1) at the input of the regulator causes a decrease in c which is especially important for $\varepsilon>A$. The presence of $\Delta\neq 0$ prevents the possibility of false inclusion of the additional term in the control signal (1) for large mismatch values and for shift of the characteristic $dU_{shift}/d\varepsilon$ along the vertical from the effect of the noise and inaccuracies of the system.

Thus, a magnetometer was developed for automatic measurement of the variations of the nonuniform magnetic field in the small gaps. For a relative gradient of $5\cdot10^{-3}$ cm^{-1}, the measurement accuracy was $5\cdot10^{-6}$ in the static mode and 10^{-4} for the harmonic variations with $\omega<1.5$ deg/sec. The range of measured variations of the magnetic field was $\pm 1\%$ of $H_{meas}\approx 1400$ oersteds, which was connected only with the limited range of frequency tuning of the measuring generator. Further decrease in the error is possible as a result of using the units with more stable characteristics which, first of all, pertains to the measuring generator. The instrument can be used as a multipurpose magnetometer and as a highly sensitive magnetic field sensor in such devices as the low acceleration meters.

BIBLIOGRAPHY

1. Zhernovoy, A. I.; Yegorov, Yu. O.; Latyshev, G. D. IFZH, No 6, 1963, p 123.

2. Skripov, F. I. DOKL. AN SSSR [Reports of the USSR Academy of Sciences], No 121, 1958, p 998.

3. Benoit, H. COMPT. REND., No 246, 1958, p 3053.

4. Dekhtyarenko, P. I.; Kovalenko, V. P. OPREDELENIYE KHARAKTERISTIK ZVEN'YEV SISTEM AVTOMATICHESKOGO REGULIROVANIYA [Determination of the Characteristics of the Elements of Automated Control Systems], Energiya, 1973.

5. Smith, O. J. M. AVTOMATICHESKOYE REGULIROVANIYE [Automatic Regulation], Fizmatgiz, 1962.

6. Bakli, P. S. "Automatic Control of Processes with Pure Delay," TRUDY I KONGRESSA IFAK [Works of the First Congress of the IFAC], Vol 1, USSR Academy of Sciences, 1961.

NATURAL OSCILLATIONS OF A CYLINDRICAL RESONATOR PARTIALLY FILLED WITH ANISOTROPIC DIELECTRIC

[Article by Yu. I. Meshcheryakov, I. N. Toptygin]

[Text] The problem of determining the natural frequencies of resonators partially filled with anisotropic dielectric is encountered in plasma physics when calculating quantum amplifiers and generators and also a number of microwave devices in which it is necessary to insure vacuum thermal insulation between the dielectric and the walls of the resonator. The complete solution of the problems for all-possible types of oscillations and the high degree of anisotropy of the dielectric is highly complicated. However, in the case of low anisotropy this problem can be solved by the methods of perturbation theory.

As the undisturbed system it is natural to select a resonator in which the anisotropic dielectric (uniaxial crystal having dielectric constants $\varepsilon_{||}$ and $\varepsilon_{\perp}$) is replaced by an isotropic dielectric with the dielectric constant $\varepsilon_0=\varepsilon_{\perp}$. Then the perturbation parameter for the completely filled resonator will be $(\varepsilon_{||}-\varepsilon_{\perp})/\varepsilon_{\perp}$, and for partial filling this parameter decreases naturally. For a ruby which is used in quantum amplifiers and generators ($\varepsilon_{\perp}=9.95$, $\varepsilon_{||}=11.73$), the perturbation parameter is 0.18.

Thus, the problem of calculating the natural frequencies is broken down into two parts: calculation of the natural frequencies of the resonator partially filled with isotropic dielectrics; determination of the corrections for anisotropy.

We shall consider that the cylindrical ruby rod is coaxial to the resonator, and the axis of anisotropy of the ruby is perpendicular to the axis of symmetry of the system. Let us first consider the TE oscillations in the undisturbed system. For them $E_z=0$, and H_z is determined from the solution of the wave equation

$$\Delta H_z+\varepsilon_0 k_0^2 H_z=0, \quad k_0=\omega/c,$$

where $\varepsilon_0=1$ outside the dielectric. The remaining projections of the vectors E and H can be expressed in terms of H_z using the Maxwell equations.

The field components satisfying the boundary conditions $E_T=0$ on the ends of the resonator z=0 and z=h can be expressed in terms o f H_{1z} and H_{2z}:

$$\left.\begin{aligned} H_{1z} &= J_m(\varkappa_1 r)\begin{pmatrix}\cos m\alpha\\ \sin m\alpha\end{pmatrix}\sin kz;\\ H_{2z} &= [CJ_m(\varkappa_2 r)+DN_m(\varkappa_2 r)]\begin{pmatrix}\cos m\alpha\\ \sin m\alpha\end{pmatrix}\sin kz.\end{aligned}\right\} \qquad (1)$$

Here $m=0, 1, 2, \ldots; \quad k=\pi p/h; \quad p=0, 1, 2, \ldots; \quad \varkappa_1=\sqrt{\varepsilon_0 k_0^2-k^2};$
$\varkappa_2=\sqrt{k_0^2-k^2}.$

The boundary conditions for the field components are

$$\begin{aligned} &E_{2\alpha}=0 \quad \text{for} \quad r=a;\\ &E_{1\alpha}=E_{2\alpha}; \quad E_{1z}=E_{2z}; \quad H_{1z}=H_{2z} \quad \text{for} \quad r=b. \end{aligned} \qquad (2)$$

From these conditions, it is necessary to determine the constants C and D and also the natural frequencies. It is easy to see that the factually asymmetric solutions ($m\neq 0$) do not satisfy the boundary conditions (2) if the resonator is incompletely filled with dielectric. In this case, there are no individual TE and TM oscillations in the investigated system; some of their superpositions are characteristic types. For the axially symmetric oscillations (m=0) the set of boundary conditions gives the following transcendental equation for determining the natural frequencies:

$$\frac{\varkappa_2 J_1(\varkappa_1 b)}{\varkappa_1 J_0(\varkappa_1 b)}=\frac{J_1(\varkappa_2 b)N_1(\varkappa_2 a)-J_1(\varkappa_2 a)N_1(\varkappa_2 b)}{J_0(\varkappa_2 b)N_1(\varkappa_2 a)-J_1(\varkappa_2 a)N_0(\varkappa_2 b)}. \qquad (3)$$

For large ε_0 when the value of χ_2 can be made purely imaginary it is necessary to replace the function $J_m(\chi_2 r)$ in formulas (1) by $I_m(\chi_2 r)$ and $N_m(\chi_2 r)$ by $K_m(\chi_2 r)$, that is, by the modified Bessel functions, and by χ_2 we mean the value of $(k2-k_0^2)^{1/2}$. Then we shall reduce equation (3) to the following:

$$\frac{\varkappa_2 J_1(\varkappa_1 b)}{\varkappa_1 J_0(\varkappa_1 b)}=\frac{I_1(\varkappa_2 b)K_1(\varkappa_2 a)-I_1(\varkappa_2 a)K_1(\varkappa_2 b)}{I_0(\varkappa_2 b)K_1(\varkappa_2 a)+I_1(\varkappa_2 a)K_0(\varkappa_2 b)}. \qquad (4)$$

In the case of a wholly filled resonator (a=b) the equation for the natural frequencies $(J_m'(\chi_1 a)=0$ for any m. The analogous equations occur for oscillations of the TM type. One of the families of curves obtained by the numerical solution of equation (4) for the lowest TE type ($\varepsilon_0=9.95$, p=1, m=0, $2a=1.2\cdot 10^{-2}$ m) is presented in Fig 1.

Now let us proceed to the calculation of the corrections to the natural frequencies caused by anisotropy of the dielectric. Let us present only certain final expressions.

The first-order corrections to the natural frequencies are determined from the secular equation

$$|\Omega_{\sigma\sigma'} - \Delta\omega_\mu^{(0)}\delta_{\sigma\sigma'}| = 0,$$

where

$$\Omega_{\sigma\sigma'} = -\frac{\omega_\mu^{(0)}\int \mathbf{E}^0_{\mu\sigma}\hat{\Delta\varepsilon}\,\mathbf{E}_{\mu\sigma'}\,dV}{2\varepsilon_0\int|\mathbf{E}_{\mu\sigma}|^2\,dV}; \quad (\hat{\Delta\varepsilon})_{ik} = \varepsilon_{ik} - \varepsilon_0\delta_{ik},$$

$E_{\mu\alpha}$ are the eigenfunctions of the undisturbed problem; μ is the set of three eigenvalues which determine the resonator frequency; $\sigma=1,2$ is the type of polarization inasmuch as the frequencies corresponding to the axially asymmetric modes are doubly degenerate.

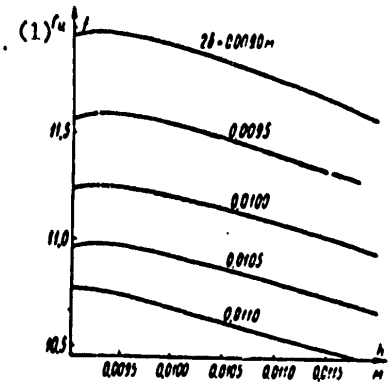

Figure 1

Key:
1. hertz

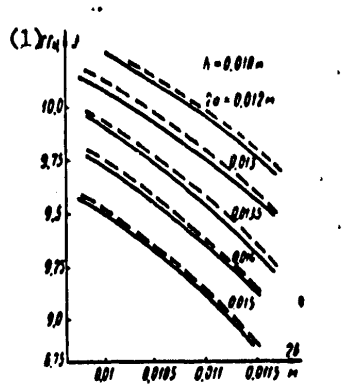

Figure 2

Key:
1. gigahertz

For the TE oscillations with m=0 from the presented formulas we obtain

$$\Delta\omega = -\omega^{(0)}\frac{\varepsilon_\parallel - \varepsilon_\perp}{\varepsilon_\perp}\,\frac{\int_a^b J_1^2(x_1 r)\,r\,dr}{\int_a^b J_1^2(x_1 r)\,r\,dr + Q}, \qquad (5)$$

where

$$Q = J_1^2(x_1 b)\int_a^b\left\{\frac{J_1(x_2 r)K_1(x_2 a) - K_1(x_2 r)I_1(x_2 a)}{I_1(x_2 b)K_1(x_2 a) - K_1(x_2 b)I_1(x_2 a)}\right\}^2 r\,dr.$$

For a resonator wholly filled with dielectric, there is a simple formula

$$\Delta\omega = -\omega^{(0)}(\varepsilon_\parallel - \varepsilon_\perp)/\varepsilon_\perp.$$

Among the TM oscillations there are types which do not depend on the coordinates (including the basic oscillation). These types are not influenced by the anisotropy of the dielectric, $\Delta\omega=0$. The TM oscillations with $k\neq0$ and $m\neq1$ in the completely filled resonator experience the following shift under the effect of the dielectric anisotropy:

$$-\omega^{(0)}(\varepsilon_{\parallel}-\varepsilon_{\perp})\,4\varepsilon_{\perp}.$$

The oscillation frequencies with $k\neq0$ and $m=1$ are split each in two:

$$\omega^{(0)}+\Delta\omega_1 \text{ and } \omega^{(0)}+\Delta\omega_2,$$

where

$$\Delta\omega_1=-\omega^{(0)}\frac{\varepsilon_{\parallel}-\varepsilon_{\perp}}{\delta\varepsilon_{\perp}};\quad \Delta\omega_2=-3\omega^{(0)}\frac{\varepsilon_{\parallel}-\varepsilon_{\perp}}{\delta\varepsilon_{\perp}}.$$

The spacing between them in the case of a ruby is $0.045\,\omega^{(0)}$. In Fig 2 we have the experimental (solid curve) and the theoretical (dotted curve) values of the natural frequencies of the TE oscillations with $m=0$ considering the corrections calculated by formula (5). It is possible to explain the small divergences by the effect of the elements of the coupling of the resonator to the wave guide and also the finite magnitude of the conductivity of the resonator wall.

Then let us estimate the energy distribution of the electromagnetic field between the dielectric and the unfilled region of the resonator. For the basic TE type oscillations the computer calculations used the energy ratio of ≈500 for a ruby on a frequency of $f=9370$ megahertz, that is, in practice all the energy is concentrated in the dielectric.

The filling coefficient η of the resonator using the paramagnetic material is equal to the product K_vK_p, where K_v is the volumetric filling coefficient, K_p is the use coefficient of the paramagnetic material, the calculation of which can be performed by the known formulas.[1] The calculations for the resonator $2a=1.47\cdot10^{-2}$ m in diameter with a ruby rod with a diameter of $2b=1.3\cdot10^{-2}$ m gives $\eta=0.955$. The presented example indicates that the application of the cylindrical resonator with TE oscillations insures a highly effective use of the paramagnetic material in the quantum amplifier.

---

[1] A. Sigmen, MAZERY [Masers], Mir, 1966.

DECELERATING STRUCTURES OF THE "LADDER" AND "MEANDER" TYPE AND THEIR USE IN MICROWAVE STRUCTURES

[Article by V. V. Batygin, S. Ye. Drozdetskiy, B. G. Matisov, Yu. A. Nonin, A. A. Rumyantsev, I. N. Toptygin]

[Text] At the present time the electromagnetic decelerating structures are finding broader and broader application in the development of microwave elements such as delay lines, phase shifters, traveling wave filters and masers. Therefore the theoretical and experimental study of these structures is of unquestioned practical interest.

Analytical and Numerical Calculations of the Decelerating Structure in the H-Type Wave Guide

In the traveling wave masers, the ladder type decelerating structure usually is placed in the wave guide together with the active material for which ruby is most frequently used (ε=10). The application of a wave guide with rectangular cross section does not make it possible to create an optimal structural design of the maser, for the deceleration coefficient turns out to be small, and the use coefficient of the active material turns out to be low. As the calculation performed below indicates, the application of the H-type wave guide is more prospective. This wave guide and also the other complex forms of wave guides with a ladder baffle were investigated by Butcher [1], who was limited to the case of the absence of a dielectric. However, inasmuch as the dielectric constant of the maser crystals is high, the partial filling of the wave guide with the dielectric essentially changes its properties, and in real cases the Butcher results are inapplicable.

Let us consider the wave guide, the shape of the cross section of which is depicted in Fig 1. The dielectric will be considered isotropic, the ladder baffle is in the plane of y=0, the planes are oriented parallel to the x-axis. Inasmuch as in real cases the wave length is large by comparison with the system period, we shall solve the problem in the approximation of an anisotropically conducting plane. Let us first find the partial solutions of the Maxwell equations for the region I($-a<x\leq a$, $-g\leq y\leq g$) satisfying all of the boundary conditions except the conditions for $y=\pm g$,

$$x = \pm a, \quad E_{1y} = E_{1z} = H_{1x} = 0; \tag{1}$$
$$x = \pm b, \quad E_{1y} = E_{2y}, \quad E_{1z} = E_{2z}, \quad H_{1y} = H_{2y}, \quad H_{1z} = H_{2z}; \tag{2}$$
$$y = 0, \quad E_{1x} = E_{2x} = H_{1x} = H_{2x} = 0, \quad x = 0, \quad H_{2z} = H_{3y} = 0. \tag{3}$$

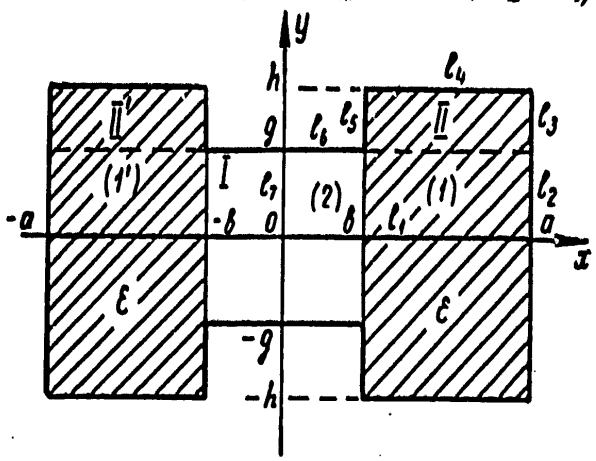

Figure 1

Integrating the Maxwell equation by the standard methods, it is possible to obtain partial solution which satisfies the conditions (1)-(3) of two types: the transverse-electric and transverse-magnetic systems with respect to the axis of anisotropy (the x axis)

TE type:

$$\left.\begin{aligned} &E_{xn} = 0; \quad H_{xn} = \frac{i(\gamma^2 - \beta_n^2)}{k_0 \beta_n} X_n(x) \operatorname{sh} \beta_n y; \\ &E_{yn} = -(i\gamma\, \beta_n) X_n(x) \operatorname{sh} \beta_n y; \quad H_{yn} = (i\, k_0) X_n'(x) \operatorname{ch} \beta_n y; \\ &E_{zn} = X_n(x) \operatorname{ch} \beta_n y; \quad H_{zn} = -(\gamma\, k_0 \beta_n) X_n'(x) \operatorname{sh} \beta_n y. \end{aligned}\right\} \tag{4}$$

Here

$$X_n(x) = \begin{cases} \sin \alpha_n (a - x); & b \leq x \leq a; \\ |\sin \alpha_n (a - b) \cos \alpha_n' b| \cos \alpha_n' x; & -b \leq x \leq b; \\ \sin \alpha_n (a + x); & -a \leq x \leq -b; \end{cases}$$

the eigenvalues β_n and α_n' are expressed in terms of α_n, the propagation constant γ, the dielectric constant ε and $k_0 = \omega/c$;

$$\beta_n^2 = \alpha_n^2 + \gamma^2 - k_0^2 \varepsilon; \quad \alpha_n'^2 = \alpha_n^2 - k_0^2 (\varepsilon - 1).$$

The eigenvalues α_n are the solution of the transcendental equation

$$\alpha_n \operatorname{ctg} \alpha_n (a-b) = \sqrt{\alpha_n^2 - k_0^2(\varepsilon-1)} \operatorname{tg} \left(\sqrt{\alpha_n^2 - k_0^2(\varepsilon-1)}\, b\right). \qquad (5)$$

Let us limit ourselves to the investigation of only the positive solutions of (5), and let us number them in increasing order. It is necessary to include the values of α_n for which α_n' becomes an imaginary value equal to $i[k_0^2(\varepsilon-1)-\alpha_n^2]^{1/2}$. Here the trigonometric functions containing α_n' are replaced by hyperbolic functions. The eigenfunctions $X_n(x)$ are continuous together with their first derivative, and they form a system of mutually orthogonal eigenfunctions of the hermetian operator:

TM type:

$$\left.\begin{aligned} &H_{zn}' = 0; \quad E_{zn}' = \frac{i(\mu_n^2 - \gamma^2)}{\gamma\varepsilon(x)} \Phi_n'(x) \operatorname{sh} \mu_n y; \\ &H_{yn}' = -ik_0 \Phi_n(x) \operatorname{sh} \mu_n y; \quad E_{yn}' = -\left(i\mu_n/\gamma\varepsilon(x)\right) \Phi_n'(x) \operatorname{ch} \mu_n y; \\ &H_{xn}' = (k_0\mu_n/\gamma) \Phi_n(x) \operatorname{ch} \mu_n y; \quad E_{xn}' = \varepsilon^{-1}(x) \Phi_n'(x) \operatorname{sh} \mu_n y. \end{aligned}\right\} \qquad (6)$$

Here

$$\varepsilon(x) = \varepsilon = \text{const} \quad \text{for} \quad b \leqslant |x| \leqslant a; \quad \varepsilon(x) = 1 \quad \text{for} \quad |x| \leqslant b,$$

and the eigenfunctions $\phi_n(x)$ are defined by the expression:

$$\Phi_n(x) = \begin{cases} (\varepsilon/\sigma_n) \cos \sigma_n (a-x), & b \leqslant x \leqslant a; \\ \sin \sigma_n (a-b) \sin \sigma_n' x/\sigma_n' \cos \sigma_n' b, & -b \leqslant x \leqslant +b; \\ -(\varepsilon/\sigma_n) \cos \sigma_n (a+x), & -b \leqslant x \leqslant -a. \end{cases}$$

The eigenvalues

$$\mu_n^2 = \sigma_n^2 + \gamma^2 - k_0^2\varepsilon; \quad \sigma_n'^2 = \sigma_n^2 - k_0^2(\varepsilon-1)$$

are expressed in terms of the solutions of the transcendental equation

$$\sigma_n \operatorname{tg} \sigma_n (a-b) = \varepsilon\sigma_n' \operatorname{ctg} \sigma_n' b.$$

It is also necessary to consider the solutions which correspond to the imaginary σ_n', replacing the trigonometric functions by hyperbolic functions.

The eigenfunction $\phi_n(x)$ and the function $(1/\varepsilon(x))\phi_n'(x)$ are continuous in the entire region of $-a \leqslant x \leqslant a$. The functions $\phi_n(x)$ are orthogonal with weight $1/\varepsilon(x)$ in this interval.

The general solution in the region I will be found in the form of infinite series with respect to the eigenfunctions (4) and (6), and in

region II, in the form of series with respect to trigonometric and hyperbolic functions satisfying all of the boundary conditions except the conditions for $y=\pm g$. When recording these series it is necessary to consider the properties of evenness or oddness of the corresponding field components. In order to determine four of the infinite system of expansion coefficients it is necessary to use the condition of the field components for $y=g$ which have the usual form, and the orthogonality of the system of functions X_n, Φ_n. Let us note that X_n and Φ_n are mutually orthogonal on the basis of their different evenness. The condition of resolvability of the infinite system of algebraic equations obtained as a result of these operations with respect to the expansion coefficient is equality of the determinant of the system to zero.

In spite of the extraordinary complexity of the dispersion equation relating γ to k_0, it must be solved numerically, breaking the series by which the solution is expressed and equating the corresponding truncated determinant to zero. Although the strict proof of the convergence of this procedure is not available, comparatively close results obtained from the equality of the determinants of different orders to zero indicate quite rapid convergence. For example, for the case of $\varepsilon=10$, $s=(b-a)/2a=0.25$, $g/2a=0.05$, $h/2a=0.25$, $\eta=2a\omega/\pi c=0.4$, the equality of the determinant 2X2, 4X4, 6X6 to zero gave values of the root $\zeta=2a\gamma/\pi$ equal to 1.868, 1.874, 1.918 respectively.

The calculation was performed on the Ural-2 and M-20 computers. Several versions were calculated for a ruby ($\varepsilon=10$) with different parameters (see Table 1). The versions were calculated for determinants with dimensionality 8X8 and 10X10. Table 2 shows the energy losses in different sections of the wave guide wall W_1, the energy fluxes q, the damping coefficient α_1 the filling coefficients K for the direct wave in the 90° mode and K for the return wave in the push-pull mode.

Table 1

(1) Варианты	Параметры (2)					
					ε	
	s	g	h	τ_1	8×8	10×10
I	0,45	0,1	0,25	0,323	1,974	1,998
II	0,45	0,2	0,25	0,345	1,728	1,751
III	0,375	0,2	0,5	0,390	1,640	—

Key:
1. Version
2. Parameters

A comparison of the field components at the boundary of regions I and II indicates that their difference does not exceed 20%. The components E_x and H_x constitute an exception, but they are small with respect to absolute magnitude.

The standard values of the deceleration coefficient $S=c/v_{ф}=d\zeta/d\eta$ depend sharply on the value of the parameter s. For $\varepsilon=10$ in the middle (operating) part of the pass band, they are equal to 5 to 15 for $s=0.125$ to 0.25, and they rise to 10-30 for $s=0.375$ and even to 100-200 for $s=0.45$. The large values of the deceleration coefficient are achieved in the wave guide with narrow and shallow longitudinal grooves. For example, for $s=0.45$, $g/2a=0.2$, $h/2a=0.25$, we obtain $S=100$, and for $s=0.45$, $g/2a=0.1$, $h/2a=0.28$ we have $S=200$.

Table 2

(1) Параметры	(2) Варианты				
	I		II		III
	8×8	10×10	8×8	10×10	8×8
W_1	1,548	1,541	1,512	1,490	1,101
W_2	1,364	1,346	1,966	1,935	1,826
W_3	0,492	0,464	0,127	0,123	0,758
W_4	0,559	0,541	0,676	0,652	0,104
W_5	0,005	0,007	0,003	0,001	0,126
W_6	0,015	0,030	0,002	0,004	0,070
W_7	0,002	0,012	0,000	0,002	0,014
q_1	0,003	0,001	0,000	0,054	0,010
q_2	0,005	0,004	0,000	0,000	0,007
a	0,001	0,001	0,007	0,011	0,000
K	0,502	0,503	0,490	0,491	0,511
$\tilde{K}$	0,677	0,678	0,671	0,691	0,726

Key:
1. Parameters
2. Versions

Calculation of the Ladder Structure with Respect to Perturbation Theory

For small differences in shape of the wave guide from rectangular the deceleration factor and other parameters of the wave guide with ladder decelerating structure and dielectric rods can be obtained in analytical form by perturbation theory. Omitting the details of the calculations, let us present the dispersion functions (in the dimensionless variables η, ζ)

$$\eta = \frac{1}{\sqrt{\varepsilon}}\left[1 - \frac{\sin\pi(1-2s)}{\pi}\,\frac{\operatorname{sh}\left(\pi\frac{h-g}{a}\right)}{\operatorname{sh}\pi\frac{h}{a}}\right], \qquad (7)$$

and also the retardation coefficient

$$S = \frac{a\sqrt{\varepsilon}}{h\sin\pi(1-2s)}\cdot\frac{\operatorname{sh}^2\pi\frac{h}{a}}{\operatorname{sh}\pi\frac{g}{a} - \frac{g}{h}\operatorname{ch}\pi\frac{h-g}{a}\operatorname{sh}\pi\frac{h}{a}}.$$

The propagation constant ζ varies within the limits from zero to infinity, and the transmitted frequency η, within the limits of the band

$$\Delta\eta = \frac{h-g}{h}\sin\frac{\pi(1-2s)}{\pi\sqrt{\varepsilon}}.$$

Smallness of the second term in parentheses in formula (7) by comparison with one is a condition of applicability of perturbation theory.

For masers, the product of the retardation coefficient times the transmitted frequency band is an important parameter. Using the formulas presented above, it is easy to obtain the following expression:

$$\Delta f S_{\text{раб}} = \frac{4a\sqrt{\varepsilon}}{\pi h} f_{\text{раб}},$$
(1)

Key:
1. operating

where $S_{\text{operating}}$ corresponds to the minimum of the curve $S(\eta)$, and Δf and $f_{\text{operating}}$ are the band width and the operating frequency.

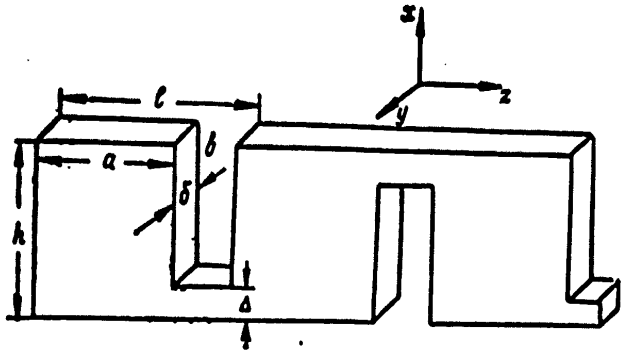

Figure 2

The coefficient of ohmic losses in decibels/centimeter is determined by the energy dissipation in the wave guide walls and in the decelerating structure. For the investigated system it is given by the formula

$$\alpha = 69{,}4\frac{1}{\lambda_{\text{раб}}\sin\pi(1-2s)}\sqrt{\frac{f_{\text{раб}}}{s}}\frac{h}{h-g}\frac{a}{h}\left[1+\frac{a}{h}(0{,}32+0{,}81k)\right].$$

Here k is the ratio of the strip width to the period of the structure. Let us note that the small parameters 1-2s and h-g are introduced into the denominator. Therefore the increase in deceleration leads to an increase in losses.

Decelerating Structure of the Meander Type

A distinguishing feature of the transmitting line of the meander type is the fact that the group propagation rate of the oscillations in it turns out to be much smaller than for the purely geometric deceleration, and at the same time this rate bends weakly on the frequency in a sufficiently broad frequency band. This makes it highly prospective to use the meander line in many electronic devices.

Let us consider the structure of the meander type which is located in a vacuum (Fig 2). It is convenient to use a rectangular coordinate system. The thickness of the strips δ in the direction of the y-axis is assumed to be negligibly small so that the structure can be considered plane and located in the xz plane. Let us first perform the calculation under the assumption of infinite conductivity of the strips.

Inasmuch as a meander is an infinitely long periodic structure with the period $l=a+b$, at the corresponding points of the structure removed from each other by the period, the elecromagnetic field can be distinguished only by the phase factor

$$H(x, y, z, t) = \sum_{n=-\infty}^{\infty} H_n(x, y) \exp[i(\omega t - \beta_n z)] = \\ = H_0(x, y, z) \exp\left[i\left(\omega t - \frac{vz}{l}\right)\right], \qquad (8)$$

where

$$\beta_n = \frac{v + 2\pi n}{l}, \quad H_0(z + l) = H_0(z).$$

Just as in the paper by Butcher [1] in which a study was made of a strip structure in a vacuum, we shall consider the solution of the Maxwell equations in the form of the TEM waves. The absence of the TM and TE type waves is connected with the proposed smallness of the ratio δ/a: the presence, for example, of the component $E_x \neq 0$ would cause disturbance of the boundary conditions for the tangential component of the electric field in the meander cross connection region.

The two-dimensional Laplace equation [2] is satisfied by all of the field components in the TEM wave and the complex potential $W=U+iV$, where $E=-\nabla U$, $H=-\nabla V$. Here the potential $W(z+iy)$ is a regular function of the complex argument $\phi=z+iy$. The Laplace equation and also the boundary conditions both within the limits of the bands and in the region between them turn out to be satisfied if we select the complex potential in the following form

$$W(\varphi) = \int_{+\infty}^{\varphi} d\eta \frac{\exp\left[(\pi - v)\frac{\eta}{l} i\right]}{f(\eta)}; \quad f(\eta) = \frac{l}{\pi}\left(\sin^2\frac{\pi b}{2l} - \sin^2\frac{\pi\eta}{l}\right)^{1/2}.$$

It is easy to see that the potential W satisfies the conditions of periodicity of the type of (8).

If we shift the meander in the z direction by l and then carry out reflection in the x=0 plane, we obtain the initial structure; therefore we form the superposition

$$\tilde{W} = W(0)\cos kx + CW(\pi + 0)\sin kx,$$

having the property

$$\tilde{W}(-x, y, z + l) = \tilde{W}(x, y, z)\exp(-i\theta); \quad C = \text{const.}$$

Then equating the difference of the electric potentials and currents at the edge points P, Q of the cross connections to zero (since the indicated points are truncated), after a number of simple transformations we obtain the following dispersion equation for the meander (see Fig 3)

$$\operatorname{ctg}^2\frac{kh}{2} = \operatorname{tg}\frac{\theta}{2}\,\frac{U\left(\frac{a}{l}, \theta\right)U\left(\frac{b}{l}, \theta + \pi\right)}{U\left(\frac{b}{l}, \theta\right)U\left(\frac{a}{l}, \theta + \pi\right)}, \tag{9}$$

where

$$U(x, y) = \int_{-\frac{\pi}{2}x}^{\frac{\pi}{2}x} \frac{dt\cos\left[\left(1 - \frac{y}{\pi}\right)t\right]}{\left(\sin^2\frac{\pi x}{2} - \sin^2 t\right)^{1/2}}, \tag{10}$$

$k=\omega/c$ is the propagation constant $\theta=2\pi l/\lambda$.

The decleration coefficient $S_0 = \frac{c}{l}\frac{d\omega}{d\theta}$. In particular, if $a \ll l$, then from (9), (10) we have $S_0 \approx h/b$ which corresponds to geometric deceleration ($h \gg b$); if $b \ll l$, then $S_0 = \pi h/l$. In the presence of a dielectric with the constant ε, the deceleration coefficient will become equal to $S=\chi S_0$, where $\chi=\sqrt{\varepsilon}$ is the index of refraction. When a dielectric is located on one side of the meander with a constant ε_1, and on the other side with a constant ε_2, then the calculation leads to the following effective index of refraction:

$$\varkappa = \left(\frac{\varepsilon_1\varepsilon_2(\varepsilon_1 + \varepsilon_2)}{\varepsilon_1^2 + \varepsilon_2^2}\right)^{1/2}.$$

Let us present the final results for the meander in the form of simple formulas convenient for engineering calculations:

Deceleration coefficient:

$$S = \frac{\pi h}{b}\sqrt{\frac{l}{b}}\,0{,}238 \quad \text{for} \quad b/l \ll 1;$$

the ohmic Q-factor

$$Q_0 = 4l\sqrt{\frac{f_\mu}{\rho}}\,\frac{1+\frac{2l}{\pi h}}{\frac{a}{t}+\frac{\Delta b}{th}+\frac{\delta_1 h+b_1}{th}};$$

the wave impedance of the meander

$$Z = \frac{hZ_0}{8\ln 4\sqrt{\pi\beta}},$$

where f_μ is the frequency in gigahertz; ρ is the specific resistance in ohm-cm; l is the period of the structure in cm; ε is the dielectric constant of the paramagnetic material; $\beta = b/l \ll 1, Z_0\sqrt{\mu/\varepsilon}$. More detailed calculations have been performed in the report.

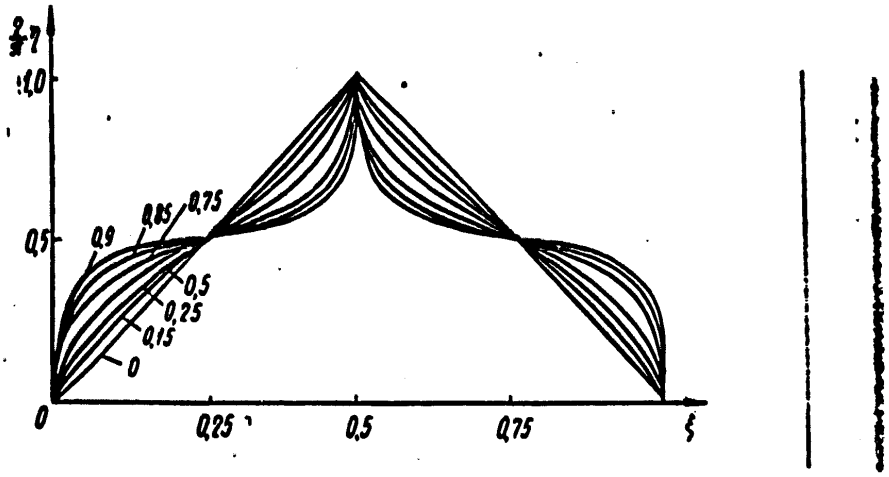

Figure 3

The results obtained above demonstrated that on the basis of the ladder type decelerating structure it is possible to create both a traveling wave maser and a delay line with good operating parameters. The ladder type decelerating system is not inferior with respect to its operating qualities to the comb type, and in many respects it is superior to it. As for comparison of the ladder and meander type decelerating systems, it is necessary to note that in these structures the product of the pass band times the decelerating coefficient remains approximately constant, but the deceleration coefficient of the meander cannot in practice be more than 100.

The data from calculating the decelerating structures of the "meander" and "ladder" types will permit the following conclusion to be drawn: the use of the decelerating structure of the "ladder" type is expedient when creating quantum paramagnetic traveling wave amplifiers, delay lines and filters with a pass band to 100 megahertz; the use of the decelerating structure of the "meander" type is expedient when creating quantum paramagnetic traveling wave amplifiers and phase shifters with a pass band of more than 100 megahertz.

BIBLIOGRAPHY

1. Butcher, P. N. PROC. IEE, Part B, No 14, 1957, p 177.

2. Landau, L. D.; Lifshits, Ye. M. ELEKTRODINAMIKA SPLOSHNYKH SRED. [Electrodynamics of Continuous Media], Fizmatgiz, 1959.

THEORETICAL STUDY OF THE LINE SHIFT OF THE SUPERFINE STRUCTURE OF HYDROGEN ATOMS IN A HELIUM ATMOSPHERE

[Article by Vl. V. Batygin, N. A. Lapuk, B. G. Matisov]

[Text] Recently the line shift of the superfine structure of hydrogen atoms in an atmosphere of inert gas has turned out to be an object of broad experimental [1-2] and theoretical [4-8] interest. The recent experimental progress took the form of measuring the superfine shift in a broad temperature range [3]; at the same time more data appeared which were subject to explanation by the theory.

In the proposed paper the exchange perturbation theory method is applied to the calculation of spin densities on the nucleus of a hydrogen atom at a finite distance from the helium atom. The exact calculation of the spin densities is the most complex problem in theoretical investigations of the superfine shift and broadening (see [6], [8]).

An electron of the hydrogen atom in the normal state has an orbital moment of $\ell=0$; therefore the hamiltonian of the electron-nuclear interaction leading to superfine splitting is described with good precision by the Fermi contact interaction.

The local shift of the atomic level caused by the approach of the buffer atom to it by distance R is defined as

$$\Delta\omega(R)=\omega(R)-\omega_0=\frac{16\pi\mu_0\mu(2I+1)}{3}\Delta\rho(R). \qquad (1)$$

Here $\omega(R)$ is the spacing between levels of the superfine structure coinciding in atomic units with the frequency of the corresponding transition; $\omega_0\equiv\omega(R=\infty)$; $\Delta\rho(R)=\rho(R)-\rho_0$ is the change in the spin density $\rho(R)$ of the electrons of the system on the nucleus of the active atom

$$\rho(R)=N\frac{(\psi(R,x)\,|\,S_1z\delta(r_{01})\,|\,\psi(R,x))}{(\psi(R,x)\,|\,\psi(R,x))};$$

$\rho_0=\rho(R=\infty)$; N is the number of electrons in the system; x is the set of spatial and spin variables. In the case of a hydrogen atom in the

ground state $\rho_0 = (1/2)\Psi_0^2(0) = 1/(2\pi)$, where $\Psi_0(r_{a1}) = (1/\sqrt{\pi})\exp(-r_{a1})$ is the wave function of the ground state of the hydrogen atom (the nucleus at the point a).

Let us write the expression for the local relative level shift of the superfine structure of the hydrogen atom (indeed, also, any alkali atom) excited by the presence of a buffer helium atom at a distance R from it (for detailed conclusions see [7], report IV)

$$\delta\omega(R) = \frac{\Delta\omega(R)}{\omega_0} = \frac{s_0}{1-s_0} - \frac{q}{(1-s_0)^2} + \frac{1-\frac{q}{1-s_0}}{(1-s_0)\rho_0}\,\mathrm{Re}\,(\Phi_0(1)|\delta(r_{a1})|\Delta\Phi(1)) -$$
$$- \frac{1-\frac{q}{1-s_0}}{(1-s_0)\rho_0}\,\mathrm{Re}\,(\Phi(2)|\delta(r_{a1})|\Phi(1)) + \frac{1-\frac{q}{1-s_0}}{2(1-s_0)\rho_0}\,(\Delta\Phi(1)|\delta(r_{a1})|\Delta\Phi(1)) +$$
$$+ \frac{1-\frac{q}{1-s_0}}{2(1-s_0)\rho_0}\,\mathrm{Re}\,(\Phi(2)|\delta(r_{a1})|\Phi(3)). \qquad (2)$$

Here

$$\Phi(1) = \Phi_0(1) + \Delta\Phi(1) \equiv \Phi(r_1, r_2, r_3) = \Psi_0(r_1)\,\phi_{00}(r_2, r_3) + \Delta\Phi(r_1, r_2, r_3) -$$

is the asymmetric wave function of the H-He system; $\phi_{00}(r_2, r_3)$

is the wave function of the ground state of the helium atom with the nucleus at the point b; $\Delta\Phi$ is the variation of the wave function of the H-He system taking into account the interaction of the hydrogen atom with the helium atom;

$$s_0 = (\Phi_0(1)|\Phi_0(2)); \quad q = q_0 - q_1; \quad q_0 = (\Delta\Phi(1)|\Delta\Phi(1)); \quad q_1 = (\Delta\Phi(1)|\Delta\Phi(2)). \qquad (3)$$

Formula (2) is accurate to second order inclusively with respect to the small value of $\Delta\Phi$.

In order to calculate the local shift it is necessary to know the wave function of the H-He system for finite distances between the hydrogen and helium nuclei. For this purpose we shall use one of the most developed versions of the exchange perturbation theory taking into account the Pauli principle -- the ALBAX exchange perturbation theory [10]. We do not want to deal with the difficulties connected with ambiguity of the expansions of the exchange perturbation theory here (see, for example, [11]).

On the basis of the formalism developed in [10], let us write the wave function and the energy of the ground state ($^2\Sigma^+$) of the H-He system with accuracy to the second order of smallness with respect to the perturbation inclusively:

$$\psi = A\Phi(1) = \psi_0 + \sum_k a_k \psi_k, \qquad (4)$$

Here A is the antisymmetrization operator, and the expansion coefficient

$$a_k = b_k + c_k + d_k, \qquad (5)$$

where b_k and c_k are the first order terms with respect to the perturbation:

$$b_k = \frac{1}{3}\frac{V_{k0} - U_{k0}}{E_0 - E_k}; \quad c_k = \frac{1}{3}\frac{s_{k0}}{1 - s_0}\frac{V_{00} - W_{00}}{E_0 - E_k}, \quad k \neq 0;$$
$$b_0 = \frac{1}{3}\sum_k{}' \frac{s_{0k}}{1 - s_0}\frac{V_{k0} - U_{k0}}{E_0 - E_k}; \quad c_0 = \frac{1}{3}\frac{V_{00} - W_{00}}{(1 - s_0)^2}\sum_k{}' \frac{|s_{0k}|^2}{E_0 - E_k};$$

and d_k are the terms of second order of smallness with respect to perturbation equal to

$$d_0 = -\frac{1}{18}\sum_k{}' \frac{1}{(E_0 - E_k)^2}\left[|V_{0k}|^2(1 + s_0) - W_{0k}V_{k0} - V_{0k}U_{k0}\right] +$$
$$+ \frac{1}{18}\sum_{k,l}{}' \frac{1}{(E_0 - E_k)(E_0 - E_l)}(V_{0k}s_{kl}V_{l0} - 2s_{0k}V_{kl}V_{l0}); \qquad (6)$$

$$d_k = \frac{1}{9}\frac{1}{(E_0 - E_k)}\sum_l{}' \frac{1}{E_0 - E_l}\left[V_{kl}V_{l0} - W_{kl}V_{l0} - V_{kl}U_{l0} - \right.$$
$$\left. - V_{k0}s_{0l}V_{l0} - s_{k0}|V_{0l}|^2\right], \quad k \neq 0. \qquad (7)$$

Here

$$V_{kl} = (\Phi_k(1)|V(1)|\Phi_l(1)); \quad W_{kl} = (\Phi_k(1)|V(1)|\Phi_l(2));$$
$$U_{kl} = (\Phi_k(2)|V(1)|\Phi_l(1)); \quad s_{kl} = (\Phi_k(1)|\Phi_l(2)); \quad \Phi_k(1) = \Psi_k(1)\varphi_{fg}(2, 3);$$
$$\Psi_k(1) \equiv \Psi_k(r_1);$$

$\varphi_{fg}(2, 3) \equiv \varphi_{fg}(r_2, r_3)$ are the coordinate wave functions, respectively, of the hydrogen atom in the state h=(n,ℓ,m) with energy ε_h and the helium atom in the stage f,g with energy ε_{fg}, and

$$V(1) \equiv V(1, 2, 3) = -\frac{1}{r_{a2}} - \frac{1}{r_{a3}} - \frac{2}{r_{b1}} + \frac{2}{R} + \frac{1}{r_{12}} + \frac{1}{r_{13}}.$$

The energy of the H-He system described by the wave function (4)

$$E = E_0 + E^{(1)} + \frac{1}{3(1 - s_0)}\sum_k{}' \frac{|V_{0k} - W_{0k}|^2}{E_0 - E_k} + \frac{E^{(1)2}}{3(1 - s_0)}\sum_k{}' \frac{|s_{0k}|^2}{E_0 - E_k} +$$
$$+ 2\mathrm{Re}\left[\frac{E^{(1)}}{3(1 - s_0)}\sum_k{}' \frac{s_{0k}\cdot V_{k0} - U_{k0}}{E_0 - E_k}\right].$$

Here

$$E^{(1)} = \frac{V_{00} - W_{00}}{1 - s_0}.$$

In formulas (6) and (7) the terms of order exp (-2ZR) and less are omitted (Z=1.6875).

A careful analysis of formula (2) indicates that a significant contribution to the local shift $\delta\omega(R)$ is made only by the first four terms. The first two terms are the overlap integrals. The wave function of the ground state of the helium atom will be approximated by the product of two single-electron wave functions in the approximation of the effective charge Z=1.6875

$$\varphi_{00}(2, 3) = \varphi_0(2)\,\varphi_0(3) = \frac{Z^3}{\pi}\exp\left[-Z(r_{b2} + r_{b3})\right],$$

where r_{b2}, r_{b3} are the distances from the electrodes 2, 3 to the nucleus b. The overlap integral S0 will be expressed here in terms of the overlap integral S of the single-electron orbitals

$$S = \int \Psi_0^*(1)\,\varphi_0(1)\,dV_1, \qquad (8)$$

for which there is a simple formula (see, for example, [12], the appendix):

$$s_0 = |\Phi_0(1)|\Phi_0(2)| = S^2.$$

It is obvious that the first term of (2) depends only on the zero-approximation wave functions and, consequently, does not depend on the choice of the version of the relative perturbation theory. All of the remaining terms (2) are sensitive to the choice of the version of the relative perturbation theory.

The second term of (2) includes the value of q determined according to (3) through $\Delta\Phi$. With precision to second order with respect to the perturbation V

$$\Delta\Phi(1) = \sum_k a_k \Phi_k(1), \qquad (9)$$

where a_k is defined by formula (5). Using (9), for q_0 we obtain the following expression (hereafter in the coefficient a_k we shall neglect the terms of order exp (-3R) and smaller):

$$q_0 = \sum_{k,l} a_k^* a_l (\Phi_k|\Phi_l) \simeq \frac{1}{9}\sum_k{}' \frac{|V_{k0} - U_{k0}|^2}{(E_0 - E_k)^2}. \qquad (10)$$

The exact calculation of the sum (10) is extraordinarily difficult for two reasons: a) it is necessary to know all of the eigenfunctions for the helium atom; b) U_{k0} is the matrix element of the exchange time containing highly complex molecular integrals -- the electron exchange and the hybrid integrals in the arbitrary excited state, including the continuous spectrum.

Therefore, in order to estimate (10) we shall use the known Unsold procedure consisting in taking some average value of $(E_0-E_k)^{-2}$ outside the summation sign in (10) with subsequent summation over the complete set of states k:

$$q_0 = \frac{1}{9}\sum_h' \frac{|V_{h0} - U_{h0}|^2}{(E_0 - E_h)^2} \cong \frac{2}{9}\lambda^3 (V^2)_{00}.$$

Here we take λ according to Adrian [4]

$$\lambda = -\frac{1}{E_a + E_b},$$

where

$$E_a = \frac{I_a + E_{1a}}{2} \text{ and } E_b = \frac{I_b + E_{1b}}{2}, \quad E_a, E_b > 0 -$$

are the mean excitation energies of the atoms a and b where I is the ionization potential and E_1 is the excitation energy of the atom to the first level.

The estimation of q_1 using the unsolved Unsold procedure indicates that q_1 contains an additional smallness of the order of the overlap integral and is small by comparison with q_0. Thereofre we shall write q in the form

$$q \cong q_0 \cong \frac{2}{9} \frac{|V^2|_{00}}{(E_a + E_b)^2}.$$

Let us substitute expression (9) for $\Delta\Phi(1)$ in the third term (2).

$$\frac{1}{\rho_0} \mathrm{Re}\,(\Phi_0(1)|\delta(r_{a1})|\Delta\Phi(1)) = 2\left(b_0 + c_0 + d_0 + \sum_h' (b_h + d_h)\frac{\Psi_h(0)}{\Psi_0(0)}\right). \quad (11)$$

It is necessary to note that only the ground state of the helium atom and also only the s-state of the hydrogen atom ($\Psi_h(0)=0$ for $\ell \neq 0$) participates in the spectral sum (11) as a result of the presence of the factor $\delta(r_{a1})$ in the third term. The wave functions of the s-state are real, and the Re sign can be omitted in (11). The q and s_0 which are small by comparison with one are also omitted. The following sum enters into (11)

$$\left.\begin{aligned} &\frac{2}{\Psi_0(0)}\sum_h' b_h \Psi_h(0) = \Omega_1 + \Omega_2; \\ &\Omega_1 = \frac{2}{3\Psi_0(0)}\sum_h' \frac{V_{h0}\Psi_h(0)}{E_0 - E_h}; \\ &\Omega_2 = -\frac{2}{3\Psi_0(0)}\sum_h' \frac{U_{h0}\Psi_{h0}(0)}{E_0 - E_h}. \end{aligned}\right\} \quad (12)$$

The matrix element of the nonexchange type

$$V_{h0} = (\Phi_h(1)|V(1)|\Phi_0(1)) =$$

$$= -\left(\Phi_h(1)\left|\Pi(r_1) = 2\left(\frac{1}{r_{b1}} + Z\right)\exp(-2Zr_{b1})\right|\Phi_0(1)\right)$$

is expressed in terms of the electric potential $\Pi(r_1)$ of the helium barge field at the point where the electron 1 is located.

The sum (12) contains the exchange type matrix elements; therefore (see the above) we also used the Unsold procedure for calculation of it. However, the characteristic difficulty is encountered here -- the product $\delta(r_{a1})V(2)$ arises. It is an operator which is defined improperly, for it contains the term $\delta(r_{a1})/r_{a1}$ which is meaningless. Accordingly, the term $-1/r_{a1}$ with the "dangerous" denominator $r_{a1}=0$ must be isolated and investigated accurately without applying the Unsold averaging to it.

The first term together with the fourth (in the fourth term it is sufficient to limit ourselves to wave functions in the zero approximation) gives the local shift in the zero approximation of $\delta\omega^{(0)}(R)$.

Let us write the final expression for the local relative shift of the line of the superfine structure of the hydrogen atom:

$$\delta\omega(R) = \delta\omega^{(0)}(R) - \frac{1,41}{9}\left(\frac{2}{E_a} + \frac{3}{E_a+E_b}\right)\Pi^2 + \frac{2}{3\Psi_0(0)}\sum_h{}' \frac{\Psi_h(0)\Pi_{h0}}{E_h - E_0} - \\ - \frac{2\lambda'}{3}(W_{00} + SN_0) - \frac{2S}{3\Psi_0(0)}\sum_h{}' \frac{\Psi_h(0)N_h}{E_h - E_0}, \qquad (13)$$

$$N_h = \int \frac{\Psi_h^*(1)\varphi_0(1)}{r_{a1}}\,dV_1, \quad W_{00} = (\Phi_0(1)|V(1)|\Phi_0(2)).$$

The averaging parameter λ' is estimated from a comparison of the numerical values for the spectral sums which are calculated exactly and the application of the Unsold procedure.

The summation in (13) also implies integration over a continuous spectrum of the hydrogen atom. A detailed calculation of these sums can be found in [7, report IV]. It is necessary to note that when calculating Σ_{hB} (13) we were actually able for the first time to perform the integration over the continuous spectrum.

Formula (13) which we obtained for the local shift has quite understandable physical meaning in contrast to the results of [6, 8]. The first term of $\delta\omega^{(0)}(R)$ in (13) was reckoned for the first time in the work by Clark [5]. He did not obtain the other terms inasmuch as he was limited to the wave function in the zero approximation. This led to the fact that his theoretical result for the shift differed from the experimental result by two times.

The first term (the Van der Waals type) was present already in Adrian's work [4]; as for the remaining terms, they occur as a result of the application of the more successive method of relative perturbation theory.

We also used another method of calculating $\delta\omega(R)$ (in the first order) with respect to the ALBAX relative perturbation theory which gets around

the difficult calculation of the spectral sums. The differential equation was solved directly for the first correction to the wave function $\phi^{(1)}(1) \equiv \Delta\phi(1)$ which according to the ALBAX relative perturbation theory was written in the form:

$$(H_0(1) - \varepsilon^{(0)})\Phi^{(1)}(1) + \frac{1}{3}\left\{[V(1) - E^{(1)}]\Phi_0(1) - \right.$$
$$\left. - \frac{1}{2}[V(2) - E^{(1)}]\Phi_0(2) - \frac{1}{2}[V(3) - E^{(1)}]\Phi_0(3)\right\} = 0. \qquad (14)$$

Here

$$H_0(1) = \sum_{i=1}^{3}\left(-\frac{1}{2}\cdot\Delta_i\right) - \frac{1}{r_{a1}} - \frac{2}{r_{b2}} - \frac{2}{r_{b3}} + \frac{1}{r_{23}};$$
$$V(2) = -\frac{1}{r_{a2}} - \frac{1}{r_{a1}} - \frac{2}{r_{b2}} + \frac{2}{R} + \frac{1}{r_{12}} + \frac{1}{r_{23}},$$

and the perturbation V(3) corresponds to the case where the electron 3 is on the hydrogen atom.

Here it was possible to obtain an explicit expression for the sum $\Omega_1+\Omega_2$, avoiding the extremely difficult calculation of the molecular two-center integrals containing the wave functions of the excited state and more difficult subsequent summation with respect to these states including integration of the continuous spectrum. A detailed derivation of the formulas is contained in the diploma work of N. A. Lapuk written in 1974.

Now let us present the results of the numerical calculations. In Table 1 the following are compared: a) individual contributions to the local shift calculated by formula (13); b) local shift obtained by us with other theoretically calculated shifts [8] and [6]; c) the interaction potentials between the hydrogen and helium atoms.

Table 1

R(a. e.)	$\delta\omega^{(0)}(R)\times10^3$	$\Omega_1\times10^3$	$\Omega_2\times10^3$	(1) Члены второго порядка малости	$\delta\omega(R)\times10^3$			$U(R)\times10^3$		
					наш результат (2)	по [8] (3)	по [6] (4)	наш результат (2)	по [8] (3)	по [6] (4)
4	6,730	−1,558	6,787	−0,265	11,694	14,643	11,913	2,768	2,883	2,63
5	1,196	−0,307	1,442	−0,0695	2,261	2,726	2,472	0,387	0,361	0,369
6	0,195	−0,0539	0,256	−0,0233	0,373	0,326	0,349	0,028	−0,0058	0,0257
7	0,0304	−0,00914	0,0422	−0,00922	0,0543	−0,063	0,037	−0,0106	−0,0344	−0,0108
8	0,00456	−0,00136	0,00658	−0,00414	0,00544	−0,098	0,019	−0,0088	−0,0231	−0,0057
9	0,00066	−0,00024	0,00099	−0,00204	−0,00063	−0,042	0,002	−0,0050	−0,0126	−0,0049
10	0,00010	−0,00005	0,00016	−0,00108	−0,00087	−0,017	—	−0,0028	−0,0066	−0,0027
11	0,00001	−0,00001	0,00002	−0,00061	−0,00058	−0,008	—	−0,0016	—	−0,0034

Key:

1. Terms of second order of smallness
2. Our results
3. According to [8]
4. According to [6]

Table 2

Температура K (1)	Относительный сдвиг в 10^{-9} тор (2)			
	(3) Расчет			Эксперимент
	по (1)	по (13)	по (8)	
	(4)	(5)	(6)	(7)
173	4,56	4,31	—	4,6
223	4,21	3,97	—	4,3
273	3,95	3,71	—	4,0
323	3,75	3,52	3,40	3,61 ±0,19
373	3,58	3,36	3,35	3,62
423	3,44	3,23	3,31	3,48
473	3,32	3,11	3,26	3,36
523	3,21	3,01	3,21	3,26
573	3,11	2,92	3,14	3,24
623	3,03	2,84	3,12	3,18
673	2,95	2,77	3,08	3,12

Key:

1. Temperature, °K
2. Relative shift in 10^{-9} torr
3. Calculation
4. According to (1)
5. According to (13)
6. According to (8)
7. Experiment

Note. The result of the calculation according to [6] for T=323°K was $4.28 \cdot 10^{-9}$ torr.

As is obvious from Table 1, the primary contribution to the local shift at intermediate distances R~4 to 6 atomic units is made by the local shift of zero order $\delta\omega^{(0)}(R)$ and the exchange term Ω_2. The nonexchange sum Ω_1 is negative for all R and is about 25% of the shift $\delta\omega(R)$. A comparison of the local shifts obtained by Davison and Liew, Das and Ray and by us indicates that our $\delta\omega(R)$ is closer to the shift from [6], but in contrast to it has small negative part. The local shift from [8] has the same property.

It is necessary to note that the accurate calculation of the nonexchange sum and also one of the exchange sums and mainly with the "dangerous" denominator r_{al}^{-1} demonstrated that at intermediate distances the discrete spectrum makes a 5 to 10-fold more significant contribution than the continuous spectrum which to some degree justifies the application of the Unsold averaging in the other sums. In the sums with respect to discrete spectrum, in turn, the primary contribution is usually made by the first term (n=2). For example, in the sum Ω_1 for R=5 to 6 the contribution of the first term is 80 to 90%. Thus, our calculations confirm the neglecting of the higher excited states in other papers (apparently, we succeeded for the first time in correctly considering the contribution from the higher excited states, including from the continuous spectrum). According to formulas (1), (13) presented in reference [9], the observed (averaged over the distances R) relative shift $f_p=\Delta/(p\omega_0)$ was calculated, where p is the pressure of the buffer gas in torrs. The results are presented in Table 2.

BIBLIOGRAPHY

1. Anderson, L. W.; Pipkin, F. W.; Baird, J. C. PHYS. REV., No 122, 1961, p 1962.

2. Pipkin, F. M.; Lambert, R. H. PHYS. REV., No 127, 1962, p 787.

3. Wright, J. J.; Balling, L. C.; Lambert, R. H. PHYS. REV., No A1, 1971, p 1018.

4. Adrian, F. J. J. CHEM. PHYS., No 32, 1960, p 972.

5. Clarke, G. A. J. CHEM. PHYS., No 36, 1962, p 2211.

6. Das, G.; Ray, S. PHYS. REV. LETT., No 24, 1970, p 1391.

7. OTCHETY LPI VNITITS [Reports of the Leningrad Polytechnical Institute VNITITs], I, B 067234, 1970; II, B 109317, 1971; III, B 190191, 1972; IV, B 268901, 1973.

8. Davison, W.; Liew, Y. C. J. PHYS. B: ATOM. MOL., No 5, 1972, p 309.

9. Batygin, Vl. V.; Batygin, Vit. V.; Guzhva, Yu. G.; Ivanov, A. N. See the present collection, p 105.

10. Ad van der Avoird, J. CHEM. PHYS., No 47, 1967, p 3649.

11. Certain, P. R.; Hirschfelder, J. O.; Kolos, W.; Wolniewioz, L. J. CHEM. PHYS., No 49, 1968, p 24.

12. Gombash, P. PROBLEMA MNOGIKH CHASTITS V KVANTOVOY MEKHANIKE [Problem of Many Particles in Quantum Mechanics], IL, 1953.

THEORY OF LINE SHIFTS AND BROADENINGS OF THE SUPERFINE TRANSITION OF AN ATOM IN A BUFFER GAS ENVIRONMENT

[Vl. V. Batygin, Vit. V. Batygin, Yu. G. Guzhva, A. N. Ivanov]

[Text] The phenomena of line shift and broadening of the superfine transition of atoms in a buffer gas environment have been quite deeply and completely investigated in the papers with double optical resonance of alkali atoms and in creating frequency standards on the principle of optical pumping. The theoretical studies are less complete. Several papers are known which are devoted to the calculation of the collision shift of the frequency, for example, [1-5]. However, the line width was not calculated in any of them. The purpose of this paper is to fill this gap to some extent -- to obtain calculation expressions for the line shifts and broadenings of the superfine structure with zero intensity of the pumping field and the microwave field.

At the present time in all the known papers [1-5] for calculation of the collision shift of the line frequency of the superfine transition of an active alkali or hydrogen atom in a buffer gas, the following formula is used:

$$\Delta = N_B \int_0^\infty \exp\left(-\frac{U(R)}{kT}\right) \Delta\omega(R) \cdot 4\pi R^2 dR, \qquad (1)$$

where

$$\Delta\omega(R) = \omega(R) - \omega_0; \qquad (2)$$

ω_0 is the frequency of the superfine transition of the isolated active atom; $\Delta\omega(R)$ is the local shift of the frequency occurring on fastening the atom of buffer gas at a distance R from the active atom $A(\omega_0 \equiv \omega(\infty))$; N_B is the concentration of the buffer atoms; U(R) is the energy of interaction of the active and buffer atoms; T is the gas temperature; k is the Boltzmann constant. Formula (1) can be written on the basis of the obvious statistical arguments which, however, will not permit anything to be said about the line width (neither about collision or doppler width) and the width was not calculated in any of the papers [1-5].

General expressions for the shifts and broadenings have been found in correlation theory; see, for example, [6, 7]. However, it was not possible with their help to achieve agreement with the experiment for the line shift in contrast to formula (1). The fact that for collision broadening Γ_{coll} values were obtained which exceed the observed ones by several orders, was especially inconvenient. From correlation theory the conclusion would be drawn that the Foley ratio must be satisfied [8]:

$$\Gamma_{coll} |\Delta| \sim 1. \qquad (3)$$

Nevertheless, from the experiment it follows that in the microwave band at pressures of less than 100 torr the collision broadening is less by several orders than the shift, and expression (3) is thus grossly violated. We investigated this problem in 1969-1973 [9, 10]. The reason for such significant constriction of the lines is the random wanderings of the phase of the emitted field in accordance with the previously stated qualitative arguments [11]. In order to obtain the calculation formulas for the shift and broadening, it turned out to be necessary to consider the distortion of the trajectories of the colliding atoms.

Basic Propositions

In the estimates discussed below we shall take the values of the parameters that are standard for the gas cells of atomic frequency standards with optical pumping, for example, [11]. The derived formulas indeed have broader applicability.

For these values of the parameters the following theoretical propositions are satisfied:

1) The primary role is played by short binary collisions of the active atom with the buffered ones -- the impact approximation $\tau_0 \gg t_{coll}$;

2) The relative motion of the active and buffer atoms is quasiclassical so that it is possible to talk about the classical theory, the target parameters ρ, and so on;

3) The condition $\lambda \gg L$ of the Dicke effect is satisfied;

4) The energy of the superfine interaction is small so that $\Delta\omega(R)t_{coll} \ll 1$ for real R (or $\Delta t_{coll} \ll 1$);

5) The adiabatic collision broadening is large by comparison with nonadiabatic

$$\Gamma_a \gg \Gamma_{Ha}$$

(the transverse relaxation time is $1/\Gamma_a$, and the longitudinal is $1/\Gamma_{Ha}$).

Correlation Theory

Under the conditions of applicability of the impact approximation the trajectory of the active atom is a broken line on which the length ℓ_ν of each ν-th of the rectilinear sections of the free path is large by comparison with the length of the collision section in which the trajectory break occurs. The doppler shift and the broadening corresponding to it which occurs as a result of averaging of the shifts with respect to directions is basically observed on the rectilinear section of the trajectory of the active element, the collision shifts and broadening, on the breaks of the trajectory when on approach of the atoms atomic transitions are realized leading to nonadiabatic broadening Γ_{Ha}, and the line frequency ω_0 emitted by the isolated atom is shifted by $\Delta\omega(R)$. The modulation of the frequency ω occurring as a result of the fact that R varies with time causes shift of the line and adiabatic broadening of it.

According to correlation theory of the emission line width, the form of the line is a Fourier transform from the correlator

$$\Phi_f(\tau) = \ll F_{ii}(\tau) F_{ii}(0) \gg \qquad (4)$$

the matrix element $F_{ff}(t)$ from the interaction F of the active atom with the microwave field between the initial $\psi_i(t)$ and final $\psi_f(t)$ states of the moving active atom. The angular brackets << >> in (4) denote averaging with respect to the set of random collisions, each of which is characterized by the target parameter ρ_ν and the relative initial velocity v_ν of the colliding active and buffer atoms, the random path lengths ℓ and the absolute velocities $v_{A\nu}$' of the atom A on the ν-th rectilinear section and also the random numbers n of collisions for the time τ.

Let us denote by $V(t)=\Sigma_\nu V_\nu$ the perturbation potential of the superfine interaction caused by random collisions with buffered atoms. In the impact approximation this potential is the sequence of independent random shocks V_ν. The diagonal matrix elements V_ν are causing local shift (2). The nondiagonal elements V_ν describe the departures from the initial state on collision. Selecting the direction of observation of the quantum after the z-axis, let us write the matrix element

$$F_{ii}(\tau) = F_{ii}(0) \exp\left(i\omega_0\tau + i\sum_{\nu=1}^{n}\Phi_\nu\right),$$

where

$$\Phi_\nu = x_\nu + \eta(\rho_\nu, v_\nu) + \frac{i}{2}\zeta(\rho_\nu, v_\nu); \qquad (5)$$

$$x_\nu = \frac{\omega_0}{c}\frac{v_{Az}}{v_{A\nu}} l_\nu = 2\pi\frac{l_\nu}{\lambda}\frac{v_{Az}}{v_{A\nu}}; \qquad (6)$$

$$\eta(\rho_\nu, v_\nu) = \frac{1}{\hbar}\int_{-\infty}^{+\infty}(V_{ii,\nu}(t) - V_{ff,\nu}(t))\,dt = \int_{-\infty}^{+\infty}\Delta\omega(R_\nu(t))\,dt. \qquad (7)$$

For calculation details let us refer to reports [9], [10]. Here χ_ν is the random doppler phase shift of the matrix element in the ν-th element of the free path; $\eta(\rho_\nu, v_\nu)$ is the random collision phase shift of an adiabatic nature for the ν-th collision; $\zeta(\rho_\nu, v_\nu)$ is the probability of departure of the atom A from the states i and f to other possible states, and the meaning of Φ_ν is obvious from (5).

General Expressions for Shifts and Broadenings

Within the framework of the impact approximation, the theory of Poisson random impacts is applicable. The probability that n impacts took place in the time τ is determined by the Poisson distribution

$$W_n = (\bar{n}^n/n!)\exp(-\bar{n}),$$

where $\bar{n}=\tau/\tau_0$ is the average number of collisions in the time τ. After averaging over n we obtain

$$\Phi_f(\tau) = |F_{if}(0)|^2 \exp\left[i(\omega_{if} + \Delta + i\Gamma/2)\tau\right], \tag{8}$$

where

$$i\Delta - \frac{\Gamma}{2} = \frac{1}{\tau_0}\left\langle \exp\left\{i\left[\chi(l, v_A) + \eta(\rho, v) + \frac{i}{2}\zeta(\rho, v)\right]\right\} - 1\right\rangle. \tag{9}$$

Here the angular brackets < > denote averaging over the entire remaining random variables l, v_A, ρ, v. The phase shifts χ, η are defined by the formulas (6), (7) in which the indexes ν can be omitted, for the probability distributions for l_ν, $v_{A\nu}$, ρ_ν, v_ν obviously do not depend on ν.

The form of the line corresponding to the correlator (8) is found to be Lorentian with shifts Δ and broadening Γ determined with respect to (9).

On satisfaction of the above-enumerated propositions, the phase shifts are small by comparison with one $|\chi| \sim 2\pi L/\lambda \leq 0.1$, $|\eta| \leq 0.1$ (see below and also [11] p 72), $\zeta \sim \eta^2 \leq 0.01$. Here it is possible to expand the exponent in (9) in a series, omitting all the terms above second order:

$$\left.\begin{aligned} &\Delta = \Delta_{cr} = \frac{1}{\tau_0}\langle\eta\rangle; \\ &\Gamma = \Gamma_{cr} + \Gamma_D; \quad \Gamma_{cr} = \Gamma_a + \Gamma_{aa}; \\ &\Gamma_a = \frac{1}{\tau_0}\langle\eta^2\rangle; \quad \Gamma_{aa} = \frac{1}{\tau_0}\langle\zeta\rangle; \quad \Gamma_D = \frac{1}{\tau_0}\langle\chi^2\rangle. \end{aligned}\right\} \tag{10}$$

Key: coll

The averaging with respect to the velocities v_A, v_B (10) is carried out with respect to the Maxwell distribution dw_v, with respect to the free path lengths L, with distribution $dw_l = (1/L)\exp(-l/L)$, with respect to the target distances with distribution $dw_\rho = 2\pi\rho d\rho/\sigma_0$ for $\rho < r_0$, $\sigma_0 = \pi r_0^2$ is the

gas kinetic cross section. For $\rho \leq r_0$ the classical investigation of scattering is unsuitable. However, the functions under the integral sign contain the factor $\eta(\rho, v)$ which rapidly decreases with an increase in ρ, and we shall integrate with respect to ρ to ∞. Noting that $\tau_0 v_0 = 1/N_B \bar{v}$ we obtain

$$\Delta = \frac{1}{\tau_0} \langle \eta \rangle = N_B \bar{v} \int_0^\infty dw_v \int_0^\infty \eta(\rho, v) \cdot 2\pi\rho \, d\rho; \qquad (11)$$

Γ_a differs from (11) by replacement of η by $\eta^2/2$.

It is inexpedient to express the nonadiabatic broadening by integrals of this type; it is better to note that $\langle \zeta \rangle$ is connected, by definition, with the cross section σ of inelastic relaxation collision by the expression $\langle \zeta \rangle = N_B v_0 \tau_0$, so that $\Gamma_{Ha} = N_B \bar{v} \sigma$.

As for Γ_D, as a result of the simple structure of expression (6) for the phase χ, averaging with respect to Maxwell and with respect to dw_v can be performed to the end. While writing the calculations (see [9], Chapter I) we obtained the known Dicke expression [12]:

$$\Gamma_D = (8\pi^2/3) L \bar{v} / \lambda^2.$$

From (10) it is obvious that in accordance with the experiment, $\Gamma_a / |\Delta| \sim |\langle \eta \rangle| \leq 10^{-1}$. Thus, the Foley expression (3) does not necessarily follow from the correlation theory.

Calculation Formulas for Adiabatic Shift and Broadening

Formulas of the type of (11) include $\eta(\rho, v)$ determined according to (7) by a single integral with respect to t. Accordingly, Δ is depicted by a triple integral with respect to v, ρ, t, and Γ_a, by the quadruple integral. Part of the integrations can be performed in general form. It is advantageous to make the transition from integration with respect to t to integration with respect to R using the expression $dR = \dot{R} dt$ which can be written in the form:

$$dt = \frac{dR}{v} \left(1 - \frac{2U(R)}{Mv^2} - \frac{\rho^2}{R^2}\right)^{-1/2}. \qquad (12)$$

Physically (12) takes into account the distortion of the trajectories A and B. The integration with respect to v and ρ is satisfied in general form. Referring to [9], Chapter 1, §2 for the calculation details, we present the final result:

$$\Delta = 4\pi N_B \int_0^\infty \exp\left[-\frac{U_1 R^2}{kT}\right] F\left(\frac{U_1 R}{2kT}\right) \Delta w(R) R^2 \, dR. \qquad (13)$$

Here F is the temperature form factor:

$$F(x) = \frac{4|x|}{\pi} \exp(x) \left[K_1(|x|) - K_0(|x|) \operatorname{sign} x\right]; \qquad (14)$$

$K_1(x)$, $K_0(x)$ are the MacDonald functions.

It is significant that the formula (13) has a reasonable structure of the statistical formula (1) differing from it only by the form factor F. The general behavior of the factors exp(-U/kT) and F exp (-U/kT) is close. Since $\Delta\omega(R)$ decreases with an increase in R and R~5 to 6 turns out to be the most significant region with respect to R in the integral (13) as demonstrated by the calculations, the results of calculating the shift with respect to (1) and with respect to (13) must be close (see below), differing by no more than 10 to 20%. Here formula (13) usually gives a smaller value than (1). Let us note that by small modification of the presented conclusion which is natural from the point of view of the structure of the majority of formulas for kinetic coefficients, in formula (13) instead of (14) it is possible to obtain the form factor

$$F_1(x)=\begin{cases} 1 \text{ for } x>0, \\ \frac{1}{\sqrt{\pi}}\exp(2x)\sqrt{-2x}-\frac{1}{2}\Phi(\sqrt{-2x}) \text{ for } x<0, \end{cases} \quad (15)$$

where Φ is the probability integral. Usually $F_1(x)$ for all x is quite close to 1. In order to obtain (15), in the initial expression (11) it is necessary to introduce the average velocity v under the integral sign with respect to v and replace it by the variable velocity v.

Let us note that the approximation of rectilinear trajectories [6], [7] is unsuitable in the case of lines with superfine structure, for it erodes the basic fact of smallness of the phase η in a significant region R (for more details see [9]).

When calculating the adiabatic broadening in general form it is necessary to perform only integration with respect to ρ. Introducing the notation

$$x=\frac{Mv^2}{2kT}+W(R'); \quad v_0=\sqrt{2kT/M},$$

where W(R')=U(R')/kT for U(R')>0; W(R')=0 for U(R')<0; M is the reduced mass A and B, we obtain

$$\Gamma_a=\frac{32N_B}{v_0}\int_0^\infty R\,dR\int_0^R R'\,dR'\,\Delta\omega(R)\,\Delta\omega(R')\exp[-W(R')]\times$$
$$\times\int_0^\infty dx\,\frac{\exp(-x)}{\sqrt{x+W(R')}}\ln\left|\frac{R\sqrt{x+W(R')-W(R)}-R'\sqrt{x}}{R\sqrt{x+W(R')-W(R)}-R'\sqrt{x}}\right|. \quad (16)$$

When writing (16) we made a simplification of little significance consisting in replacing the true value of U(R) by 0 for U(R)<0.

From (16) we see that the adiabatic broadening, just as the shift, is expressed in terms of the local shift $\Delta\omega(R)$ and the interaction energy U(R). Formulas (14)-(16) are new.

Results of Calculating Adiabatic Shifts and Broadening

Let us present the results of the performed shift calculations by formula (13) with the thermal form factor (14) for the systems H-He, Li^7-He, Na^{23}-He for various temperatures. Let us compare them with the calculations with respect to (1), which corresponds to F=1 and with the experiment (Table 1 and Table 2 in [13]), where the relative shift $f_p=\Delta/(\omega_0 p)$ is presented (p is the pressure of the buffer gas) in units of 10^{-9} $torr^{-1}$. The values of the local shift are taken from references [3, 5]. The results of the calculation presented in these papers are supplemented for a number of temperatures by our results. The results of the calculation and the experiments agree on the whole satisfactorily. The difference between formulas (1) and (13) is 8-13%. In all cases the form factor decreases the value of the shift. For the H-He system with local shift from [2] consideration of the form factor improved the agreement with the experiment; for the same system from [5], it became noticeably worse, and for the systems Li^7-He and Na^{23}-He the experiment "forked."

Table 1

T K	Li^7—He			Na^{23}—He		
	(1) Расчет		Эксперимент по [3] (4)	(1) Расчет		Эксперимент по [3] (4)
	по (13) (2)	по (1) (3)		по (13) (2)	по (1) (3)	
295	—	—	—	61,3	72,2	67,5
373	—	—	—	55,6	61,4	—
387	51,3	55,5	54,7	—	—	—
473	47,1	50,8	—	49,8	54,4	—

Key:
1. Calculation
2. With respect to (13)
3. With respect to (1)
4. Experiment according to [3]

The results of the calculations of the adiabatic broadening by formula (16) are presented in Tables 2 and 3. The calculations were performed for the same versions as above. The absolute values of the adiabatic broadening are presented in Table 2, and its relative values $\delta\Gamma_a=\Gamma_a/(\omega_0 p)$ in Table 3 along with the values of the ratio of the adiabatic broadening to shear and the absolute transition frequency.

It is impossible to compare the values obtained for Γ_a with the experiment at the present time, for they are small and are completely shaded out by the stronger broadening effects.

Our calculations have thus confirmed that actually powerful constriction of the superfine transition line takes place $\Gamma_a/|\Delta| \sim 10^{-4}$ to 10^{-3} by comparison with the theoretical predictions, not taking into account the distortion of the trajectories according to which the Foley ratio (3) must occur.

Table 2

T K	$\Gamma_0 \cdot 10^{-3}$ Гц тор (1)			
	H—He		Li^7—He	Na^{23}—He
	$\Delta\omega(R)$ из [5] (2)	$\Delta\omega(R)$ из [2] (2)		
300	0,248	0,181	—	47,5
323	0,248	0,182	—	—
373	0,246	0,183	7,04	—
473	0,241	0,184	6,50	43,2

Key:
1. hertz/torr
2. from

Table 3

	H—He		Li^7—He	Na^{23}—He
	$\Delta\omega(R)$ из [5]	$\Delta\omega(R)$ из [2]	T=473 K	
	T=323 K			
$\delta\Gamma_0 \cdot 10^{12}$ тор$^{-1}$ (1)	0,175	0,128	7,6	24,4
$\lvert\Gamma_0'/\Delta\rvert \cdot 10^4$	0,460	—	1,4	36,0
$\omega_0 \cdot 10^{-9}$ Гц (2)	1,4204	—	0,8035	1,7716

Key:
1. torr
2. hertz

Table 4

Смесь (1)	$\sigma_{эксп}$ см^2 (2)	$\sigma_{теор}$ см^2 (3)	
		наш расчет (4)	по [16]
Rb—Ar	$3,7 \cdot 10^{-22}$ $1,1 \cdot 10^{-22}$	$4,8 \cdot 10^{-22}$	$1,9 \cdot 10^{-22}$
Rb—Kr	$5,9 \cdot 10^{-21}$ $7,3 \cdot 10^{-21}$ $2,3 \cdot 10^{-20}$	$2,4 \cdot 10^{-21}$	$4,8 \cdot 10^{-21}$
Rb—Xe	$1,3 \cdot 10^{-20}$ $1,3 \cdot 10^{-20}$	$1,5 \cdot 10^{-20}$	$1,0 \cdot 10^{-20}$

Key:
1. Mixture
2. σ_{exp} cm^2
3. σ_{theor} cm^2
4. our calculation

Results of Calculating Adiabatic Broadening

In the paper by Hermann[14], the relaxation cross section of the spin of the valence electron of an alkali metal atom was calculated on interaction with the buffer gas atoms. The calculated value turned out to be in poor agreement with the experiment, for example, for the Rb-He pair we obtain $\sigma_{theor}=3.84\cdot10^{-24}$ cm^2, and $\sigma_{exp}=6.25\cdot10^{-25}$ cm^2. It is possible to think that one of the causes of divergence of the theoretical and experimental values is failure to consider the distortions of the trajectories of the interacting atoms in reference [14].

For the relaxation cross section σ we were able to obtain the closed formula considering the distortions of the trajectory which we shall not present in view of the insufficient space (see [9, 10]). This formula was used to calculate the inelastic collision cross section $\sigma=\Gamma_{Ha}/(\bar{v}N_B)$ for certain A-B pairs. The results are partially presented in Table 4. They are compared with the experimental [14, 15] and theoretical results [16].

Obviously, it is possible to talk about the existence of agreement between the theory and the experiment. Our formula predicts a sharp increase in cross section at low temperatures. This temperature range still has not been investigated experimentally.

BIBLIOGRAPHY

1. Robinson, L. B. PHYS. REV., No 117, 1960, p 1275.

2. Das, G.; Ray, S. PHYS. REV. LETT., No 24, 1970, p 1391.

3. Ray, S.; Das, G.; Maldonado, P.; Wahl, A. C. PHYS. REV., No A2, 1970, p 2196.

4. Kunik, D.; Kaldor, U. JOURN. CHEM. PHYS., No 55, 1971, p 4127.

5. Davisson, W.; Liew, Y. C. JOURN. PHYS. B: ATOM. MOLEC. PHYS., No 5, 1972, p 309.

6. Sobel'man, I. I. VVEDENIYE V TEORIYU ATOMNYKH SPEKTROV [Introduction to the Theory of Atomic Spectra], Fizmatgiz, 1963.

7. Gersten, J. I.; Foley, H. M. PHYS. REV., No 182, 1969, p 24.

8. Foley, H. M. PHYS. REV., No 69, 1946, p 616.

9. Report of the Leningrad Polytechnical Institute on Topic 5229, II, 1971, VNITITs B-109317.

10. Report of the Leningrad Polytechnical Institute on Topic 7006, IV, 1973, VNITITs B-268901.

11. Grigor'yants, V. V.; Zhabotinskiy, M. Ye.; Zolin, V. F.; KVANTOVYYE STANDARTY CHASTOTY [Quantum Frequency Standards], Nauka, 1968.

12. Dicke, R. H. PHYS. REV., No 89, 1953, p 472.

13. Batygin, V. V.; Lapuk, N. A.; Matisov, B. G. See the present collection, p 99.

14. Hermann, R. M. PHYS. REV., No 136A, 1964, p 1576.

15. Violino, P. SUPPL. EL NUOVO CIM., No 6, 1968, p 440.

16. Happer, W. REV. MOD. PHYS., No 44, 1972, p 5.

10845
CSO: 8044/0436

- END -